มหาวิทยาลัยมหิดล
คณะแพทยศาสตร์โรงพยาบาลรามาธิบดี

มหาวิทยาลัยมหิดล
คณะทันตแพทยศาสตร์

The 47th Annual Meeting of The Pharmacological and Therapeutic Society of Thailand

Global Trends and Emerging Innovations in Pharmacology

13-15 May 2026 At Meeting Room, 10th Floor, Bajrakitiyabha Building, Phramongkutklao Hospital

This publication includes abstracts of invited speakers, poster abstract and papers presented at the 47th Annual Meeting of the Pharmacological and Therapeutic Society of Thailand (PTST) under the theme "Global Trends and Emerging Innovations in Pharmacology". The conference was held at Pramongkutklao College of Medicine, Bangkok during 13-15 May 2026, organized by Faculty of Medicine Ramathibodi Hospital, Mahidol University; Faculty of Dentistry, Mahidol University and Pramongkutklao College of Medicine.

Disclaimer

Matters of copyright of all images and text associated with the abstracts and papers within the Proceedings of the 47th Annual Meeting of the Pharmacological and Therapeutic Society of Thailand are the responsibility of the authors. The PTST does not accept responsibility for any liabilities arising from the publication of any of the submissions.

Copyright

Published by The Pharmacological and Therapeutic Society of Thailand (PTST).

National Library of Thailand Cataloging in Publication Data

Proceedings of the 45th International Meeting of the Pharmacological and Therapeutic Society of Thailand.-- Bangkok : The Pharmacological and Therapeutic Society of Thailand, 2024.
140 p.

1. Pharmacy. I. Title.

615.1
ISBN 978-616-94260-1-1

Table of Content

Table of Content

Table of Content

"Global Trends and Emerging Innovations in Pharmacology"

13–15 May 2026

It is my great pleasure to welcome all participants to the Annual Conference of the Pharmacological and Therapeutic Society of Thailand (PTST 2026). This conference brings together researchers, clinicians, and scholars to exchange knowledge and explore advancements under the theme "Global Trends and Emerging Innovations in Pharmacology."

The program has been thoughtfully designed to cover key areas in modern pharmacology. Highlights include the Chiravat Sadavongvivad Memorial Lecture, international collaboration with the Japanese Society for the Study of Xenobiotics (JSSX), and the Ouay Ketusingh Honorary Award Lecture. Scientific sessions span important topics such as herbal interventions in metabolic disorders, gene therapy and novel drug delivery systems, pharmacology education, and translational research.

In addition to plenary lectures and symposia, the conference features technical seminars, poster and oral presentations, and interactive workshops on simulation- and game-based learning. These activities aim to foster collaboration, innovation, and professional development among participants.

On behalf of the Society, I extend my sincere appreciation to all speakers, organizers, and participants for their valuable contributions. I hope this conference will inspire meaningful discussions, strengthen collaborations, and advance pharmacological research at both national and global levels.

Associate Professor Rattima Jeenapongsa, Ph.D.

President

The Pharmacological and Therapeutic Society of Thailand (PTST)

Annual Conference 2026

Message from the Chair

Distinguished Guests, Esteemed Colleagues, and Friends,

On behalf of the organizing committee, it is my great honor, as Chairman of the 47th Annual Meeting of the Pharmacological and Therapeutic Society of Thailand, to warmly welcome you to our 2026 conference. We are delighted to gather as a dynamic scientific community dedicated to advancing pharmacological research and improving global health.

This year's theme, **"Global Trends and Emerging Innovation in Pharmacology,"** reflects the rapid transformation of our field. From natural products and phytopharmaceutical development to gene therapy and novel anticancer strategies using advanced synthesis techniques, our program highlights the breadth of innovation shaping modern therapeutics. We will also address the challenges of cross-species medication use, underscoring the global and translational relevance of pharmacological science.

Beyond the scientific sessions, this meeting serves as a vital platform for collaboration, mentorship, and professional partnership. Through interdisciplinary dialogue and shared expertise, we continue to strengthen our collective impact and shape the future of pharmacology.

I would like to extend my sincere appreciation to our distinguished speakers, sponsors, organizing committee members, and dedicated staff for their invaluable contributions. Most importantly, I thank all participants for your presence and engagement, which truly enrich this annual gathering.

As Chairman, I am confident that this meeting will inspire new ideas, foster meaningful collaborations, and advance innovative solutions for the benefit of patients and communities worldwide.

Thank you, and I wish you a productive and inspiring conference.

Assoc. Prof. Pornpun Vivithanaporn

Faculty of Medicine Ramathibodi Hospital

Mahidol University

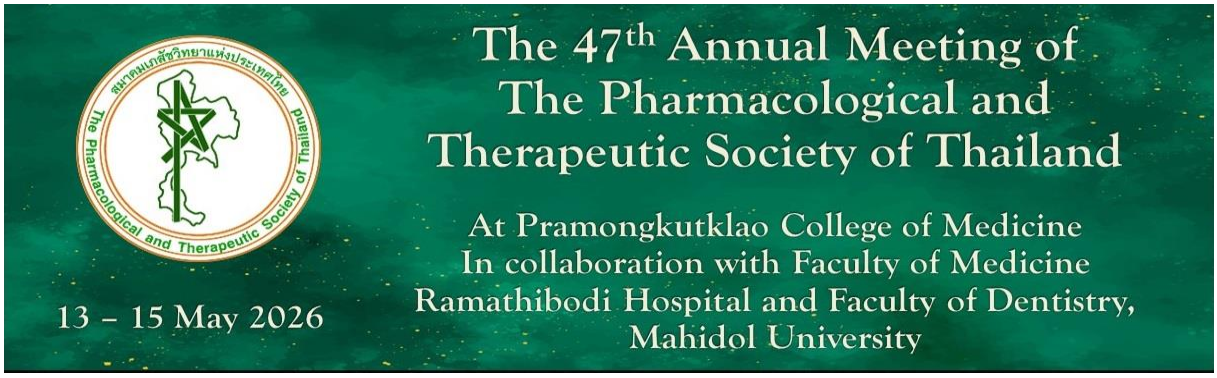

Conference Program

13 May 2026	
08.00 – 08.30	Registration
08.30 – 09.00	Welcome Ceremony Associate Professor Pornpun Vivithanaporn, Ph.D. Chair of the Organizing Committee (PTST2026) Colonel Associate Professor Janeyuth Chaisakul, Ph.D. Co-chair of the Organizing Committee (PTST2026) Associate Professor Rattima Jeenapongsa, Ph.D. President of the Pharmacological and Therapeutic Society of Thailand *Moderated by Lieutenant Colonel Thishnapha Vudhironarit, Ph.D.*
09.00 – 10.00	Chiravat Sadavongvivad Memorial Lecture (English) "Natural Products and Longevity Medicine: Exploring Novel Pathways for Healthy Aging" Professor Lijun Liu, M.D., Ph.D. *Moderated by Assistant Professor Tipparat Parakaw, Ph.D.*
10.00 – 10.20	Morning refreshment and poster session
10.20 – 11.20	Invited speaker from the collaboration project between the Japanese Society for the Study of Xenobiotics (JSSX), and the Pharmacological and Therapeutic Society of Thailand (PTST) "The Role of the Mucus Layer in Pharmacokinetics and Pharmacological Effects, and Its Molecular Basis" Associate Professor Hisanao Kishimoto, Ph.D. Department of Biopharmaceutics, School of Pharmacy, Tokyo University of pharmacy and Life Sciences (TUPLS) *Moderated by Jiranan Chotitumnavee, Ph.D.*
11.20 – 11.50	Ouay Ketusingh Honorary Award Ceremony and Award Lecture Professor Uraiwan Panich, M.D., Ph.D. *Moderated by Lieutenant Colonel Thishnapha Vudhironarit, Ph.D.*
11.50 – 12.05	Technical Seminar I – Kyberlife

Program Schedule

12.05 – 13.00	Lunch
13.00 – 14.30	Symposium I: Herbal Interventions in Metabolic Disorders: Mechanisms and Translational Insights (English) "Lipid-lowering effects of fingerroot extract against hyperlipidemia induced fatty liver: From bench back to communities" (45 min) Associate Professor Chutima Vaddhanaphuti, Ph.D. Department of Physiology, Faculty of Medicine, Chiang Mai University "Effects of herbal medicines on gut microbiomes" (30 min) Assistant Professor Pisut Pongchaikul, Ph.D. Chakri Naruebodindra Medical Institute, Faculty of Medicine Ramathibodi Hospital, Mahidol University *Moderated by Pinnakarn Techapichetvanich, Ph.D.*
14.30 – 14.45	Technical Seminar II – Fortis trading
14.45 – 15.45	Afternoon refreshment and poster session
15.45 – 16.30	"Updates and challenges in antimalarials in Thailand" Lieutenant General Professor Mathirut Mungthin Phramongkutklao College of Medicine *Moderated by Colonel Associate Professor Janeyuth Chaisakul, Ph.D.*
16.30 – 17.30	Annual member meeting of the Pharmacological and Therapeutic Society of Thailand
18.00 – 20.30	Social dinner and honoring ceremony
14 May 2026	
08.30 – 09.00	Registration
9.00 – 9.45	Plenary session I (Thai) "Phytopharmaceutical product development against COVID outbreaks: A lesson learned from the COVID working group of Mahidol University" Associate Professor Phisit Khemawoot Chakri Naruebodindra Medical Institute, Faculty of Medicine Ramathibodi Hospital, Mahidol University *Moderated by Krit Rattanawonsakul, Ph.D.*
9.45 – 10.00	Technical Seminar III – Bara Scientific
10.00 – 10.30	Morning refreshment and poster session
10.30 – 11.15	Oral presentation from selected abstract *Moderated by Professor Pithi Chanvorachote, Ph.D.* *and Colonel Associate Professor Janeyuth Chaisakul, Ph.D.*
11.15 – 12.00	"Dengue Vaccines: An Update" Major General Professor Veerachai Watanaveerade Department of Pharmacology, Phramongkutklao College of Medicine *Moderated by Lieutenant Colonel Thishnapha Vudhironarit, Ph.D.*

Program Schedule

12.00 – 13.00	Lunch
13.00 – 13.45	Plenary session II (Thai) "Why Human Medications Can't Always Be Used in Animals?" Professor Amnart Poapolathep, Ph.D. Faculty of Veterinary Medicine, Kasetsart University *Moderated by Lieutenant Colonel Associate Professor Nattapon Jaisupa, Ph.D.*
13.45 – 14.30	Symposium III: Venom and Toxins in Pharmacology Education Colonel Associate Professor Janeyuth Chaisakul, Ph.D. Department of Pharmacology, Phramongkutklao College of Medicine *Moderated by Lieutenant Colonel Associate Professor Nattapon Jaisupa, Ph.D.*
14.30 – 15.15	Symposium IV: Novel pharmacological approaches "HDAC8 PROTACs as novel anticancer drugs" Jiranan Chotitumnavee, Ph.D. Department of Pharmacology, Faculty of Dentistry, Mahidol University *Moderated by Lieutenant Colonel Associate Professor Nattapon Jaisupa, Ph.D.*
15.15 – 15.30	Afternoon refreshment
15.30 – 16.00	Poster award announcement and Closing ceremony *Moderated by Lieutenant Colonel Associate Professor Janeyuth Chaisakul, Ph.D. and Assistant Professor Tipparat Parakaw, Ph.D.*
15 May 2026	
08.30 – 09.00	Registration
09.00 – 11.00	Simulation center at Phramongkutklao College of Medicine Lieutenant Colonel Thishnapha Vudhironarit, Ph.D.
OR	
09.00 – 11.00	Game-based learning for pharmacology teaching workshop Associate Professor Pornpun Vivithanaporn Chakri Naruebodindra Medical Institute, Faculty of Medicine Ramathibodi Hospital, Mahidol University Associate Professor Sirada Srihirun Department of Pharmacology, Faculty of Dentistry, Mahidol University
11.00 – 12.00	Phaya Thai Palace

Natural Products and Longevity Medicine: Exploring Novel Pathways for Healthy Aging

Professor Lijun Liu, MD., Ph.D.

College of Life and Health Sciences, Northeastern University, Shenyang, China

Abstract

Although modern medicine has significantly extended human lifespan, the bottleneck in absolute lifespan and the severe lag in healthspan constitute an urgent "longevity double gap." Facing aging as a highly complex systemic degenerative process,traditional single-target intervention strategies are often limited by compensatory physiological effects. Therefore, longevity medicine urgently requires a new-generation intervention paradigm with a holistic approach.

Breaking through the limitations of single-pathway interventions, this presentation proposes the "Cell Cycle Clock" as the ultimate integration hub for upstream aging stress signals and the arbiter of cell fate. We posit that the true biological age of an organ is fundamentally determined by the cell cycle homeostasis of its functional "On-duty cells." Based on this underlying mechanism, we innovatively introduce "The O3 Framework" for full life cycle cellular management. This paradigm encompasses Optimal Genesis (protecting the quiescent niche of stem cells), Optimal Vigor (maintaining the high-efficiency G1 phase of on-duty cells), and Optimal Clearance (precisely inducing targeted apoptosis in senescent cells).

Research has demonstrated that natural active products, with their advantages in multi-target network synergy, can gently and systematically remodel the complex cell cycle network, making them ideal candidates to actualize the O3 Framework. To this end, we have established a multidimensional natural product discovery platform integrating AI-driven 3D structural prediction, network pharmacology, and high-content phenotypic screening. Next, we will highlight the empirical anti-aging data of representative natural compounds identified through this pipeline. Finally, we will objectively address the core challenges in the clinical translation of longevity interventions—such as balancing cellular rejuvenation with tumorigenic risk, and overcoming bioavailability barriers—and provide future perspectives on the translational potential of natural products in longevity medicin

The Role of the Mucus Layer in Pharmacokinetics and Pharmacological Effects, and Its Molecular Basis

Associate Professor Hisanao Kishimoto, PhD

Department of Biopharmaceutics, School of Pharmacy, Tokyo University of Pharmacy and Life Sciences.

Abstract

Mucus layer that covers the various mucosal epithelial surfaces in the body and plays a dynamic barrier protecting against infections and foreign particles. At the same time, it forms an unstirred water layer in the vicinity of epithelial cells, and has long been considered as a primary barrier to the absorption of a wide range of drugs. However, many studies have focused only on the mucus layer as part of the mucosa or have relied on indirect observations, and the detailed molecular mechanisms underlying drug transport across the mucus layer remain unclear. In particular, the pharmaceutical and pharmacological roles of mucins—the main structural components of the mucus layer—are not yet fully understood. In this presentation, we will introduce our recent findings on the impact of the mucin layer on drug absorption, with particular emphasis on the physiological properties of mucus and the distinct expression patterns of membrane-bound and secreted mucins.

Lipid-lowering effects of fingerroot extract against hyperlipidemia induced fatty liver: from bench back to communities

Associate Professor Chutima S. Vaddhanaphuti, Ph.D.

Innovative Research Unit of Epithelial Transport and Regulation (iETR), Department of Physiology, Faculty of Medicine, Chiang Mai University, Chiang Mai, Thailand

Abstract

Boesenbergia rotunda (L.) Mansf, known as fingerroot or krachai, is widely grown in the Southeast Asia and commonly used as a spice. Previous studies have shown that fingroot extract (FR) exerted anti-oxidant, anti-inflammation, antidiabetic, antimicrobial, anticancer, and hepatoprotective activity in both the in vitro and in vivo models. With this knowledge asset, we further investigated the effects of FR on cholesterol homeostasis and its mechanisms of action against metabolic dysfunction-associated steatotic liver disease (MASLD). Results showed that after MASLD rats received either single treatment of FR and simvastatin alone or FR combined with a half-dose of simvastatin for 3 months, the plasma LDL-cholesterol, total cholesterol, and triglyceride levels were significantly decreased, corresponding with the hepatic lipid contents, insulin resistant, oxidative stress, and inflammation. The molecular mechanisms of FR have shown to involved with inhibiting intestinal cholesterol absorption. This study suggest that consuming FR product could be an alternative supplement for both healthy and hyperlipidemia to prevent the incidence of non-communicable diseases. Besides, it also provides opportunities for Thai manufacturers to add healthy and economic values and widen customer targets in the country and around world. Thailand's FR product could serve as an example and a model for an alternative medicine industry at national and international levels.

Acknowledgement:

This work was supported by the Chao Phya Abhaibhubejhr Hospital Foundation, Prachinburi, Thailand and Chiang Mai University, Chiang Mai, Thailand.

The effect of Ocimum sanctum extract on gut microbiome change after taking high-fat diet

Assistant Professor Pisut Pongchaikul, M.D., Ph.D.

Chakri Naruebodindra Medical Institute, Faculty of Medicine Ramathibodi Hospital, Mahidol University.

Abstract

High-fat diet (HFD)-induced gut dysbiosis is a key driver of metabolic syndrome, disrupting microbial metabolism, gut barrier integrity, and inflammatory balance. Our study highlights the microbiome-restorative potential of Ocimum sanctum L. (Holy basil) extract in an HFD-induced mouse model.

OSLY significantly reshaped the HFD-associated microbiome, enriching short-chain fatty acid–producing commensals while suppressing pathobionts. A substantial proportion of disrupted taxa were restored toward a normal diet–like profile, with the strongest effects observed at higher doses. At the community level, OSLY reduced microbiome divergence and rendered treated samples indistinguishable from healthy controls.

These findings position OSLY as a potent, microbiome-targeted, prebiotic-like phytotherapeutic with promising translational potential for metabolic syndrome management.

Keywords: Ocimum sanctum; gut microbiota; metabolic syndrome; high-fat diet; 16S rRNA; Rescue Index; dysbiosis

Updates and challenges in antimalarials in Thailand

Lieutenant General Professor Mathirut Mungthin

Phramongkutklao College of Medicine

Abstract

Thailand's progress toward malaria elimination is characterized by a significant epidemiological transition. While aggressive deployment of artemisinin-based combination therapies (ACTs) and the "1-3-7" surveillance protocol have reduced Plasmodium falciparum to historic lows, Plasmodium vivax has emerged as the dominant species, now constituting over 95% of indigenous cases. This shift necessitates a re-evaluation of radical cure strategies and resistance monitoring.

This presentation focuses on the Clinical Practice Guidelines for The Treatment of Malaria for Physicians, Thailand 2025, by the Committee on Malaria Drug Policy and treatment Guideline, The Ministry of Public Health, highlighting the adoption of tafenoquine as a single-dose radical cure for *P. vivax*. To mitigate the risk of drug-induced hemolysis inherent to 8-aminoquinolines, the guidelines mandate the integration of point-of-care (POC) quantitative G6PD testing. This diagnostic precision enables the safe administration of both tafenoquine and the conventional 14-day primaquine regimen, addressing the biological challenges of hypnozoite-mediated relapse.

Despite regional gains, the persistence of multidrug-resistant (MDR) *P. falciparum* along the Myanmar and Cambodia borders remains a global health priority. These border zones act as reservoirs for parasites exhibiting reduced susceptibility to both artemisinin derivatives and partner drugs. The transmission of MDR strains is further complicated by high population mobility and the prevalence of asymptomatic, sub-patent infections among forest-goers and migrant workers. Sustaining elimination requires proactive molecular surveillance to detect "early warning" genetic signatures. Continuous monitoring of the pfcrt, pfmdr1, pfk13, and pfpm2/3 loci is essential to inform evidence-based shifts in national first-line drug policies and to preempt the cross-border dissemination of resistant phenotypes.

Phytopharmaceutical product development against COVID outbreaks: A lesson learned from the COVID working group of Mahidol University

Associate Professor Phisit Khemawoot, Ph.D.

Chakri Naruebodindra Medical Institute, Faculty of Medicine Ramathibodi Hospital, Mahidol University.

Abstract

In 2020, the emergence of the SARS-CoV-2 virus triggered multiple waves of the COVID-19 pandemic. In response, the Faculty of Medicine Ramathibodi Hospital and the Faculty of Science at Mahidol University collaborated to identify potential antiviral treatments derived from Thai medicinal herbs. Through High-Throughput Screening (HTS) in laboratory settings, researchers discovered two potent active compounds capable of neutralizing SARS-CoV-2 at concentrations below 10uM, Andrographolide (from Green Chiretta) and Panduratin A (from Fingerroot).

In animal studies using hamster models showed that both extracts significantly reduced inflammation in SARS-CoV-2 infected hamsters. Notably, the Green Chiretta extract demonstrated a 100% survival rate in animal models infected with the highly virulent Delta variant. Despite its potency, Andrographolide suffers from low water solubility and poor absorption in the digestive tract. Therefore, the research team developed an enhanced formulation using widely available pharmaceutical solubilizers. Tests in beagle models confirmed that this new formulation significantly improved the absorption of Andrographolide.

As the pandemic subsided following the Omicron wave, the team began repurposing these potent herbal extracts to target Neglected Tropical Diseases (NTDs) and Non-Communicable Diseases (NCDs). The research process, along with the challenges faced during the pandemic, will be presented to share insights on herbal drug discovery and development. These "lessons learned" aim to provide a valuable roadmap for participants to better prepare for and respond to potential future pandemic

Why Human Medications Cannot Always Be Used in Animals?

Professor Amnart Poapolathep, D.V.M., Ph.D.

Department of Pharmacology, Faculty of Veterinary Medicine, Kasetsart University

Abstract

Currently, veterinary pharmacotherapy encompasses both pharmaceuticals specifically developed and approved for animal use and selected human medicines that are utilized off-label in veterinary practice. The incorporation of human medicines is driven by several scientific and practical considerations. Notably, the availability of species-specific veterinary drugs remains limited for many conditions, particularly in minor species, exotic animals, and rare disease presentations. In addition, the substantial cost and time associated with the development, registration, and approval of veterinary-specific pharmaceuticals constrain the number of products available on the market, thereby necessitating the use of alternative therapeutic options. Despite these considerations, the extrapolation of human medicines to animals remains a significant concern in veterinary medicine, especially in companion animal practice, where individualized treatment is common. Drugs that are safe and effective in humans cannot be assumed to exhibit comparable safety or efficacy across animal species. This limitation reflects fundamental interspecies differences in physiology, biochemistry, and genetic determinants that influence drug disposition and response. Such differences affect pharmacokinetic processes—including absorption, distribution, metabolism, and excretion—as well as pharmacodynamic interactions at the molecular and cellular levels. Species-specific metabolic capacity represents a critical determinant of drug safety. For example, cats exhibit limited activity in certain drug conjugation pathways, resulting in reduced metabolic clearance and increased susceptibility to toxicity from compounds such as acetaminophen. Furthermore, allometric differences in body size and metabolic rate complicate dose extrapolation, increasing the risk of subtherapeutic exposure or overdose. The presence of excipients in human formulations, such as xylitol, which may be highly toxic to animals, further underscores the complexity of cross-species drug use. The widespread availability of over-the-counter (OTC) medications further exacerbates this issue, as unsupervised use by pet owners can lead to dosing errors, adverse reactions, and delayed diagnosis. These considerations highlight the necessity for a thorough understanding of species-specific pharmacology. The use of human medicines in animals should therefore be undertaken only under the guidance of veterinary professionals to ensure both safety and therapeutic efficacy.

Keywords: Human medications, Veterinary medicine, Pharmacokinetics, Pharmacodynamics, Drug toxicity, Interspecies different

Venoms and Toxins in Pharmacology

Janeyuth Chaisakul, MSc, PhD.

Department of Pharmacology, Phramongkutklao College of Medicine, Bangkok, Thailand

Background:

Snakebite envenoming is responsible for mortality and morbidity worldwide, especially in Thailand. As a One Health challenge, this issue intersects human, animal, and environmental health, necessitating a multifaceted approach for comprehensive management. Snake venoms are a mixture of enzymes and highly specific toxins which may induce effect independently or synergistically, targeted against vital physiological processes. However, a lack of clinical experience may limit the learning ability to make the connection between basic toxicology of snake venom and clinical knowledges in preclinical students. In fact, clinical correlations using case-based learning in medical education are an effective tool that assist students to correlate basic science concepts with medical applications. Using the common case study would simplify the complexity of medical lesson. In this study, we evaluated the learning outcome of case-based learning using a snakebite envenomed case with neurotoxicity in 2nd year premedical class.

Summary of Work:

Inhibitory effect of snake venom neurotoxin was applied as a part of neurotransmitter regulation and function lecture. A case of Malayan krait envenomed patient with neurotoxicity was introduced to 103 second-year medical students in order to demonstrate the abnormal mechanism of cholinergic neurotransmission in real-world scenario. Five questions (1 recall, 2 application and 2 understanding items) related to the snakebite envenomed case were used to measure learning outcomes. A satisfaction evaluation of teaching technique was also determined.

Summary of Results: Obtained data from final examination showed that more than 40% of enrolled students reached ≥ 80% of the final score. Satisfaction evaluation of teaching technique was 4.47±0.79 from the total of 5. Some students also continued performing laboratory research in snakebite envenoming in their 4th year medical class.

Discussion and Conclusion: Case-based learning using snakebite envenomed case (*i.e.* snakebite-induced neurotoxicity) appeared to be an effective tool for enhancing clinical knowledge in premedical students. Other clinical outcomes such as hematotoxicity or nephrotoxicity can be applied as a case study.

Take-home Message(s): Clinical scenario related to snakebite envenoming can be used in pre-clinical classes, not only in lecture but also applying in other designs such as group discussion and practical laboratory classes to enhance student experience.

Key words: Premedical students: Neurotoxicity: snakebite: Case based learning: venoms: toxins

Novel Pharmacological Approaches "HDAC8 PROTACs as novel anticancer drugs"

Jiranan Chotitumnavee, Ph.D.

Department of Pharmacology, Faculty of Dentistry, Mahidol University

Abstract

Conventional chemotherapy remains a fundamental approach in cancer therapy; however, its limited selectivity often leads to significant toxicity and suboptimal clinical outcomes. Although targeted therapies, such as small-molecule inhibitors, have improved selectivity, they remain limited by incomplete target inhibition. To address these challenges, targeted protein degradation has emerged as a promising therapeutic strategy. Proteolysis-targeting chimeras (PROTACs) induce degradation of target proteins via the ubiquitin-proteasome system, providing an alternative to conventional inhibition strategies.

Histone deacetylase 8 (HDAC8), a class I HDAC, is overexpressed in several malignancies and has been implicated in tumor progression. Although HDAC8 inhibitors have been developed, their anticancer activity has been largely restricted to hematological cancer models in vitro, with limited success in solid tumors. Notably, genetic depletion of HDAC8 by siRNA has been shown to induce cytotoxic effects in solid tumor models, highlighting its potential as a therapeutic target; however, RNA-based knockdown approaches remain clinically challenging.

To address these limitations, we developed the first HDAC8-targeting PROTAC in 2022, providing a small-molecule approach for the selective degradation of HDAC8. Our recent studies demonstrate that this PROTAC selectively degrades HDAC8 via the ubiquitin-proteasome pathway and exhibits potent anticancer activity compared to a conventional HDAC8 inhibitor in both hematological cancer and solid tumor models, while sparing normal cell viability. Mechanistic studies further reveal that this HDAC8-targeting PROTAC induces S-phase cell cycle arrest and ER stress-mediated apoptosis via activation of the IRE1α/XBP1s-JNK-CHOP pathway in a glioblastoma model.

Collectively, current evidence suggests that the HDAC8-targeting PROTAC represents a promising therapeutic strategy for cancer, with the potential to improve selectivity and efficacy compared to both selective and pan-HDAC inhibitor

High Prevalence of Actionable Pharmacogenetic Variants in Thai Psychiatric Patients: Comprehensive Profiling of 15 Clinically Relevant Genes

Wanchai Rupchaiyaphum[1,4], Naphat Sirinimnualkul[2], Chavit Tunvirachaisakul[2], Thanakit Pongpitakmetha[3], Pajaree Chariyavilaskul[3,4,*]

[1] PhD Program in Medical Sciences (Molecular Pharmacology and Advanced Therapeutics), Faculty of Medicine, Chulalongkorn University, Pathum Wan, Bangkok 10330, Thailand
[2] Department of Psychiatry, Faculty of Medicine, Chulalongkorn University, Pathum Wan, Bangkok 10330, Thailand
[3] Department of Pharmacology, Faculty of Medicine, Chulalongkorn University, Pathum Wan, Bangkok 10330, Thailand
[4] Center of Excellence in Clinical Pharmacokinetics and Pharmacogenomics, Department of Pharmacology, Faculty of Medicine, Chulalongkorn University, Pathum Wan, Bangkok 10330, Thailand

Abstract

Inter-individual variability in response to psychotropic medications remains a major challenge in psychiatric practice, frequently leading to treatment failure and adverse drug reactions. Pharmacogenetics (PGx) provides a precision framework for individualized therapy; however, comprehensive PGx data in Thai psychiatric populations remain limited. This study aimed to characterize allele, genotype, and predicted phenotype distributions of clinically actionable pharmacogenes in Thai psychiatric patients. Peripheral blood samples from 161 psychiatric outpatients at King Chulalongkorn Memorial Hospital were analyzed using a MassARRAY genotyping platform. Variants in 15 clinically actionable pharmacogenes (*CYP2B6, CYP2C9, CYP2C19, CYP2D6, CYP3A4, CYP3A5, CYP4F2, DPYD, HLA-A, HLA-B, NUDT15, SLCO1B1, TPMT, UGT1A1*, and *VKORC1*) were assessed, with predicted phenotypes assigned according to CPIC and DPWG guidelines. Participants were primarily diagnosed with major depressive disorder (29.8%), schizophrenia (26.7%), and bipolar disorder (24.2%), and were treated with diverse psychotropic regimens. Among the 15 genes analyzed, clinically actionable findings were most prominent in *CYP2C19, CYP2D6, HLA-A/B*, and *CYP3A5*. For *CYP2C19*, only 34.78% of patients were normal metabolizers, while 54.66% were intermediate or poor metabolizers, representing a substantial proportion likely to require dose adjustment or alternative therapy. *CYP2D6* intermediate metabolizers accounted for 45.96%, driven by the high prevalence of reduced-function alleles common in Asian populations (e.g.**36+*10* tandem arrangement and **10* alleles). Clinically significant HLA risk alleles associated with severe cutaneous adverse reactions were observed, including *HLA-B*15:02* (11.8%) and *HLA-A*31:01* (4.35%). Additionally, 42.86% of patients were *CYP3A5* non-expressors, whereas *CYP3A4* exhibited no detectable functional variability. These findings demonstrate a high burden of actionable pharmacogenetic variation in Thai psychiatric patients, particularly in genes influencing antidepressant and antipsychotic metabolism and mood stabilizer safety. The observed genotype-phenotype distributions highlight the

potential of PGx-guided prescribing to inform individualized treatment strategies in psychiatric care. However, interpretation should consider key limitations, including the single-center design, relatively small sample size, absence of treatment outcome data, and potential contributions of additional pharmacodynamic or polygenic factors.

Keywords: Pharmacogenetics, Psychiatry, *CYP2D6*, *CYP2C19*, *HLA*, Precision medicine

c-Myc Inhibitor 10058-F4 Suppresses Cell Proliferation and Enhances Gemcitabine Sensitivity in Human Cholangiocarcinoma Cells

Chatsiri Jesadakultavee[1], Auemduan Prawan[1], Sarinya Kongpetch[1], Piman Pocasap[1], Laddawan Sengunprai[1,*]

[1]Department of Pharmacology, Faculty of Medicine, Khon Kaen University, Khon Kaen, 40002, Thailand

Abstract

Cholangiocarcinoma (CCA) is a highly prevalent malignancy in Thailand, particularly in the Northeastern region, primarily linked to chronic *Opisthorchis viverrini* infection. This distinct etiology contributes to late-stage diagnosis, low survival rates, and chemoresistance. The oncogene c-Myc has emerged as a critical therapeutic target, as it is frequently overexpressed in various cancers, including CCA, where it drives rapid tumor progression. This study aimed to investigate the anti-tumor potential of 10058-F4, a direct c-Myc inhibitor, in the CCA cell line KKU-213A, an *O. viverrini*-associated intrahepatic CCA cell line confirmed to overexpress c-Myc protein by Western blot analysis, making it a relevant model for this investigation. The results showed that 10058-F4 effectively inhibited KKU-213A cell viability with an IC_{50} of 68.30 ± 6.69 μM at 24 h. Western blot analysis revealed that 10058-F4 significantly reduced c-Myc protein expression in CCA cells. The colony-forming ability of the cells was also suppressed by the c-Myc inhibitor treatment in a dose-dependent manner. Consistent with its growth-inhibitory effect, the c-Myc inhibitor induced cell cycle arrest at the G2/M phase. In addition to the evident G2/M arrest, 10058-F4 induced apoptosis in KKU-213A cells, as evidenced by a distinct sub-G1 apoptotic peak. Moreover, the combination of 10058-F4 (25 μM) with gemcitabine (250, 1,000, and 5,000 μM) assessed by MTT assay following 48 h treatment yielded a Combination Index (CI) of 0.00134, indicating a strong synergistic effect in suppressing KKU-213A cell viability. Collectively, suppression of c-Myc in CCA cells with 10058-F4 inhibits their growth and synergistically enhances their sensitivity to gemcitabine. Inhibition of c-Myc may be a promising approach for the CCA treatment.

Keywords: Cholangiocarcinoma, c-Myc, 10058-F4, Synergistic effect, Cell cycle arrest.

HLA Risk Alleles Associated with Antituberculosis Drug-Induced Severe Cutaneous Adverse Reactions in a Thai Population

Weenutsara Prasawang[1], Warayuwadee Amornpinyo[2], Parinya Konyoung[3], Suteeraporn Chaowattanapanit[4], Wichittra Tassaneeyakul[1], Sirimas Kanjanawart[1], Nontaya Nakkam[1*]

[1]Department of Pharmacology, Faculty of Medicine, Khon Kaen University, Khon Kaen 40002,Thailand
[2]Division of Dermatology, Department of Internal Medicine, Khon Kaen Hospital, Khon Kaen 40000, Thailand
[3]Pharmacy Unit, Udon Thani Hospital, Udon Thani 41000,Thailand
[4]Division of Dermatology, Department of Medicine, Faculty of Medicine, Khon KaenUniversity, Khon Kaen 40002, Thailand

Abstract

Antituberculosis drugs, including isoniazid, rifampicin, pyrazinamide, and ethambutol, are essential first-line therapies for tuberculosis. However, their use can be complicated by severe cutaneous adverse reactions (SCARs), such as Stevens-Johnson syndrome (SJS), drug reaction with eosinophilia and systemic symptoms (DRESS), and acute generalized exanthematous pustulosis (AGEP), which are associated with substantial morbidity and mortality. Although genetic polymorphisms in human leukocyte antigen (*HLA*) genes have been implicated in the immunopathogenesis of drug-induced SCARs, data specific to antituberculosis drug-induced SCARs remains limited. This study aimed to investigate the associations between *HLA* alleles and antituberculosis drug-induced SCARs in a Thai population. Nineteen patients with antituberculosis drug-induced SCARs, consisting of 10 SJS/TEN, 8 DRESS, and 1 AGEP patients, were enrolled in the study. Controls included 183 unrelated healthy native Thais who had no history of drug allergy. *HLA* class I (*HLA-A, HLAB*, and *HLA-C*) and class II (*HLA-DRB1*) alleles were genotyped using the polymerase chain reaction-sequence-specific oligonucleotide probes (PCR-SSOP) method. Associations were evaluated using odds ratios (ORs) with 95% confidence intervals (CIs). The results demonstrated that *HLA-B**39:09 showed the strongest and statistically significant association with increased risk of antituberculosis drug–induced SCARs (OR = 24.13, 95% CI = 4.08-142.71, P = 0.0008, Pc = 0.0373). Additional risk associations were observed for *HLA-A**29:01 (OR = 21.41, 95% CI = 1.85-248.47, P = 0.0238), *HLA-DRB1**12:01 (OR = 19.37, 95% CI =1.68-223.66, P = 0.0280), and *HLA-A**24:10 (OR = 5.53, 95% CI = 1.26-24.23, P = 0.0414). In contrast, *HLA-A**02:07 appeared to confer a protective effect (OR = 0.12, 95% CI = 0.02-0.90, P = 0.0150). These findings provide preliminary evidence that specific *HLA* alleles, particularly *HLA-B**39:09, may serve as potential genetic markers of susceptibility to SCARs associated with antituberculosis drug regimens in the Thai population. Validation in larger, multicenter, and ethnically diverse cohorts is essential to confirm these associations and establish their clinical utility.

Keywords: Antituberculosis drugs, Severe cutaneous adverse reactions, Human Leukocyte Antigen, Pharmacogenetic

Cytotoxicity effect of DNA-PK and PARP inhibitors in cholangiocarcinoma cell lines

Buntita Nadtee[1], Sarinya Kongpetch[1], Auemduan Prawan[1], Laddawan Senggunprai[1], Piman Pocasap[1,*]

[1]Departments of Pharmacology, Faculty of Medicine, Khon Kaen University, Khon Kaen 40002, Thailand

Abstract

Cholangiocarcinoma (CCA) is a highly aggressive malignancy arising from the biliary epithelium and is associated with a poor prognosis. Due to the absence of specific early symptoms, most patients are diagnosed at advanced stages when curative surgery is no longer feasible. Cisplatin-based chemotherapy remains the standard treatment for advanced CCA; however, its clinical benefit is often limited by the development of drug resistance. One major mechanism of resistance involves the activation of DNA damage response and repair pathways, enabling cancer cells to repair cisplatin-induced DNA lesions and survive. In particular, homologous recombination (HR) and non-homologous end joining (NHEJ) are key pathways responsible for repairing DNA double-strand breaks. Therefore, targeting these repair mechanisms represents a promising strategy to overcome resistance and improve therapeutic outcomes. In this study, we investigated the cytotoxic effects of (1) a PARP inhibitor (niraparib), which impairs HR, and (2) a DNA-PK inhibitor (nedisertib), which suppresses NHEJ, in CCA cell lines. Cytotoxicity was evaluated in KKU-452 and KKU-610 cells after 72 hours of treatment using the MTT assay. KKU-452 cells, which are BRCA1-proficient but harbor an ARID1A mutation, exhibited a shorter doubling time of 17.9 hours, whereas KKU32 610 cells, which are BRCA1-deficient, had a longer doubling time of 27 hours. Niraparib exhibited IC_{50} values of 37.47 μM in KKU-452 and 19.02 μM in KKU-610 cells, while nedisertib showed IC_{50} values of 6.02 μM and 32.49 μM, respectively. In addition, the IC_{50} values of cisplatin were 3.9 μM and 8.6 μM in KKU-452 and KKU-610 cells, respectively. Our results indicate that KKU-610 cells were more sensitive to niraparib (approximately two37 fold), despite being more resistant to cisplatin, suggesting reliance on alternative DNA repair pathways. In contrast, KKU-452 cells were more sensitive to nedisertib (approximately five39 fold). These differences may be associated with variations in genetic background. KKU-452 harbors an ARID1A mutation, which may affect DNA repair regulation, whereas KKU-610 carries a BRCA1 mutation that may increase sensitivity to PARP inhibition. Overall, these findings suggest that the efficacy of DNA repair inhibitors in CCA is cell type–dependent.

Keywords: Cholangiocarcinoma, Niraparib, Nedisertib, Cytotoxicity

A Non-Canonical Role for Cyclin D1/D2-CDK4: Directing Cytoskeletal Reorganization and Migration via the TGFβ-FAK-Rac1 Axis

Ruifang Guo[1], Yihang Wang[1], Lijun Liu[1,*]

[1]College of Life and Health Sciences, Northeastern University, Shenyang, Liaoning 110169, China

Abstract

Previous reports have linked cyclin D-CDK4/6 to cell motility, but a direct connection to cytoskeletal remodeling has been lacking. Here, we address this gap by combining pharmacological inhibition (Palbociclib, 1 μM, 48 h) with quantitative proteomics in HeLa cells. CDK4/6 inhibition significantly reduced lamellipodia formation, impaired focal adhesion assembly, suppressed migration and invasion. Importantly, we identify a distinct function of CDK4 that has not been described in prior mechanistic studies: CDK4-cyclin D1/D2 complexes localize to membrane ruffles, where they directly engage the cytoskeleton. By integrating proteomic and phosphoproteomic approaches, we revealed its molecular mechanism: CDK4 kinase activity maintains transforming growth factor β (TGFβ) pathway signaling through phosphorylation of Smad3 at Thr8. This phosphorylation event is critical for the expression of specific integrin subunits (α5, α6, and β1). Inhibition of CDK4 leads to diminished activation of focal adhesion kinase (FAK) and Rac1 due to the loss of these integrin subunits. Our rescue experiments further solidified this causal relationship by demonstrating that forced activation of FAK or Rac1 signaling could largely rescues both lamellipodia formation and cell migration (to 80% of control). These findings establish a previously unknown direct mechanism for CDK4 in cytoskeletal control, distinct from the well-characterized cell-cycle function. Thus, therapeutic CDK4/6 inhibitors may suppress invasion by targeting this novel cytoskeletal pathway.

Keywords: Cell migration, cyclin D, cyclin-dependent kinase 4, cytoskeletal reorganization, lamellipodia formation

Montelukast and Zafirlukast Suppress Melanoma Cell Survival and Invasiveness via Induction of Apoptosis, Autophagy, DNA damage, and ER Stress Pathways

Ratchanon Sukprasert [1,2], Titiwadee Titiwattanakarn[1], Rapeewan Setthacomkul [1], Tanapan Siangcham [2], Pornpun Vivithanaporn [1,*]

[1]Chakri Naruebodindra Medical Institute (CNMI), Faculty of Medicine Ramathibodi Hospital, Mahidol University, Bang Phli, Samut Prakarn 10540, Thailand
[2]Medical Sciences Department, Faculty of Allied Health Sciences, Burapha University, Chon Buri 20131, Thailand

Abstract

Melanoma is the most aggressive and deadly form of skin cancer, characterized by its high metastatic potential and resistance to conventional chemotherapy. In two large epidemiologic studies, asthmatic patients who used cysteinyl leukotriene receptor antagonists (LTRAs) showed a decreased risk of various cancers. Our previous studies reported that LTRAs induced cell death and inhibited proliferation of triple negative breast cancer and glioblastoma cells. The present study aimed to compare the effects of montelukast and zafirlukast on the molecular mechanisms regulating cell death in melanoma cells. The toxicity of montelukast and zafirlukast on the cell viability of melanocyte SK-MEL-5, adult human dermal fibroblast (HDF-Ad), and keratinocyte HaCaT cells was measured by MTT assays. Apoptosis and cell proliferation were determined via flow cytometry using Annexin V FITC/7-AAD and CFSE staining, respectively. The expression of mRNA and proteins related to apoptosis, autophagy, DNA damage, ER stress, migration and invasion was measured using real-time PCR and western blot analysis. The percentage of wound closure was measured using an Incucyte® Live Cell Imager. The IC50 of montelukast and zafirlukast in SK-MEL-5 cells at 24 h were 10.98±0.85 and 18.21±0.82 μM, respectively. In HDF-Ad and HaCaT, the IC50 was higher than SK-MEL-5 in both LTRA drugs. Montelukast and zafirlukast increased apoptotic cells in SK-MEL-5 and HDF-Ad cells, but only montelukast triggered apoptosis in HaCaT cells. In contrast to their effects on other cancer cells, LTRAs did not inhibit proliferation of SK-MEL-5 cells. Both LTRAs increased PARP cleavage and levels of cleaved caspase-3 in SK-MEL-5 cells. Autophagosome formation was indicated by the increase of LC-3-II levels after exposure to both LTRAs. Montelukast and zafirlukast inhibited expression of MITF, the marker of melanoma with a role in proliferation and apoptosis. The percentage of wound closure was decreased after treatment with LTRAs. LTRAs increased ER-stress-related proteins, including CHOP and XBP-1s expression. Montelukast and zafirlukast decreased invasion and migration-related genes by reducing expression of cathepsin B, MMP-2, MMP-3, and MMP-9. In conclusion, LTRAs effectively induced SK-MEL-5 cell death via multiple pathways, including apoptosis, autophagy, DNA damage, and ER stress, while also downregulating markers associated with invasion and migration.

Keywords: LTRAs, melanoma, apoptosis, migration, invasion

Anti-Inflammatory Effects of Cucurbitacin B, Cucurbitacin E, and Coccinia grandis Fruit Extract on M1 Macrophage Polarization: An In Vitro and In Silico Study

Kingkarn Rachadet[1], Sarinya Kongpetch[1] , Kampeebhorn Boonloh[1] , Rattanathorn Choonong[1] *

[1]Department of Pharmacology, Faculty of Medicine, Khon Kaen University, Khon Kaen 40002, Thailand

Abstract

Coccinia grandis, a tropical vine of the Cucurbitaceae family, is traditionally used for its anti inflammatory properties. The bitterness of its raw fruit is attributed to cucurbitacins, triterpenoid compounds with potent biological activity. This study aimed to investigate the effects of ethanolic raw C. grandis fruit extract and its major constituents, cucurbitacin B (CuB) and cucurbitacin E (CuE) on M1 macrophage polarization using integrated in vitro and in silico approaches. Human THP-1 monocytes were differentiated into macrophages with phorbol-12-myristate-13-acetate and stimulated with lipopolysaccharide to induce M1 polarization. Cytotoxicity was assessed using the MTT assay, and flow cytometry was employed to measure the expression of specific surface markers CD80/86 (M1 marker) and CD206 (M2 marker). Non-cytotoxic concentrations were identified at 125 μM for CuB and CuE and 125–250 μg/mL for the extract, maintaining cell viability above 80%. At these concentrations, treatments show attenuation of M1 polarization, while no significant induction of CD206 expression was observed. Molecular docking analysis further indicated favorable interactions of CuB and CuE with key inflammatory-related proteins, including signal transducer and activator of transcription 3, mitogen-activated protein kinase 1, vascular endothelial growth factor receptor 2 and insulin-like growth factor receptor. These findings suggest that raw *C. grandis* fruit extract and its cucurbitacins possess antiinflammatory potential through modulation of macrophage polarization and provide preliminary insight into their possible mechanisms of action.

Keywords: Coccinia grandis, Cucurbitacins, Anti-inflammatory, M1 macrophage polarization, Molecular docking

Astilbin Disrupts the Oxidative Stress–Inflammation–Lipogenesis Axis: An Integrative FTIR and Correlation Network Analysis in MAFLD Models

Saharat Kattiyanon[1], Piman Pocasap[1], Sarinya Kongpetch[1], Auemduan Prawan[1], Laddawan Senggunprai[1], Karnchanok kaimuangpak[1], Kampeebhorn Boonloh[1,2*]

[1] Department of Pharmacology, Faculty of Medicine, Khon Kaen University, Khon Kaen 40002, Thailand
[2]Cardiovascular Research Group, Khon Kaen University, Khon Kaen 40002, Thailand

Abstract

Metabolic dysfunction–associated fatty liver disease (MAFLD) is characterized by excessive hepatic lipid accumulation accompanied by oxidative stress and chronic inflammation. Palmitic acid (PA), a major saturated fatty acid, promotes lipotoxic injury by activating inflammatory signaling and dysregulating lipid metabolism. Astilbin (ASB), a bioactive flavonoid glycoside, exhibits antioxidant and anti-inflammatory properties; however, its coordinated metabolic effects in MAFLD remain unclear. This study investigated whether ASB disrupts the oxidative stress–inflammation–lipogenesis axis using integrative biochemical and FTIR-based metabolic analyses. PA-induced lipotoxicity was established in HepG2 hepatocytes, while inflammatory activation was induced in RAW 264.7 macrophages using LPS or PMA. Cytotoxicity was assessed by MTT assay. Lipid accumulation was quantified by Oil Red O staining and Fourier-transform infrared spectroscopy (FTIR) coupled with principal component analysis (PCA). Superoxide ($O_2^{\bullet-}$) and nitric oxide (NO) production were measured spectrophotometrically. Expression of metabolic and inflammatory regulators was analyzed by qRT-PCR and Western blotting. Data were analyzed using one-way ANOVA ($p < 0.05$). Pearson correlation–based network analysis integrated oxidative, inflammatory, and lipid metabolic parameters. ASB exhibited IC_{50} values of 547.9 μM in RAW 264.7 cells and 755 μM in HepG2 cells, respectively. In activated macrophages, ASB significantly reduced $O_2^{\bullet-}$and NO production and suppressed Il-6, Tnf-α, and Ccl2 expression. In PA-treated HepG2 cells, ASB decreased intracellular lipid accumulation by 35% (metformin: 48%). FTIR spectral profiling revealed reduced lipid-associated vibrational bands (2917, 2850, and 1736 cm^{-1}), indicating diminished neutral lipid deposition. PCA clearly separated control, PA, and PA+ASB groups (PC-1: 97% variance), confirming ASB-driven metabolic remodeling. Mechanistically, ASB enhanced AMPK phosphorylation while suppressing SREBP1 and FASN and restoring CPT1A expression, indicating reduced lipogenesis and enhanced fatty acid oxidation. Correlation network analysis demonstrated strong positive associations among oxidative stress, inflammatory mediators, and lipid accumulation ($r \geq 0.86–0.97$), whereas pAMPK showed consistent inverse correlations with lipogenic and inflammatory markers. Astilbin disrupts the oxidative stress–inflammation–lipogenesis axis through AMPKdependent metabolic reprogramming. Integrated FTIR metabolic fingerprinting and correlation network analysis supports its potential as a phytotherapeutic candidate for MAFLD.

Keywords: Astilbin, MAFLD, Lipotoxicity, AMPK, FTIR metabolic fingerprinting, Inflammation

Adaptive Plasticity and Steady-State Dynamics of Cholangiocarcinoma Stem Cells under Therapeutic Stress

Krittiyabhorn Kongtanawanich[1], Supawan Jamnongsong[1,2], Sunisa Prasopporn[1,2], Pornlada Likasitwatanakul[3], Seiji Okada[4], Marianne Hokland[5], Methichit Wattanapanitch[6], Siwanon Jirawatnotai[1,2,4,7,*]

[1]Department of Pharmacology, Faculty of Medicine Siriraj Hospital, Mahidol University, Bangkok, Thailand.
[2]Siriraj Center of Research Excellence for Precision Medicine and Systems Pharmacology, Faculty of Medicine Siriraj Hospital, Mahidol University, Bangkok, Thailand.
[3]Department of Medicine, Faculty of Medicine Siriraj Hospital, Mahidol University, Bangkok, Thailand.
[4]Division of Hematopoiesis, Joint Research Center for Human Retrovirus Infection, Kumamoto University, Kumamoto, Japan. [5]Department of Biomedicine, Aarhus University, Aarhus, Denmark.
[6]Siriraj Center for Regenerative Medicine, Research Department, Faculty of Medicine Siriraj Hospital, Mahidol University, Bangkok, Thailand.
[7]Faculty of Pharmacy, Silpakorn University, Nakhon Pathom, Thailand.

Abstract

Cholangiocarcinoma (CCA) presents a major clinical challenge due to its aggressive progression and profound therapeutic resistance, traits largely driven by a dynamic subpopulation of Cancer Stem Cells (CSCs). To investigate the underlying plasticity of CCA without relying on static biomarkers, this study utilized a SORE6-dsCopGFP live-reporter system. This functional approach allowed for real-time tracking of the core pluripotency factors SOX2 and OCT4 across 2D monolayers, 3D multi-spheroid cultures, and 3D multicellular spheroids, successfully identifying a highly tumorigenic SORE6^{POS} subpopulation. Our findings demonstrate that CCA cells exist in a continuous bidirectional flux. While SORE6^{POS} cells naturally differentiate, SORE6^{NEG} non-CSCs exhibit a remarkable capacity for dedifferentiation. We quantified these phenotypic transitions using 3D Surface Integrative Spheroid Profiling (3D-SiSP), enabling high-content analysis within multi-spheroid models. The biological impact of this plasticity was further validated *in vivo*. Mouse xenografts initiated from either pure SORE6^{POS} or SORE6^{NEG} populations ultimately reached a phenotypic equilibrium, displaying comparable SOX2 and OCT4 expression at the endpoint. This indicates that CCA tumors inherently adjust their CSC density to a steady-state level via spontaneous cellular reversion. Furthermore, we highlight the 3D multicellular spheroid model as an optimal platform for therapeutic screening, as its complex architecture closely mimics the protective microenvironment required to support this adaptive plasticity. Under the stress of conventional treatments, such as gemcitabine and 5-fluorouracil, we observed a critical "phenotypic switch". These chemotherapies paradoxically accelerated the dedifferentiation of surviving non-CSCs into resistant SORE6^{POS} cells, fostering a more aggressive tumor profile that evades traditional cytotoxic strategies. Conversely, targeted intervention using CDK4/6 inhibitors

(palbociclib or abemaciclib) successfully arrested this plastic cycle. By suppressing dedifferentiation and enforcing terminal differentiation, CDK4/6 inhibition effectively depleted the reservoir of chemoresistant cells. Ultimately, this work establishes that targeting the molecular drivers of phenotypic reversion provides a highly promising strategy to overcome the drug-induced plasticity defining CCA.

Keywords: Cholangiocarcinoma, Cancer Stem Cell Plasticity, Phenotypic Dedifferentiation, 3D-SiSP, CDK4/6 Inhibitors

The anti-migration and anti-invasion effects of selective HDAC8 PROTAC on U-87 MG and T98G glioblastoma brain cancer cell lines

Rapeewan Settacomkul[1], Jiranan Chotitumnavee[2], Kant Sangpairoj[3], Yukihiro Itoh[4], Takayoshi Suzuki[4], Pornpun Vivithanaporn[1,*]

[1]Chakri Naruebodindra Medical Institute (CNMI), Faculty of Medicine Ramathibodi Hospital, Mahidol University, Samut Prakarn 10540, Thailand
[2]Department of Pharmacology, Faculty of Dentistry, Mahidol University, Bangkok 10400, Thailand
[3]Department of Preclinical Science, Faculty of Medicine, Thammasat University, Pathum Thani 12120, Thailand
[4]SANKEN, Osaka University, Mihogaoka, Ibaraki-shi, Osaka 567-0047, Japan

Abstract

Glioblastoma multiforme (GBM) is the most aggressive brain tumor, characterized by extensive migratory and invasive capacities that cause therapeutic resistance and poor prognosis. Our previous report showed the cytotoxic effect of selective HDAC8 Proteolysis Targeting Chimera (H8P) against U-87 MG and T98G human glioblastoma cells with the half-maximal inhibitory concentration (IC_{50}) at 6.12 ± 1.52 μM and 22.68 ± 10.36 μM, respectively. The IC_{50} of the conventional HDAC8 inhibitor (H8i) was 47.41±3.37 μM in U-87 MG cells. Moreover, H8P demonstrated anti-cancer effects by inhibiting cell proliferation, inducing apoptosis, and triggering endoplasmic reticulum stress in U-87 MG cells. However, its anti-migratory and anti-invasive effects have not been investigated. To investigate anti-migratory effects, wound healing assays were performed in U-87 MG and T98G cells using the IncuCyte WoundMaker Tool, and images were captured at 6-hour intervals over 72 hours using the IncuCyte Live-Cell Analysis System. In U-87 MG cells treated with 5 μM H8P, the relative wound width remained at 72% at 30 hours and increased to 128% at 72 hours compared with time 0. In contrast, H8i at 50 μM showed a wound width of 50% at 30 hours and complete wound closure was observed by 60 hours. In T98G cells treated with 20 μM H8P, the wound width was 68% at 30 hours and further decreased to 39% at 72 hours relative to baseline, indicating partial wound closure. These results suggest that U-87 MG cells are more sensitive to the anti-migratory effects of H8P compared with T98G cells. The anti-invasive effect of H8P in U-87 MG cells was evaluated using a Matrigel-coated transwell invasion assay. Pre-treatment with H8P at 5 μM for 72 hours significantly reduced the number of cells invading through the Matrigel matrix by 80 % after 24 hours compared with the control group. Taken together, these findings indicate that H8P suppresses migration in both glioblastoma cell lines and effectively reduces invasion in U-87 MG cells, supporting its potential as a therapeutic candidate for attenuating GBM progression.

Keywords: HDAC8 PROTAC, glioblastoma, brain cancer, anti-migration, anti-invasion

Study of free radical generation in liver microsomes from iron overload mice using Electron Spin Resonance (ESR) spectroscopy

Supawadee Kittichaisombat[1], Noppawan Phumala Morales[2,*]

[1]Biomedical Science Program, Faculty of Sciences, Mahidol University, Bangkok 10400, Thailand
[2]Department of Pharmacology, Faculty of Sciences, Mahidol University, Bangkok 10400, Thailand

Abstract

Liver microsomes are vesicles derived from the endoplasmic reticulum that contain drug-metabolizing enzymes, including cytochrome P450 (CYP450) enzymes. The CYP2E1 enzyme plays a significant role in ethanol oxidation, and during hepatic metabolism, this enzyme actively generates reactive oxygen species (ROS). Patients with thalassemia experience defective hemoglobin synthesis, which leads to severe anemia. This condition is managed through repeated blood transfusions, which result in systemic iron overload. Excess iron promotes ROS production through the Fenton reaction, generating hydroxyl radicals (•OH). The combination of iron overload and increased ROS generation during hepatic metabolism may create a synergistic pathway for severe oxidative liver injury. This study aims to evaluate whether the condition of iron overload affects free radical production during hepatic metabolism. Liver microsomes were isolated from control and iron overload wild-type (WT) and beta-knockout (BKO) mice. The iron overload was induced by intraperitoneal injection of a total of 100 mg of iron per mouse for 5 days, and the mice were kept for 14 days before sacrifice. The liver microsomes were prepared using an ultracentrifugation technique. Tert-butyl hydroperoxide (t-BuOOH) and ethanol (EtOH) were used as substrates to assess the activity of the metabolizing enzymes. The techniques of spin trapping and Electron Spin Resonance (ESR) spectroscopy were employed to detect free radicals in the microsomal systems. When t-BuOOH was used as a substrate, both carbon-centered radicals and •OH were significantly enhanced under conditions of iron overload in both WT and BKO mice. Additionally, the metabolism of EtOH generated carbon-centered radicals, which increased slightly under iron overload conditions. Furthermore, the addition of deferiprone, an iron chelator, to the reaction mixture resulted in a marked reduction in radical signals, indicating that iron partially contributes to free radical generation. In conclusion, the generation of free radicals in mouse liver microsomes was dependent on both the enzymatic pathways and iron-mediated non-enzymatic pathways. Patients with iron overload may be susceptible to xenobiotic-induced liver damage.

Keywords: Microsomes, ESR; spin trapping, t-BuOOH, EtOH, Free radicals

Evaluation of the Anticancer Effects of Esculetin in Cholangiocarcinoma Cells

Pitchaporn Pusomta[1], Laddawan Senggunprai[1,2], Sarinya Kongpetch[1,2], Piman Pocasap[1,2], Auemduan Prawan[1,2,*]

[1] Department of Pharmacology, Faculty of Medicine, Khon Kaen University, Khon Kaen 40002, Thailand
[2] Cholangiocarcinoma Research Institute, Khon Kaen University, Khon Kaen 40002, Thailand

Abstract

Cholangiocarcinoma (CCA) is a highly aggressive biliary tract malignancy with an exceptionally high incidence in northeastern Thailand. Despite its clinical significance, treatment options remain limited. The standard first-line regimen of gemcitabine plus cisplatin offers modest benefit, as many patients develop chemoresistance over time. Dysregulation of apoptotic pathways is one of the key mechanisms underlying this resistance, which has prompted growing interest in targeting alternative cell death pathways. Among these, ferroptosis, a non-apoptotic, iron-dependent form of cell death characterized by excessive lipid peroxidation, has gained considerable attention as a potential therapeutic strategy in chemotherapy-refractory cancers.

This study examined the anti-proliferative effects of esculetin, a naturally occurring coumarin derivative, in CCA cell lines and explored its potential to induce ferroptosis.

KKU-213A, KKU-452, and KKU-100 cells were treated with esculetin (0.5–125 μM) for 24–72 hours. Cell viability was assessed by the sulforhodamine B (SRB) assay. Mechanistic studies employed co-treatment with ferrostatin-1, a selective ferroptosis inhibitor, or z-VAD-fmk, a pan-caspase inhibitor to distinguish ferroptotic from apoptotic contributions. Cisplatin was included as an apoptosis-positive control.

Esculetin reduced cell viability in a concentration- and time-dependent manner across all three lines. Ferrostatin-1 partially restored viability in KKU-213A and KKU-452 cells, supporting ferroptosis involvement, whereas this cytoprotective effect was not observed in KKU-100 cells. Conversely, z-VAD-fmk failed to attenuate esculetin-induced cytotoxicity, suggesting apoptosis was not the primary mechanism.

These findings provide preliminary evidence that esculetin engages ferroptotic cell death in certain CCA subtypes. Further molecular studies are needed to clarify the precise mechanisms involved.

Keywords: Cholangiocarcinoma, Esculetin, Ferroptosis, Cytotoxicity

Small-Molecule Inhibitors of Chromatin Reader Proteins Enhance Neuronal Resilience in *Drosophila* Amyotrophic Lateral Sclerosis Models

Salinee Jantrapirom[1,2], Chansunee Panto[2], Ranchana Yeewa[3,4], Ruedeemars Yubolphan[1], Saranyapin Potikanond[1], Luca Lo Piccolo[3]

[1] Department of Pharmacology, Faculty of Medicine, Chiang Mai University, Chiang Mai, Thailand.
[2]Drosophila Centre for Human Diseases and Drug Discovery (DHD), Faculty of Medicine, Chiang Mai University, Chiang Mai, Thailand
[3]Center of Multidisciplinary Technology for Advanced Medicine (CMUTEAM), Faculty of Medicine, Chiang Mai University, Chiang Mai, Thailand.
[4]Department of Biochemistry, Faculty of Medicine, Chiang Mai University, Chiang Mai, Thailand 50200

Abstract

Modulating epigenetic regulators is emerging as a promising strategy to enhance neuronal resilience and reveal therapeutic opportunities for neurodegenerative diseases. However, the roles of specific chromatin-associated factors in neuronal stress adaptation remain poorly defined. Using *Drosophila*, we identified the acyl-lysine chromatin reader proteins ENL/AF9 as modulators of neuronal stress resistance. Neuron-specific depletion of the ENL/AF9 homolog extended lifespan and increased oxidative stress tolerance in aged animals. To assess disease relevance, we conducted genetic modifier screens across multiple *Drosophila* neurodegeneration models. ENL/AF9 depletion robustly suppressed phenotypes in a UBQLN2-associated amyotrophic lateral sclerosis (ALS) model, with more modest effects on TDP-43 driven toxicity. To translate these findings, we tested a selective small-molecule inhibitor of ENL/AF9. Pharmacological inhibition of ENL/AF9 recapitulated key protective effects *in vivo*, including improved locomotor performance, restoration of motor neuron morphology, and reduced disease-associated cellular stress markers in the UBQLN2-ALS model. Collectively, our results identify ENL/AF9 as regulators of neuronal stress resilience and support targeting chromatin reader proteins as a potential therapeutic strategy for ALS

Keywords: Small-Molecule Inhibitors, neurodegeneration, UBQLN2-associated amyotrophic lateral sclerosis, Drosophila melanogaster

The effects of linoleic acid on HaCaT keratinocyte migration via regulation of inflammatory response

Thayapa Thaithae[1], Aradee Suratchananon[1], Kamolwat Ekmetipunth[1], Paranat Preechapanich[1], Mutita Pluempreecha[1], Tanyapohn soingam[1], Weerawadee Chandranipapongse[1], Uraiwan Panich[1],[*]

[1]Department of Pharmacology, Faculty of Medicine Siriraj Hospital, Mahidol University, Bangkok, Thailand

Abstract

Ultraviolet B (UVB) radiation is a critical environmental stressor that compromises epidermal integrity. It induces oxidative stress and inflammation, which dysregulates keratinocyte differentiation and impairs wound healing. Linoleic acid (LA), an essential fatty acid with skin barrier–supporting and antioxidant properties, may confer protective effects against UVB-induced cellular dysfunction. This study investigated whether linoleic acid could mitigate UVB-mediated suppression of keratinocyte migration by modulating inflammatory and differentiation-related gene expression. Human HaCaT keratinocytes were exposed to UVB irradiation, and 30 mJ/cm² was identified as a non-cytotoxic dose that significantly increased intracellular reactive oxygen species (ROS). Linoleic acid concentrations of 2.5, 5, and 10 μM were confirmed to be non-cytotoxic by propidium iodide (PI) flow cytometry. Keratinocyte migration was assessed using a wound scratch assay. The expression of differentiation markers (KRT1, KRT10, and IVL) and inflammatory markers (NF-κB, TNF-α, IL-6, and IκB-α) was evaluated by RT-qPCR. UVB exposure markedly delayed keratinocyte migration and upregulated differentiation markers (KRT1, KRT10, IVL). In parallel, UVB activated inflammatory signaling, evidenced by increased expression of NF-κB, TNF-α, and IL-6, and decreased levels of IκB-α. Pre-treatment with linoleic acid attenuated both inflammatory and differentiation-associated gene expression, correlating with improved keratinocyte migratory capacity. These findings indicate that linoleic acid effectively counteracts UVB-induced impairment of keratinocyte migration by suppressing inflammatory responses and restoring balanced differentiation. This evidence suggests that linoleic acid may be a promising therapeutic candidate for enhancing wound repair under UV-induced stress.

Keywords: Linoleic acid, Ultraviolet B, Keratinocyte migration, Inflammation

Application of 3D Human Liver-on-a-chip to modelling hepatic steatosis

Htun Aung Kyaw[1,2], Nadeeya Mad-adam[1], Pimonrat Ketsawatsomkron[1,2], Khanit Sa-Ngiamsuntorn[3], Kenjiro Muta[1,2,*]

[1]Chakri Naruebodindra Medical Institute (CNMI), Faculty of Medicine Ramathibodi Hospital, Mahidol University, Bang Phli, Samut Prakarn 10540, Thailand
[2]Programme in Translational Medicine, Faculty of Medicine Ramathibodi Hospital, Mahidol University, Bangkok, 10400, Thailand
[3]Department of Biochemistry, Faculty of Pharmacy, Mahidol University, Bangkok, 10400, Thailand

Abstract

Metabolic dysfunction-associated steatotic liver disease (MASLD, formerly known as non-alcoholic fatty liver disease), has complex pathology, strongly associated with obesity, type 2 diabetes and impaired lipid metabolism. The initial hallmark of MASLD is the ectopic accumulation of triglycerides within hepatocytes (i.e. hepatic steatosis), which is reversible through intensive lifestyle modifications, unlike irreversible later stages (e.g. cirrhosis and liver cancer). However, such behavioural interventions are most likely challenging to patients with MASLD. Drug development has been undertaken but often hindered by the complex pathology of MASLD and poor human translatability of currently used animal models, highlighting the necessity for human-relevant researchable platforms. Thus, being able to mimic this steatosis stage will open doors for novel pharmacological research where potential drug candidates can be tested. To achieve this, we utilized organ-on-a-chip (OOC) system lined with an immortalized hepatocyte-like cell line (imHC) which possesses a distinct lipid metabolic profile from other liver cell lines. The OOC is an in-vitro three-dimensional (3D) platform where cells can be cultured in a more physiologically relevant condition than conventional 2D platforms owing to the presence of fluid-flow and 3D cell-cell/extracellular matrix (ECM) interaction. The OOC model of steatosis was established by exposing collagen ECM-embedded imHCs to free fatty acid(s)(FFAs) including oleic acid (OA), palmitic acid (PA) or a mixture of OA and PA for 24 hours in MIMETAS OrganoPlate. Intracellular lipid accumulation was determined by staining with Bodipy dye, fluorescence intensity of which was quantified by a plate reader. For comparison, establishment of steatotic imHC in a 2D platform was attempted in a similar manner. In both imHC OOCs and 2D cultures, 24-hour exposure to either OA or OAPA caused a significant increase in fat accumulation without detectable cytotoxicity. Moreover, the OOC model successfully captured the cytotoxicity of PA, assessed by lactate dehydrogenase (LDH) assay, without significant fat accumulation. Our findings demonstrate that the imHC cell line can effectively accumulate lipids in response to FFAs in both 2D and 3D OOC environments, serving as an alternative in-vitro model of hepatic steatosis.

Keywords: metabolic dysfunction-associated steatosis liver disease (MASLD), hepatic steatosis, immortalized hepatocyte-like cell line (imHC), liver organ-on-a-chip, free fatty acid, lipotoxicity, OrganoPlate, in-vitro model

Introduction

With the current trend of increasing sedentary lifestyles and widespread consumption of calorie-dense foods, metabolic diseases have become one of the most prevalent non-communicable diseases worldwide.[1] Among them, metabolic dysfunction-associated steatotic liver disease (MASLD), once known as non-alcoholic fatty liver disease (NAFLD), represents a significant global health burden, with reported global prevalence of 38% in general adult population.[2] This rate is expected to rise with the global prevalence of MASLD projected to reach 55.7% by 2040.[3]

Clinically, MASLD progresses through four distinct phases, namely metabolic dysfunction-associated steatotic liver (MASL), metabolic dysfunction-associated steatohepatitis (MASH), liver fibrosis and cirrhosis of liver.[4] MASL is regarded as harmless steatosis while the latter stages encompass impairment of liver.[4] In worst cases the progression can even lead to hepatocellular carcinoma (HCC).[4-6] Impaired lipid metabolism is considered as "first hit" that leads to excessive accumulation of triglycerides (TGs) in liver parenchymal cells , resulting in hepatic steatosis.[5] The culprits of the "second hit" are plentiful, ranging from metabolic syndrome-related lifestyle to genetic variations and insulin resistance.[7] For years, clinical management of MASLD has largely relied on the "off-label" use of anti-inflammatory, anti-diabetic, and anti-obesity agents.[5] Though the 2024 FDA approval of resemtirom (Rezdiffra) marked a milestone for MASH treatment,[6, 8, 9] therapeutic interventions for the earlier steatotic phase remain limited.[10] This gap is exacerbated by the limitations of current preclinical platforms, which often fail to capture the complex pathophysiology of MASLD.[11]

Regarding models for MASLD, animal models, especially rodents, have been commonly used. In murine models, MASLD is normally induced by treating diets rich in fat, such as high-fat diet (HFD) or western diet (WD).[11-13] However, they frequently fail to fully recapitulate the inherent complexity and heterogenicity of human MASLD due to physiological differences among species, from gene sequence homology to immune responses and pathogenesis, which highly affect responses to medications.[11, 14] For example, certain polyunsaturated fatty acids (PUFAs) in mouse models result in reduced food intake, ameliorating bodyweight loss in mice model, which is not replicable in humans.[15, 16] These limitations have driven a demand for more physiologically relevant human-based models as alternatives to animal models.[11] This paradigm shift has been further supported by the FDA Modernization Act 3.0, which approves researchers to utilize alternative approaches, including advanced *in vitro* models and computational tools, to aid in experimenting novel drugs.[17] This calls for the establishment of more reliable *in-vitro* models to ensure their utility in future research applications.

Being inexpensive and able to be maintained using simple procedures, two-dimensional (2D) cultures in flasks and dishes have been used by various researchers for MASLD studies.[18] However, these conventional 2D models often fail to capture the sophisticated interplay of metabolism within hepatocytes and interactions with immune cells or with extracellular matrix (ECM) that drive MASLD progression, limiting their predictive value in mechanistic studies and drug response evaluation.[11, 19] Furthermore, they can only be cultured for short-term[11, 19] which make chronic, progressive disease, such as MASLD, difficult to be fully recapitulated.

To address these gaps, advanced three-dimensional(3D) systems such as Liver Organ-on-a-Chip (OOC) models of MASLD have emerged.[11] OOC is an *in-vitro*

microphysiological system, where cells are combined with extracellular matrix (ECM) compartment and medium paths to generate functional three-dimensional (3D) microenvironment.[19, 20] By culturing hepatocytes in OOCs, liver OOCs are created resembling hepatic microenvironment with a microfluidic flow, the architecture of liver lobules with hepatic cords or sinusoid-like structures, and hence better mimic the *in-vivo* hepatic environment.[20] Having flow in OOCs ensures constant perfusion of nutrients and removal of metabolic waste, ensuring higher metabolic efficiency and cell viability required for long-term cultures.[21, 22] This is particularly useful to model chronic disease conditions, such as MASLD.

Nevertheless, the validity of any *in vitro* models ultimately depends on the functional quality of the hepatocyte source. Primary human hepatocytes (PHHs) are the gold standard but with limitations such as donor variability, scarcity and a short lifespan in culture.[23] Thus, human hepatoma cell lines like HepG2 remain the most widely used cell line for MASLD studies, where they are generally induced lipid overload (i.e. steatosis) by employing palmitic acid (PA, C16:0), a saturated fatty acid, and oleic acid (OA, C18:1), an unsaturated fatty acid.[24-27] However, it is in dispute for the sole use of hepatoma-cell lines in MASLD research as they demonstrate remarkable divergence from normal hepatocyte proteomic and metabolic profiles.[11, 28, 29] Furthermore, the inherent genetic mutations within hepatoma-derived cell lines, such as the patatin-like phospholipase domain-containing protein 3 (PNPLA3) mutation in HepG2 cells[30] and Huh-7 cells,[31] confer a natural predisposition toward lipid accumulation upon FFA exposure.[32] As a result, these models may not accurately replicate the metabolic responses of individuals who do not carry this specific mutation.

Alternatively, the immortalized hepatocyte-like cell line (imHC) derived from human mesenchymal cells presents a promising human cell source.[33] It has been proven that imHCs express key hepatocyte markers (ALB, HNF-4α, CYP450s) and their use has been validated in infectious disease models.[33-40] Notably, one of the previous studies have highlighted a difference in lipid metabolism between imHC and HepG2 during dengue virus infection. imHCs demonstrated a significant larger area of lipid droplets compared to HepG2 cells and on exposure to dengue virus, these lipid droplets of imHCs experienced a significant decrease.[34] This observation postulates that imHCs may possess distinct lipid handling capabilities in response to various physiological and pathophysiological cues. Therefore, characterizing the steatosis induction in imHCs is a critical step toward establishing a valuable alternative human-derived model for MASLD research.

In order to develop a hepatic steatosis model using imHC, we are using MIMETAS OrganoPlate, a commercial OOC platform. This particular OrganoPlate has been used with HepG2 cells and shown superior functionality compared to its counterpart 2D cultures, and its ability to culture for long-term.[41] Moreover, it has also been used in modelling HepG2 OOC models by exposure to FFAs.[42]

In this study, we aim to establish and characterize a novel *in vitro* steatosis model utilizing the imHC cell line by investigating the lipogenic response of these cells to chemical induction using OA, PA and a combination of both (OAPA) to determine their capacity for lipid accumulation. Furthermore, to address the physiological limitations of monolayer cultures, this study will extend the investigation to imHC OOC models. By developing both 2D and 3D (OOC) steatotic models using imHCs, we seek to validate the potential of imHC cells as a relevant platform for future hepatic steatosis research.

Methods

Chemical preparation

Oleic acid (OA, MedChemExpress LLC, US) and palmitic acid (PA, MedChemExpress LLC, US) were dissolved in 1 mM Sodium Hydroxide (NaOH, Sigma, US) by heating at 100°C on a heat block. 10%Fatty acid free bovine serum albumin (BSA, Sigma-Aldrich, US) was made in serum-free William's E Medium (WE, Gibco, US).

Cell line

The immortalized hepatocyte-like cell line (imHC) was received as a gift from Dr. Khanit Sa-Ngiamsuntorn. The cell line was subcultured to Passage (10) and stored in cryovial at -80°C, before they were used for the experiments.

imHC 2D cultures

Cryopreserved imHC cells were initially thawed and seeded into 100 mm culture dish for recovery in complete William's E Medium (WE, Gibco, US) supplemented with 10% fetal bovine serum (FBS; Hyclone, US) and 2 mM L-glutamine (Gibco, US) and kept at 37°C in a humidified incubator with an atmosphere of 95% air and 5% CO_2. When the confluency reached 70-80% in 100 mm dish, cells were then seeded in 96-well plate in complete WE medium, at 25,000 cells/well, for 48 hours. imHC cells were then treated with 1 mM NaOH (vehicle), 0.5 mM OA, 0.5 mM PA, and a combination of both (OAPA, 0.25mM OA + 0.25 mM PA) in complete WE Medium containing 0.5% FBS and 2mM L-glutamine, supplemented with 1% fatty acid-free BSA. After 24 hours, conditioned medium was collected and cells were stained with 5 μM Bodipy (Boron-dipyrromethene, Invitrogen, Thermofisher Scientific, US) and 0.5 μg/mL DAPI (4',6 diamidino-2-phenylindole, Sigma-Aldrich, US).

imHC OOC cultures

Similar to 2D cultures, imHC cells were initially recovered in complete WE medium I 100 mm culture dishes. When the confluency reached 70-80% in 100 mm dish, the cells were resuspended in a neutralized collagen solution containing Cultrex Collagen Type I (4 mg/mL, rat tail; Bio-Techne, USA) with serum-free WE medium (WE-SF) to achieve a final cell density of 1 x 10^7 cells/ml. Subsequently, 3 μL of the cell-collagen mixture was loaded into the gel inlet chamber of a 2-lane OrganoPlate (cat# 9605-400-B, MIMETAS,The Netherlands). The cells were cultured in OrganoPlate in the presence of Complete WE Medium, supplemented with 10% FBS, for 48 hours, with regular replenishment of the medium every 24 hours. The OOC plates were incubated on a rocker (MIMETAS, The Netherlands) that slanted side-to-side at 7° every 8 min in a CO_2 incubator at 37°C. After 48 hours, imHC OOCs were treated with fatty acids, in the same manner as 2D cultures, for 24 hours. Following this, conditioned medium was collected and cells were stained with 5 μM Bodipy and 0.5 μg/mL DAPI.

Fluorescence Intensity Measurement and Fluorescence imaging

After 24 hours of fatty acid induction, conditioned medium was collected and imHC 2D cultures and OOCs were fixed with paraformaldehyde (4%PFA, Fujfilm Wako Pure Chemical Corporation, Japan) and stained with 5μM Bodipy and 0.5 μg/mL DAPI. The fluorescent intensity was measured using microplate reader (BioTek Cytation 5, Agilent Technologies, Inc., USA) and microscopy pictures were taken via inverted fluorescence

phase contrast microscope (Zeiss Axio Vert.A1, Germany) and a spinning disk confocal system (Opera Phenix Plus, Revvity, US).

LDH Assay

To assess cellular damage in imHC cells in both platforms, the enzymatic activity of lactate dehydrogenase (LDH) in the conditioned medium was evaluated using an LDH Activity Assay Kit (Sigma-Aldrich, USA) following the manufacturer's protocol (Farhana and Lappin, 2024). LDH activity was calculated from optical density measurements of absorbance at 450 nm using a microplate reader (BioTek Cytation 5Agilent Technologies, Inc., USA) every 5 min until the value of the most active sample was greater than the value of the highest standard.

Statistical analysis

All experiments were performed in 3-5 independent experiments (biological replicates, as indicated by "n" in each figure legend). The data were analyzed with GraphPad Prism software version 11 (GraphPad, USA) and expressed as mean ± standard error of the mean values (SEM). Two-way analysis of variance (ANOVA) with Tukey's multiple comparison test was used for statistical analysis of lipid accumulation while one-way ANOVA with Tukey's multiple comparison test was used for statistical analysis of LDH fold change. The results were considered statistically significant if the probability value (p) is less than 0.05.

Results

1. Establishing 2D in-vitro steatosis model

To evaluate the lipid accumulation capacity of imHC cells, we first evaluated the ability of imHC to do so by culturing in 96-well plates and cells exposed to vehicle sodium hydroxide (Veh, NaOH, 1mM), oleic acid (OA, 0.5mM), palmitic acid (PA, 0.5mM), or a mixture of OA and PA (OAPA, 0.25mM OA + 0.25mM PA) for 24 hours in complete WE medium containing 0.5% FBS and 1% fatty-acid free BSA. After 24 hours, in order to detect lipid accumulation across different treatment groups, the cells were stained with Bodipy(green), which is a commonly used dye staining neutral lipids.[43] DAPI was used as a counterstain. Morphological analysis of imHCs on exposure to OA and OAPA groups showed the presence of blackish and brownish granules compared to Veh group in brightfield microscopy. Via Bodipy staining, it could be identified that there is neutral lipid droplets accumulation in OA and OAPA groups (Fig.1). Quantitative analysis showed that cells treated with OA or OAPA exhibited a significant numerical increase in lipid accumulation compared to vehicle control (around 1.6-fold for OA group and 1.5-fold for OAPA group) (Fig. 3). On the other hand, PA group did not exhibit any noticeable lipid accumulation (Fig. 3).

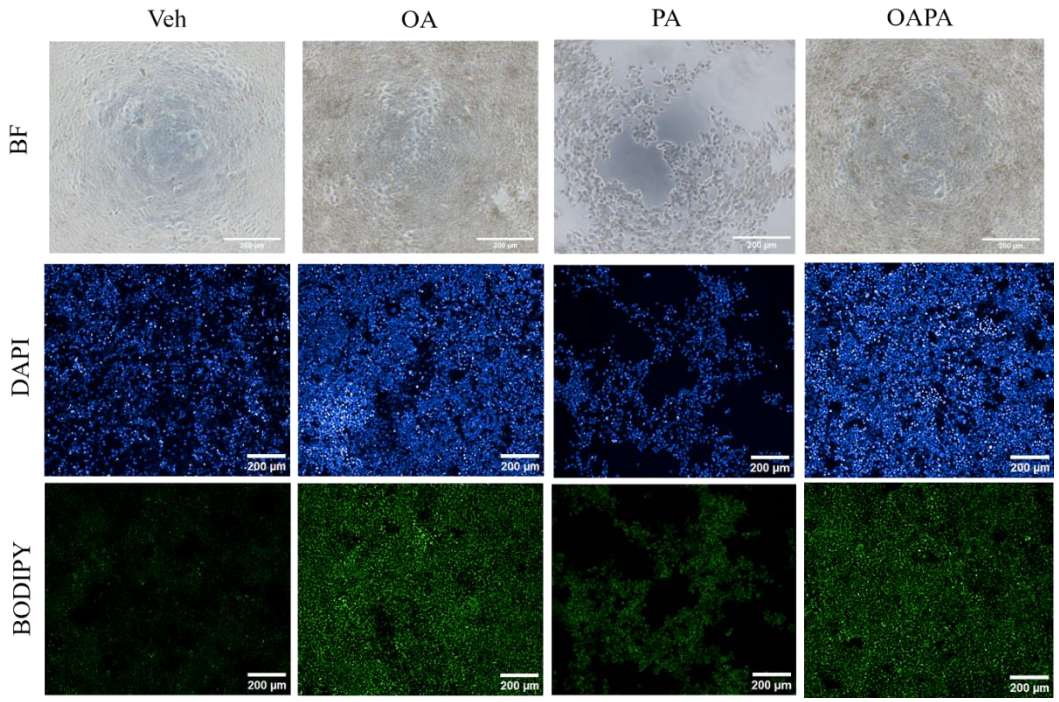

Figure 1. Representative bright field and fluorescent images at 5X magnification after induction of hepatic steatosis in imHC 2D model. imHC 2D cultures were treated with vehicle (Veh, 1 mM NaOH), oleic acid (OA, 0.5 mM), palmitic acid (PA, 0.5 mM), or a mixture of OA and PA (OAPA, 0.5 mM in total) for 24 h under complete WE medium with 0.5% FBS and 1% BSA supplement. BF = Brightfield, Veh = vehicle, OA = oleic acid, PA = palmitic acid, OAPA = combination of oleic and plamitic acid

2. Establishing 3D in-vitro OOC steatosis model

Next, we evaluated whether imHCs can accumulate lipids on exposure to different fatty acids using OOC platform. Similar to 2D in-vitro model, imHC cells were cultured in OOC platforms with vehicle NaOH, OA, PA and OAPA groups for 24 hours, followed by Bodipy staining. Interestingly, both OA and OAPA treatment groups appeared noticeably darker under brightfield microscopy, which was confirmed the presence of fat through Bodipy fluorescence (Fig. 2). Quantitative analysis revealed a statistically significant increase in intracellular lipid accumulation for both OA and OAPA groups (around 1.8- and 1.5-fold increase respectively) compared to vehicle control (Fig. 3). Similar to 2D culture, there was no noticeable lipid accumulation in PA group (Fig. 3).

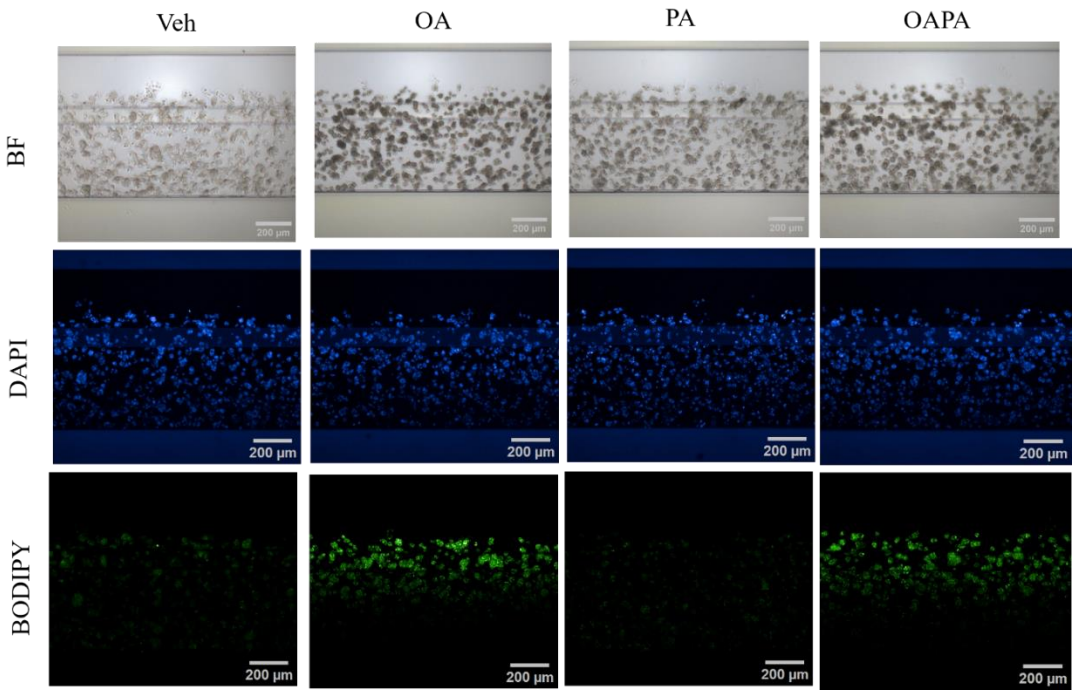

Figure 2. Representative bright field and fluorescent images at 5X magnification after induction of hepatic steatosis in imHC OOC model. imHC OOCs were treated with vehicle (Veh, 1 mM NaOH), oleic acid (OA, 0.5 mM), palmitic acid (PA, 0.5 mM), or a mixture of OA and PA (OAPA, 0.5 mM in total) for 24 h under complete WE medium with 0.5% FBS and 1% BSA supplement. BF = Brightfield, Veh = vehicle, OA = oleic acid, PA = palmitic acid, OAPA = combination of oleic and plamitic acid

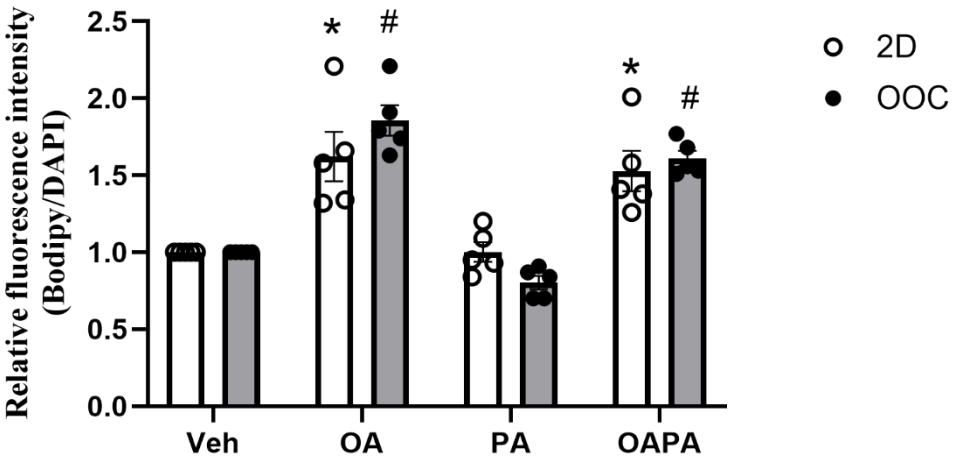

Figure 3. Quantitative analysis of relative fluorescence intensity of Bodipy/DAPI. Data are presented as mean ± SEM and analyzed by two-way ANOVA with Tukey's multiple comparison test (n=5). $^{*}p < 0.05$ versus Veh of 2D. $^{\#}p < 0.05$ versus Veh of OOC. Veh = vehicle, OA = oleic acid, PA = palmitic acid, OAPA = combination of oleic and plamitic acid

3. Identification of the effect of FFAs on imHC viability

Induction of steatosis in hepatic cells with some FFAs has been reported to be associated with cytotoxic effects.[25] In our study, imHCs on exposure to PA group showed

morphological changes in 2D culture, where the cells become rounded and lose their adherence to neighbouring cells, which are the signs of cellular injury.[44] Hence, we further assessed whether FFA-induced steatosis in both 2D and imHC OOCs was associated with cellular distress by detecting lactate dehydrogenase (LDH) activity in collected conditioned medium. LDH, a cytoplasmic enzyme, is a marker of cell membrane damage if they are found in conditioned medium.[45] OA and OAPA groups in both models, particularly in imHC OOCs, did not show any significant differences in LDH activity in response to vehicle group. On the other hand, while PA-treated groups in 2D cultures showed a numerical elevation in LDH activity (Fig. 4A) and noticeable cell loss during the staining process (Fig. 1), suggesting compromised membrance integrity, these changes were not statistically significant (Fig. 4A). In imHC OOCs, PA-treated group exhibited a statistically significant increase in LDH activity compared to all other groups (Fig. 4B). These findings highlight the replicability of lipotoxic nature of PA[25] in the imHCs, with particular significance in OOCs.

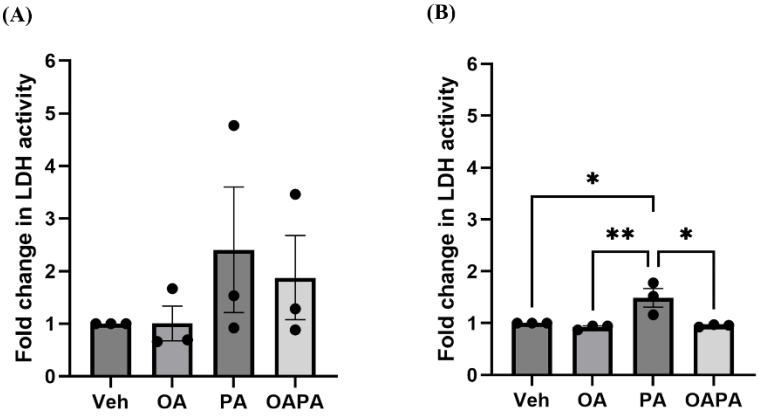

Figure 4. Fold change of LDH activity relative to vehicle control in collected conditioned medium (A) of imHC 2D cultures and (B) of imHC OOCs. Data are presented as mean±SEM and analyzed by one-way ANOVA with Tukey's multiple comparison test (n=3). * $p < 0.05$, ** $p < 0.01$. Veh = vehicle, OA = oleic acid, PA = palmitic acid, OAPA = combination of oleic and plamitic acid

In summarizing the results, imHC OOCs on exposure to OA and OAPA showed significant accumulation of lipids compared to Veh, comparable to 2D models (Fig. 3). Importantly, this steatotic response in the OA and OAPA groups in both models, occurred without associated cellular damage, mimicking the ability of imHCs to model "harmless steatosis" on exposure to OA and OAPA, regardless of the platform.

Discussion

In this study, we induced steatosis in imHCs using 2D and 3D OOC cultures, with consequent evaluation of cell viability via LDH assays. Our results revealed -

(1) **Accumulation of lipids on exposure to OA and OAPA**: OA and OAPA groups in imHC OOCs and 2D cultures exhibited a significant increase in fat accumulation compared to vehicle control, while the cells are still viable.
(2) **Lipotoxicity of PA**: PA, though did not cause noticeable lipid accumulation, showed signs of toxicity to imHCs as marked by elevation of LDH activity compared to vehicle control, where the results are significant in OOCs.

Common dietary long-chain FFAs, OA and PA, were used for steatosis induction in our study. Without incorporation of immune cells, which are generally involved in driving the MASL to steatohepatitis (MASH),[46] we aimed to solely focus on fatty-acid induced lipid accumulation, mostly resembling "hepatic steatosis" or "MASL", which is the early stage of MASLD. The use of OA and PA are also human-relevant as they have been claimed to be fats contained in normal human diet[47] and are the most abundant FFAs in liver triglycerides of patients with steatosis.[48] Notably, *in-vitro* hepatocytes can accumulate lipids on exposure to high glucose.[49] To ensure minimal involvement of other nutrients in induction of steatosis in our model, we used 0.5% FBS in order for the cells to depend more on FFAs in the culture media for their lipid accumulation.

While cancerous cell lines are commonly used in hepatic steatosis modelling,[24,25] their genetic predisposition and nonphysiological proteomic profiles limit them from their human translatability.[30] For example, previously developed HepG2 steatosis OOCs could replicate the features of MASL but failed to replicate treatment response to Pioglitazone,[42] which have been shown to effectively decrease hepatic fat accumulation in clinical trials.[50] Hence, non-cancerous hepatocyte-like cells become an alternative to model liver diseases.[51] While the major concern with these types of cells is limited life span and dedifferentiation,[52] imHC overcome these by phenotypically and metabolically stable for a life span of more than 6 months.[33,40] Hence, the shift toward the use of imHCs offers a stable, non-cancerous alternative in modelling hepatic steatosis.

The ability of imHCs to model hepatic steatosis, involves characterizing fat accumulation for steatosis and identifying the non-toxic effect of fats. It is important to note that the two FFAs we used in this study have been proven to give different effects; OA being more steatogenic while PA is considered highly cytotoxic.[24,25] In our study, on exposure to OA, imHCs in 2D cultures and imHC OOCs both showed significant steatosis effect compared to vehicle, without affecting cell viability (Fig. 3,4). This finding correlates with past studies showing a harmless steatosis effect of OA in different hepatocyte cell lines,[25,42] indicating that imHCs can accumulate lipid effectively in the similar manners as commonly used cell lines. In terms of PA, its cytotoxic effect could also be identified with a rise in LDH activity (Fig. 4). It is important to point out that while both 2D and imHC OOCs exhibited a numerical fold increase of LDH activity relative to vehicle, the significance was noticeable in OOC model only. Normally, LDH release from the cells is determined to access cellular damage by measuring the amount of LDH in collected culture medium.[45] The insignificance we saw in 2D model could be appointed to data variability, which could be explained by cellular detachment (Fig. 1) happened before LDH could be released into conditioned medium.[53] On the other hand, imHC OOCs exposed to PA maintained structural integrity (Fig. 2), while exhibiting a significant change in LDH activity relative to vehicle. This positions the imHC OOCs as a superior potential platform to 2D cultures for studying the specific mechanisms of various fatty acids on hepatocytes. Finally, OAPA exposure resulted in significant lipid accumulation relative to vehicle, with no noticeable cytotoxic effects to imHCs. This result of OAPA aligns with existing literature suggesting the protective role of OA when combined with cytotoxic PA.[25,54] Hence, we could confirm that imHCs demonstrate the ability to distinguish between metabolic lipid storage (steatosis on exposure to OA or OAPA) and lipid-induced cellular injury (lipotoxicity on exposure to PA) when exposed to FFAs in both 2D and OOCs.

OOC system is well-known for its presence of cell-ECM interactions and fluid flow, increasing physiological relevance.[19,20] In our study, we intended to see imHC OOCs

outperformed 2D cultures. Surprisingly, 2D culture gave similar responses in fat accumulation to imHC OOCs, highlighting the ability of imHC in maintaining its metabolic functionality in uptaking FFAs regardless of platforms. Nonetheless, while 2D cultures can effectively replicate hepatic steatosis, their rapid senescence after reaching confluency limits their utility for long-term culture,[19] which is an important factor in modelling later stages of chronic disease, like MASLD. The OOC system we used has been proven to sustain hepatic functions, such as albumin and urea production, for at least 14 days in long-term culture,[41,42] and hence it is uniquely positioned to mimic the chronic conditions of MASLD.

Despite the advantages of the imHC OOC model in mimicking hepatic steatosis, several limitations remain. First, our current study focused on evaluating lipid accumulation in imHCs on 24-hour exposure to FFAs. In contrast, human MASLD is a chronic, progressive condition that develops over years of persistent metabolic imbalance.[6] Taking advantage of the ability of OOC for long-term cultures,[41,42] extending the culture duration in this OOC system to 7 or 14 days would allow for the observation of chronic response on exposure to FFAs and ability to test the response of lipid lowering drugs. Potential future work involves validating the model for reversibility of lipid accumulation and predictability of the model by testing the approved drug for MASLD, Resmetirom[9], in our model. Second, while Bodipy fluorescent dye is used for quantitative analysis, its readout can be distorted by scattering or absorption of thick samples,[55] particularly in imHC OOCs, where there is presence of extracellular matrix and 3D thickness. In order to overcome this limitation, we used spinning-disk confocal microscope, which allows optical sectioning and high speed reading, producing fluorescent images with better resolution and reducing photobleaching.[56] Future studies could benefit from directly measuring the readout of fluorescence using spinning-disk confocal microscopy. Furthermore, while imHCs are used as an alternative to primary human hepatocytes, they may not fully replicate the complete metabolic and enzymatic diversity of a native human liver. Polymorphisms in genes such as PNPLA3 (patatin-like phospholipase domain-containing protein 3) or TM6SF2 are known to significantly influence individual susceptibility of lipid accumulation and the progression of MASLD[57] and the presence of the specific polymorphism in cell line could make it more susceptible to fat accumulation. Hence, future genomic characterization of the imHC line is necessary to determine if its metabolic response is representative of a high-risk or low-risk human genotype. Moreover, complementation with transcriptomic profiling to determine key human-relevant intrahepatic pathophysiological events will be further necessary to validate imHC OOCs as useful preclinical hepatic steatosis model.[11] Finally, current model only uses a single cell source of imHC, making it limited to model MASL only. Future work would benefit from co-culturing with non-parenchymal cells (such as Kupffer cells and stellate cells) that can drive MASL to MASH[46] and this could play a role in studying the disease progression.

Conclusion

In conclusion, we demonstrate that imHC cell line has the capacity for lipid accumulation upon exposure to FFAs in both 2D and OOC platforms. The lipotoxic effect from PA could also be replicated with imHCs, particularly in OOCs. Hence, imHCs play as a usable cell source for an alternative *in-vitro* model of hepatic steatosis.

Acknowledgement

This work was supported by the Program Management Unit for Competitiveness

(C01F670367 to P. K. and K.M.), and Mahidol University (FF-029/2568 to K.M., Fundamental Fund: Fiscal Year 2025, allocated by the National Science Research and Innovation Fund).

References

1. Zou B, Yeo YH, Nguyen VH, Cheung R, Ingelsson E, Nguyen MH. Prevalence, characteristics and mortality outcomes of obese, nonobese and lean NAFLD in the United States, 1999-2016. J Intern Med. 2020;288(1):139–51.
2. Younossi ZM, Golabi P, Price JK, Owrangi S, Gundu-Rao N, Satchi R, et al. The Global Epidemiology of Nonalcoholic Fatty Liver Disease and Nonalcoholic Steatohepatitis Among Patients With Type 2 Diabetes. Clin Gastroenterol Hepatol. 2024;22(10):1999–2010.e8.
3. Le MH, Yeo YH, Zou B, Barnet S, Henry L, Cheung R, et al. Forecasted 2040 global prevalence of nonalcoholic fatty liver disease using hierarchical bayesian approach. Clinical and Molecular Hepatology. 2022;28(4):841–50.
4. EASL-EASD-EASO Clinical Practice Guidelines for the management of non-alcoholic fatty liver disease. J Hepatol. 2016;64(6):1388–402.
5. Wei S, Wang L, Evans PC, Xu S. NAFLD and NASH: etiology, targets and emerging therapies. Drug Discov Today. 2024;29(3):103910.
6. Waheed A, Gul MH, Shabbir MUB, Raja HAA, Wardak AB, Hussaini H, et al. FDA approves Resmetirom: groundbreaking treatment for NASH liver scarring in moderate to advanced fibrosis. Annals of Medicine and Surgery. 2025;87(3):1088–91.
7. Mariana Verdelho M, Anna Mae D. Pathogenesis of Nonalcoholic Steatohepatitis. Gastroenterology. 2016;150(8):1769–77.
8. Konstantinos A, Theocharis K, Evangelos C, Sven F, Georgios G. Insights into the results of Resmetirom trials: Can a thyroid hormone receptor agonist be the holy grail of MASH therapy? Pharmacology & Therapeutics. 2025;268:108811.
9. Shakeel L, Shaukat A, Akilimali A. Resmetirom: A Breakthrough in the Treatment of Metabolic Dysfunction-Associated Steatotic Liver Disease (MASLD). Health Sci Rep. 2025;8(6):e70920.
10. Zhang X, Lau HC, Yu J. Pharmacological treatment for metabolic dysfunction-associated steatotic liver disease and related disorders: Current and emerging therapeutic options. Pharmacol Rev. 2025;77(2):100018.
11. Leslie J, Krishnamurthy KA, Gopalsamy IK, Inacio P, Huch M, Gallage S, et al. Metabolic dysfunction-associated steatotic liver disease and steatohepatitis-associated hepatocarcinoma preclinical models. Nature Reviews Gastroenterology & Hepatology. 2026.
12. Vacca M, Kamzolas I, Harder LM, Oakley F, Trautwein C, Hatting M, et al. An unbiased ranking of murine dietary models based on their proximity to human metabolic dysfunction-associated steatotic liver disease (MASLD). Nat Metab. 2024;6(6):1178–96.
13. Im YR, Hunter H, de Gracia Hahn D, Duret A, Cheah Q, Dong J, et al. A Systematic Review of Animal Models of NAFLD Finds High-Fat, High-Fructose Diets Most Closely Resemble Human NAFLD. Hepatology. 2021;74(4):1884–901.
14. Jiang C, Li P, Ruan X, Ma Y, Kawai K, Suemizu H, et al. Comparative Transcriptomics Analyses in Livers of Mice, Humans, and Humanized Mice Define Human-Specific Gene Networks. Cells. 2020;9(12).
15. Hunter H, de Gracia Hahn D, Duret A, Im YR, Cheah Q, Dong J, et al. Weight loss, insulin resistance, and study design confound results in a meta-analysis of animal models of fatty liver. Elife. 2020;9.
16. Konuma K, Itoh M, Suganami T, Kanai S, Nakagawa N, Sakai T, et al. Eicosapentaenoic acid ameliorates non-alcoholic steatohepatitis in a novel mouse model using melanocortin 4 receptor-deficient mice. PLoS One. 2015;10(3):e0121528.

17. Carratt SA, Zuch de Zafra CL, Oziolor E, Rana P, Vansell NR, Mangipudy R, et al. An industry perspective on the FDA Modernization Act 2.0/3.0: potential next steps for sponsors to reduce animal use in drug development. Toxicol Sci. 2025;203(1):28–34.
18. Yun J, Jeon TJ, Kim SM. Current Advances and Future Perspectives of Liver-on-a-Chip Platforms Incorporating Dynamic Fluid Flow. Biomimetics (Basel). 2025;10(7).
19. Donato MT, Gallego-Ferrer G, Tolosa L. In Vitro Models for Studying Chronic Drug-Induced Liver Injury. Int J Mol Sci. 2022;23(19).
20. Hassan S, Sebastian S, Maharjan S, Lesha A, Carpenter AM, Liu X, et al. Liver-on-a-Chip Models of Fatty Liver Disease. Hepatology. 2020;71(2):733–40.
21. Abbott RD, Raja WK, Wang RY, Stinson JA, Glettig DL, Burke KA, et al. Long term perfusion system supporting adipogenesis. Methods. 2015;84:84–9.
22. Yu F, Deng R, Hao Tong W, Huan L, Chan Way N, IslamBadhan A, et al. A perfusion incubator liver chip for 3D cell culture with application on chronic hepatotoxicity testing. Sci Rep. 2017;7(1):14528.
23. Lauschke VM, Shafagh RZ, Hendriks DFG, Ingelman-Sundberg M. 3D Primary Hepatocyte Culture Systems for Analyses of Liver Diseases, Drug Metabolism, and Toxicity: Emerging Culture Paradigms and Applications. Biotechnol J. 2019;14(7):e1800347.
24. Gomez-Lechon MJ, Donato MT, Martinez-Romero A, Jimenez N, Castell JV, O'Connor JE. A human hepatocellular in vitro model to investigate steatosis. Chem Biol Interact. 2007;165(2):106–16.
25. Ricchi M, Odoardi MR, Carulli L, Anzivino C, Ballestri S, Pinetti A, et al. Differential effect of oleic and palmitic acid on lipid accumulation and apoptosis in cultured hepatocytes. J Gastroenterol Hepatol. 2009;24(5):830–40.
26. Alkhatatbeh MJ, Lincz LF, Thorne RF. Low simvastatin concentrations reduce oleic acid-induced steatosis in HepG(2) cells: An in vitro model of non-alcoholic fatty liver disease. Exp Ther Med. 2016;11(4):1487–92.
27. Breher-Esch S, Sahini N, Trincone A, Wallstab C, Borlak J. Genomics of lipid-laden human hepatocyte cultures enables drug target screening for the treatment of non-alcoholic fatty liver disease. BMC Med Genomics. 2018;11(1):111.
28. Molinaro A, Becattini B, Solinas G. Insulin signaling and glucose metabolism in different hepatoma cell lines deviate from hepatocyte physiology toward a convergent aberrant phenotype. Sci Rep. 2020;10(1):12031.
29. Shi J, Wang X, Lyu L, Jiang H, Zhu HJ. Comparison of protein expression between human livers and the hepatic cell lines HepG2, Hep3B, and Huh7 using SWATH and MRM-HR proteomics: Focusing on drug-metabolizing enzymes. Drug Metab Pharmacokinet. 2018;33(2):133–40.
30. Green CJ, Johnson D, Amin HD, Sivathondan P, Silva MA, Wang LM, et al. Characterization of lipid metabolism in a novel immortalized human hepatocyte cell line. Am J Physiol Endocrinol Metab. 2015;309(6):E511–22.
31. Min HK, Sookoian S, Pirola CJ, Cheng J, Mirshahi F, Sanyal AJ. Metabolic profiling reveals that PNPLA3 induces widespread effects on metabolism beyond triacylglycerol remodeling in Huh-7 hepatoma cells. Am J Physiol Gastrointest Liver Physiol. 2014;307(1):G66–76.
32. Luukkonen PK, Nick A, Hölttä-Vuori M, Thiele C, Isokuortti E, Lallukka-Brück S, et al. Human PNPLA3-I148M variant increases hepatic retention of polyunsaturated fatty acids. JCI Insight. 2019;4(16).
33. Sa-Ngiamsuntorn K, Thongsri P, Pewkliang Y, Wongkajornsilp A, Kongsomboonchoke P, Suthivanich P, et al. An Immortalized Hepatocyte-like Cell Line (imHC) Accommodated Complete Viral Lifecycle, Viral Persistence Form, cccDNA and Eventual Spreading of a Clinically-Isolated HBV. Viruses. 2019;11(10).

34. Kongmanas K, Punyadee N, Wasuworawong K, Songjaeng A, Prommool T, Pewkliang Y, et al. Immortalized stem cell-derived hepatocyte-like cells: An alternative model for studying dengue pathogenesis and therapy. PLoS Negl Trop Dis. 2020;14(11):e0008835.
35. Pewkliang Y, Rungin S, Lerdpanyangam K, Duangmanee A, Kanjanasirirat P, Suthivanich P, et al. A novel immortalized hepatocyte-like cell line (imHC) supports in vitro liver stage development of the human malarial parasite Plasmodium vivax. Malar J. 2018;17(1):50.
36. Pongjantarasatian S, Kadegasem P, Sasanakul W, Sa-Ngiamsuntorn K, Borwornpinyo S, Sirachainan N, et al. Coagulant activity of recombinant human factor VII produced by lentiviral human F7 gene transfer in immortalized hepatocyte-like cell line. PLoS One. 2019;14(8):e0220825.
37. Sa-Ngiamsuntorn K, Hongeng S, Wongkajornsilp A. Development of Hepatocyte-like Cell Derived from Human Induced Pluripotent Stem cell as a Host for Clinically Isolated Hepatitis C Virus. Curr Protoc Stem Cell Biol. 2017;42(1):4A 13 1–4A 34.
38. Sa-Ngiamsuntorn K, Suksatu A, Pewkliang Y, Thongsri P, Kanjanasirirat P, Manopwisedjaroen S, et al. Anti-SARS-CoV-2 Activity of Andrographis paniculata Extract and Its Major Component Andrographolide in Human Lung Epithelial Cells and Cytotoxicity Evaluation in Major Organ Cell Representatives. J Nat Prod. 2021;84(4):1261–70.
39. Sa-Ngiamsuntorn K, Thongsri P, Pewkliang Y, Borwornpinyo S, Wongkajornsilp A. A Competent Hepatocyte Model Examining Hepatitis B Virus Entry through Sodium Taurocholate Cotransporting Polypeptide as a Therapeutic Target. J Vis Exp. 2022(183).
40. Sa-Ngiamsuntorn K, Wongkajornsilp A, Phanthong P, Borwornpinyo S, Kitiyanant N, Chantratita W, et al. A robust model of natural hepatitis C infection using hepatocyte-like cells derived from human induced pluripotent stem cells as a long-term host. Virol J. 2016;13:59.
41. Jang M, Neuzil P, Volk T, Manz A, Kleber A. On-chip three-dimensional cell culture in phaseguides improves hepatocyte functions in vitro. Biomicrofluidics. 2015;9:034113.
42. Wiriyakulsit N, Keawsomnuk P, Thongin S, Ketsawatsomkron P, Muta K. A model of hepatic steatosis with declined viability and function in a liver-organ-on-a-chip. Sci Rep. 2023;13(1):17019.
43. Govender T, Ramanna L, Rawat I, Bux F. BODIPY staining, an alternative to the Nile Red fluorescence method for the evaluation of intracellular lipids in microalgae. Bioresour Technol. 2012;114:507–11.
44. Lee J, Lilly GD, Doty RC, Podsiadlo P, Kotov NA. In vitro Toxicity Testing of Nanoparticles in 3D Cell Culture. Small. 2009;5(10):1213–21.
45. Kumar P, Nagarajan A, Uchil P. Analysis of Cell Viability by the Lactate Dehydrogenase Assay. Cold Spring Harbor Protocols. 2018;2018:pdb.prot095497.
46. Yang Z, Zhao J, Xie K, Tang C, Gan C, Gao J. MASLD development: From molecular pathogenesis toward therapeutic strategies. Chin Med J (Engl). 2025;138(15):1807–24.
47. Kien C, Bunn J, Stevens R, Bain J, Ikayeva O, Crain K, et al. Dietary intake of palmitate and oleate has broad impact on systemic and tissue lipid profiles in humans. The American journal of clinical nutrition. 2014;99.
48. Araya J, Rodrigo R, Videla LA, Thielemann L, Orellana M, Pettinelli P, et al. Increase in long-chain polyunsaturated fatty acid n - 6/n - 3 ratio in relation to hepatic steatosis in patients with non-alcoholic fatty liver disease. Clin Sci (Lond). 2004;106(6):635–43.
49. Lu Y, Zhang G, Shen C, Uygun K, Yarmush ML, Meng Q. A novel 3D liver organoid system for elucidation of hepatic glucose metabolism. Biotechnol Bioeng. 2012;109(2):595–604.
50. Blazina I, Selph S. Diabetes drugs for nonalcoholic fatty liver disease: a systematic review. Syst Rev. 2019;8(1):295.
51. Li S, Huang SQ, Zhao YX, Ding YJ, Ma DJ, Ding QR. Derivation and applications of human hepatocyte-like cells. World J Stem Cells. 2019;11(8):535–47.
52. Sampaziotis F, Segeritz CP, Vallier L. Potential of human induced pluripotent stem cells in studies of liver disease. Hepatology. 2015;62(1).

53. Chao ES, Dunbar D, Kaminsky LS. Intracellular lactate dehydrogenase concentration as an index of cytotoxicity in rat hepatocyte primary culture. Cell Biology and Toxicology. 1988;4(1):1–11.
54. Zeng X, Zhu M, Liu X, Chen X, Yuan Y, Li L, et al. Oleic acid ameliorates palmitic acid induced hepatocellular lipotoxicity by inhibition of ER stress and pyroptosis. Nutrition & Metabolism. 2020;17(1):11.
55. Reiche MA, Aaron JS, Boehm U, DeSantis MC, Hobson CM, Khuon S, et al. When light meets biology – how the specimen affects quantitative microscopy. Journal of Cell Science. 2022;135(6).
56. Oreopoulos J, Berman R, Browne M. Spinning-disk confocal microscopy: present technology and future trends. Methods in cell biology. 2014;123C:153–75.
57. Chen Y, Du X, Kuppa A, Feitosa MF, Bielak LF, O'Connell JR, et al. Genome-wide association meta-analysis identifies 17 loci associated with nonalcoholic fatty liver disease. Nat Genet. 2023;55(10):1640–50.

The Effect of Cisplatin Chemotherapy on Stress Granule Formation in Neuroblastoma Cells

Saneeya Jongjarean[1], Natthaporn Sueangoen[2], Duangporn Saengwimol[2], Atthapol Srimongkol[2], Usanarat Anurathapan[4], Parith Wongkittichote[4] and Rossukon Kaewkhaw[1, 3*]

[1]Program in Translational Medicine, Faculty of Medicine Ramathibodi Hospital, Mahidol University, Thailand
[2]Research Center, Faculty of Medicine Ramathibodi Hospital, Mahidol University, Bangkok, Thailand
[3]Chakri Naruebodindra Medical Institute, Faculty of Medicine Ramathibodi Hospital, Mahidol University, Samut Prakan, Thailand
[4]Department of Pediatrics, Faculty of Medicine Ramathibodi Hospital, Mahidol University, Bangkok, Thailand

Abstract

Neuroblastoma is an aggressive pediatric malignancy, and MYCN amplification is associated with rapid progression and treatment resistance. Cisplatin, a DNA-damaging agent used in neuroblastoma therapy, triggers broad cellular stress responses. Stress granules (SGs) are cytoplasmic ribonucleoprotein condensates that assemble during stress and have been implicated in cancer cell survival and chemotherapy tolerance; however, the impact of cisplatin on SG dynamics in neuroblastoma remains unclear. We investigated cisplatin-associated SG phenotypes in four neuroblastoma cell lines spanning distinct clinical origins and MYCN status: SK-N-BE(2) (bone marrow metastasis; MYCN-amplified), SK-N-AS (bone marrow metastasis; MYCN-non-amplified), NB69 (primary tumor; MYCN-non-amplified), and LA-N-2 (relapse tumor; MYCN-amplified). Cells were treated with cisplatin, and sodium arsenite served as a positive control for canonical SG induction. SGs were assessed by immunofluorescence staining of G3BP1 and quantified as G3BP1-positive puncta per field, normalized to DAPIstained nuclei (puncta per nucleus), expressed relative to the arsenite condition within each line. Sodium arsenite robustly induced SG formation across all cell lines, confirming SG assembly competence. In contrast, cisplatin produced predominantly diffuse G3BP1 staining with minimal puncta in SK-N-BE(2), NB69, and LA-N-2, whereas SK-N-AS showed more punctate G3BP1 structures after cisplatin exposure. Importantly, cisplatin pre-treatment markedly suppressed subsequent arsenite-induced SG assembly across all lines, indicating that cisplatin reduces SG assembly capacity in neuroblastoma cells in both MYCN-amplified and nonamplified backgrounds. Together, these findings identify cisplatin as a modulator of SG biology in neuroblastoma and suggest that this drug's DNA-damage stress can impair canonical SG assembly. Further work defining the composition and functional consequences of cisplatininduced G3BP1 condensates, particularly in SK-N-AS, and linking SG suppression to cell fate may reveal SG-linked vulnerabilities relevant to therapy and chemoresistance in high-risk neuroblastoma.

Keywords: Neuroblastoma, Cisplatin, Stress granule, Pediatric cancer, G3BP1, Chemoresistance, MYCN

Introduction

Neuroblastoma (NB) is an aggressive cancer primarily affecting infants and children. It commonly originates in the adrenal glands, although it can also develop in other parts of the body. Neuroblastoma represents around 8-10% of all childhood cancers and remains challenging to treat, especially when diagnosed in its advanced stages. A major factor driving its aggressive nature is the amplification of the MYCN gene, which leads to rapid tumor gro*WT*h and contributes to poor prognosis and resistance to treatment[1, 2]. Despite the use of cisplatin as part of aggressive chemotherapy regimens, high-risk neuroblastoma patients still face unsatisfactory treatment outcomes. This highlights the need for more effective therapeutic approaches[3]. Cisplatin is one of the most used chemotherapeutic drugs and is effective against a range of cancers, including neuroblastoma. The drug works mainly by causing DNA damage through the formation of covalent DNA adducts. Cisplatin binds to purine bases, particularly at the N7 position of guanine, leading to the formation of intrastrand and interstrand crosslinks. This blocks the processes of DNA replication and transcription, resulting in cell cycle arrest and ultimately, apoptosis[4, 5]. While the role of cisplatin in treating cancer is well established, its effectiveness is often limited by the development of chemoresistance, where cancer cells manage to evade the toxic effects of the drug. Chemoresistance occurs through mechanisms such as DNA repair, drug efflux, and modulating cellular stress responses, which may include the formation of stress granules (SGs) [6, 7]. SGs are non-membranous aggregates of RNA and proteins that form in response to various cellular stressors, such as DNA damage, oxidative stress, and exposure to chemotherapy. SGs act as protective structures by sequestering untranslated mRNA and translation initiation factors, effectively halting the synthesis of potentially harmful proteins. This allows cells to conserve energy and protect themselves from apoptosis during stress conditions[7, 8]. In cancer cells, SGs have been linked to chemoresistance, as their formation can prevent apoptosis and help cells survive the stress of chemotherapy[9, 10]. However, the role of SGs in cisplatin resistance is not yet fully understood, and studies on this topic present conflicting results. Some suggest that SGs act as a protective mechanism, while others propose that their formation may actually hinder the cell's ability to adapt to stress[11]. Recent studies have highlighted the potential of cisplatin to induce SG formation, but the specific dynamics of SGs in response to cisplatin remain unclear. Some studies indicate that cisplatin induces SG formation as part of the stress response, while others suggest that cisplatin disrupts SG dynamics by interfering with protein translation and mRNA processing, leading to impaired SG formation[12]. Additionally, cisplatin may interact directly with SG proteins, potentially altering their composition and preventing proper SG assembly[13]. Given these findings, the objective of this study is to investigate the effect of cisplatin on SG formation in neuroblastoma cell lines. Specifically, we aim to visualize SG formation following cisplatin treatment using immunofluorescence (IF) staining with G3BP1, a well-established marker of SGs. We will use SK-N-BE (2), SK-N-AS, NB-69, and LA-N-2 neuroblastoma cell lines, which include both MYCN-amplified and non-amplified models, additionally allowing us to explore whether the neuroblastoma cell line influences SG formation in response to cisplatin treatment.

Methods

Cell Culture

Cell line	SK-N-BE(2)	SK-N-AS	NB69	LA-N-2
Origin	Bone marrow metastasis	Bone marrow metastasis	Primary tumor	Relapse tumor
MYCN Amplification	YES	NO	NO	YES

Neuroblastoma cell lines used in this study included SK-N-BE(2) (MYCN-amplified), SK-NAS (MYCN non-amplified), NB-69 (MYCN non-amplified), and LA-N-2 (MYCN-amplified). These cell lines were obtained from ATCC and cultured in RPMI-1640 medium (Thermo Fisher Scientific) supplemented with 10% fetal bovine serum (FBS) (Thermo Fisher Scientific) and 1% penicillin-streptomycin (Thermo Fisher Scientific). Cells were maintained in a humidified incubator at 37°C with 5% CO2 and passaged when they reached 70-80% confluence. For experimental purposes, cells were plated at a density of 1×10^5 cells per well in 24-well plates and allowed to adhere overnight.

Cisplatin Treatment

Cisplatin treatments were performed using the half-maximal inhibitory concentration (IC50) Cisplatin was dissolved in sodium chloride (NaCl) to create a 10 mM stock solution. The IC50 concentration of cisplatin was calculated for each cell line, then diluted in RPMI-1640 medium for treatment. Cells were exposed to cisplatin at the calculated IC50 concentration for 24 hours, with a NaCl vehicle control group included to account for any effects of the solvent. Following the 24-hour treatment, cells were washed twice with PBS to remove any residual cisplatin and were subsequently prepared for immunofluorescence (IF) staining.

Cell line	SK-N-BE(2)	SK-N-AS	NB69	LA-N-2
IC_{50}	1.15 μg/ml (3.84 μM)	1.87 μg/ml (6.24 μM)	0.34 μg/ml (1.12 μM)	1.37 μg/ml (4.56 μM)

Sodium Arsenite Treatment

Sodium arsenite (HIMEDIA, Hi-AR™) was used as a positive control for stress granule formation. Cells were treated with 0.5 mM sodium arsenite for 1 hour, a concentration and treatment time known to induce stress granule formation. Following treatment, cells were washed twice with PBS to remove any residual sodium arsenite and were then prepared for subsequent immunofluorescence (IF) staining to assess stress granule formation.

Immunofluorescence Microscopy

Neuroblastoma cell lines (SK-N-BE (2), SK-N-AS, NB-69, and LA-N-2) were plated in 24- well plates and treated with cisplatin as previously described. After treatment,

cells were fixed with 4% paraformaldehyde (Sigma-Aldrich) for 15 minutes at room temperature. Following fixation, cells were permeabilized with PBS containing 0.1% Triton X-100 (PBST) for 20 minutes at room temperature to allow antibody penetration. To block non-specific binding, cells were incubated with 3% BSA (Bovine Serum Albumin) in PBST for 30 minutes. After blocking, cells were incubated overnight at 4°C with the primary antibody, anti-G3BP1 (Abcam, Cambridge, UK) at a dilution of 1:500 to detect stress granules (SGs). After primary antibody incubation, cells were washed three times with washing buffer to remove unbound antibody.

Next, cells were incubated with the Alexa Fluor 488-conjugated secondary antibody (Thermo Fisher Scientific) diluted 1:1000 in 1% BSA in TBS for 1.5 hours at room temperature in the dark. After washing with washing buffer, cells were stained for nuclei using DAPI (Thermo Fisher Scientific) for 15 minutes at room temperature. After all staining steps, cells were mounted with Mounting reagent to preserve fluorescence and prevent photobleaching. Imaging was performed using Confocal Microscope with filter sets for DAPI (blue), Alexa Fluor 488 (green). Images were captured at 63× magnification. The images were processed and analyzed using ImageJ software (NIH, Bethesda, MD, USA).

Results

1. Stress granule formation in response to cisplatin in neuroblastoma cell line

Immunocytochemical analysis of G3BP1 revealed cell line–dependent stress granule (SG) responses to cisplatin compared with untreated controls. SG burden was quantified by counting G3BP1-positive puncta and normalizing to the number of DAPI-stained nuclei in the same field (SG puncta per nucleus), and values were expressed relative to the sodium arsenite (SA) condition within each cell line (SA set to 100%). In SK-N-BE(2), NB-69, and LA-N-2, G3BP1 staining after cisplatin exposure was predominantly diffuse/weak, with few discrete puncta, consistent with minimal SG condensation under cisplatin stress (Figure 2A, 2C, and 2D). In contrast, SK-N-AS showed prominent punctate G3BP1 assemblies after cisplatin treatment, reaching approximately ~30- 40 % of the SA-induced SG burden (Figure 2B), indicating that cisplatin can drive SG-like puncta formation in this line. As z showed a diffuse G3BP1 pattern under cisplatin, although this observation is limited by the number of lines tested.

2. Cisplatin pre-treatment suppresses sodium arsenite–induced stress granule assembly across neuroblastoma lines

Because several cell lines exhibited diffuse G3BP1 staining after cisplatin exposure, we hypothesized that cisplatin impairs SG assembly capacity, potentially disrupting a stressadaptive response used by cancer cells under chemotherapy. To test this, cells were treated with cisplatin for 24 h, followed by 1 h SA exposure to induce SGs (Cis + SA condition). Cisplatin pre-treatment markedly reduced SA-induced SG burden across all lines (Figure 4A, 4B, 4C, 4D). Relative SG burden in the Cis + SA condition fell to approximately ~50% in SKN-BE (2), ~3% in SK-N-AS, ~30-40% in NB-69, and ~28–30% in LA-N-2, compared with 100% in SA-only controls (Figure 1E, 2E ,3E, and 4E).

In contrast, robust punctate G3BP1- positive SGs were readily detected in SA-treated cells without prior cisplatin exposure (Figure 3A, 3B, 3C, and 3D). Together, these results indicate that cisplatin blunts subsequent SG assembly in response to a canonical SG inducer, consistent with the diffuse G3BP1 pattern observed in several lines after cisplatin alone. In SK-N-AS, cisplatin alone produced SG-like puncta, yet cisplatin pre-treatment still strongly suppressed SA-induced SG assembly, suggesting that cisplatin may affect SG assembly and/or maturation in a context-dependent manner.

Immunocytochemical analysis of stress granule (SG) formation in SK-N-BE (2), NB-69, and LAN-2 cells showed that cisplatin treatment at its IC_{50} concentration resulted in diffuse and weak G3BP1 staining, with only a few discrete cytoplasmic puncta, indicating limited SG formation, similar to the vehicle control (Figure 1A, 1C, 1D). Interestingly, when cells were treated with sodium arsenite (SA) after cisplatin (24 hours of cisplatin followed by 1 hour of SA), the number and size of SGs were still lower compared to cells treated with SA alone. This pattern was consistent across all tested cell lines, including SK-N-BE (2), NB-69, and LAN-2, suggesting that cisplatin disrupts SG assembly, possibly by preventing the formation or disassembling pre-existing SGs. Quantification of SGs (Figure E) further confirmed that cisplatin reduced the number of SGs compared to sodium arsenite treatment, highlighting cisplatin's inhibitory effect on SG formation. In contrast, in SK-N-AS cells, cisplatin treatment still induced more SGs than the control (Figure 2A), indicating that cisplatin partially induces formation did not increase compared to cisplatin treatment alone (Figure 2D).

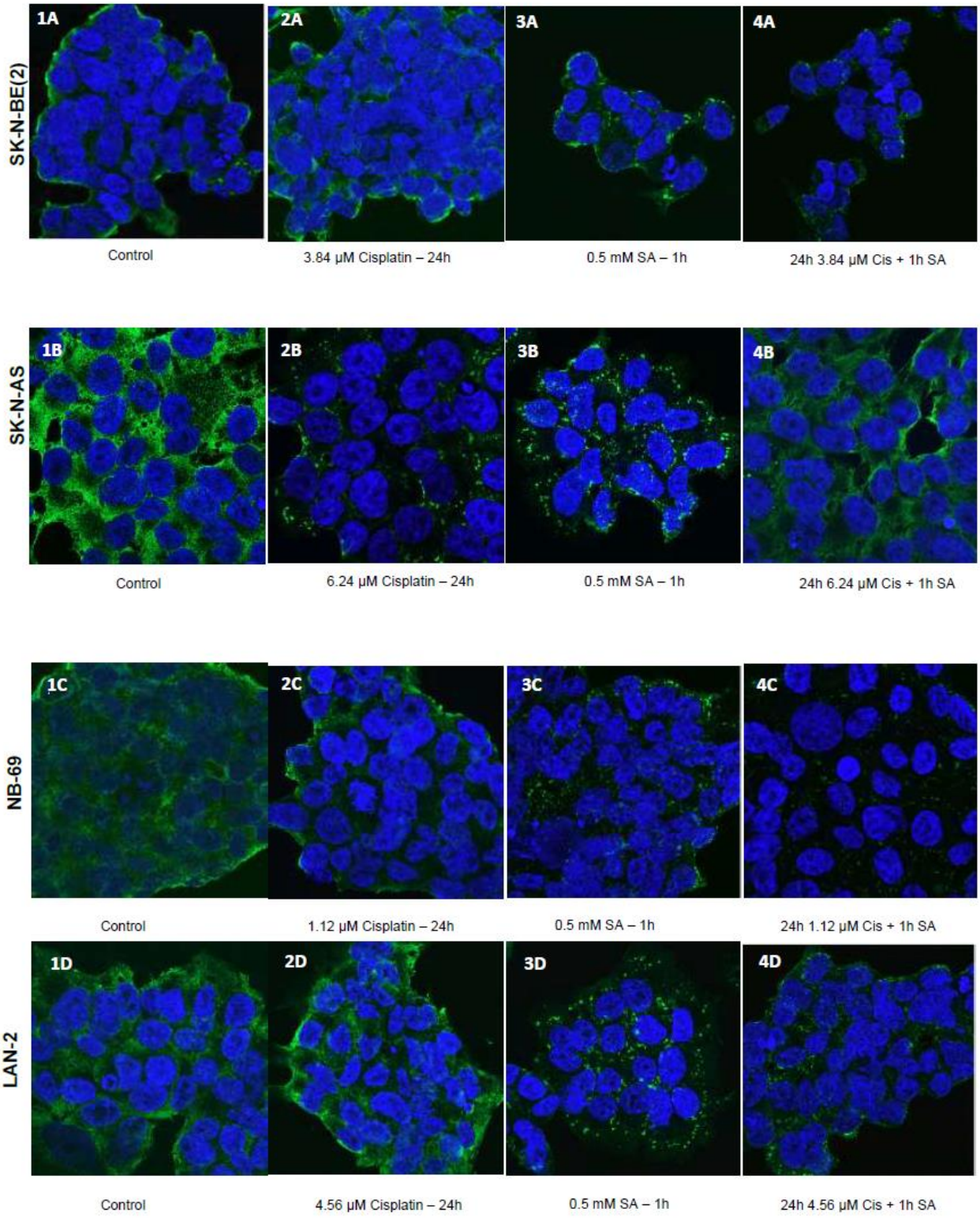
SK-N-BE(2)
1A
2A
3A
4A
Control
3.84 µM Cisplatin – 24h
0.5 mM SA – 1h
24h 3.84 µM Cis + 1h SA
SK-N-AS
1B
2B
3B
4B
Control
6.24 µM Cisplatin – 24h
0.5 mM SA – 1h
24h 6.24 µM Cis + 1h SA
NB-69
1C
2C
3C
4C
Control
1.12 µM Cisplatin – 24h
0.5 mM SA – 1h
24h 1.12 µM Cis + 1h SA
LAN-2
1D
2D
3D
4D
Control
4.56 µM Cisplatin – 24h
0.5 mM SA – 1h
24h 4.56 µM Cis + 1h SA

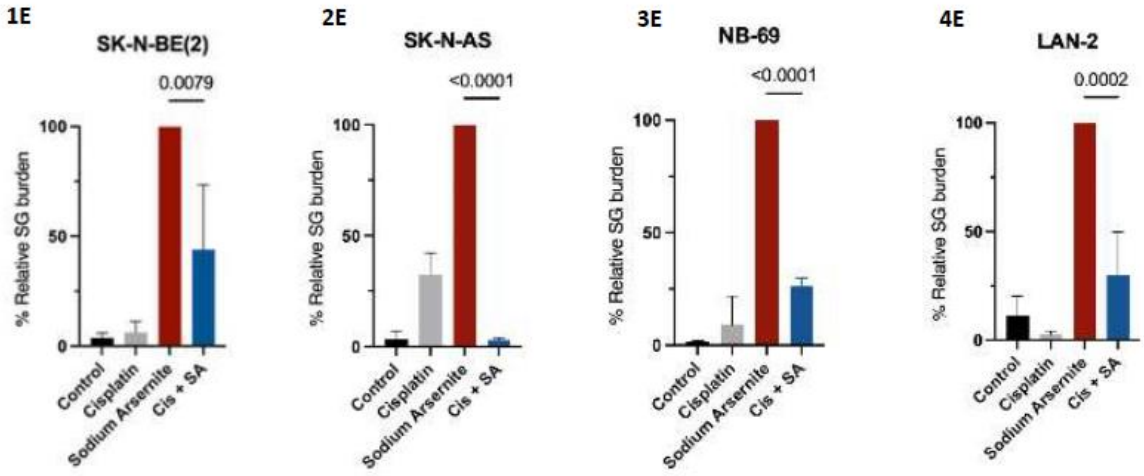

Figure. Cisplatin alters G3BP1-positive stress granule (SG) assembly in neuroblastoma cell lines and suppresses arsenite-induced SG formation.

(A–D) Representative immunofluorescence images of G3BP1 (green; SG marker) and DAPI (blue; nuclei) in four neuroblastoma cell lines treated with: untreated control, sodium arsenite (SA; 0.5 mM, 1 h), cisplatin (IC_{50} dose, 24 h), or cisplatin (IC_{50} dose, 24 h) followed by SA (0.5 mM, 1 h). Cisplatin IC_{50} concentrations were: (A) SK-N-BE (2), 3.84 μM; (B) SK-NAS, 6.24 μM; (C) NB-69, 1.12 μM; and (D) LA-N-2, 4.56 μM. (E) SG burden quantification.

G3BP1-positive puncta were counted per field and normalized to the number of DAPIstained nuclei in the same field (puncta per nucleus). Values are presented as relative SG burden, with the SA-only condition set to 100% for each cell line, enabling comparison of cisplatin and cisplatin plus SA effects within each line.

Discussion and conclusion

Our results indicate that cisplatin alters G3BP1 condensation behavior in neuroblastoma cells and, importantly, reduces the capacity to assemble canonical SGs in response to a subsequent acute stressor. Across both MYCN-amplified (SK-N-BE (2), LA-N-2) and MYCN nonamplified (SK-N-AS, NB-69) cell lines, cisplatin pre-treatment markedly suppressed SAinduced SG assembly, as reflected by a reduced SG burden (G3BP1 puncta per nucleus). This suggests that cisplatin can impair stress granule assembly competence, and that this effect is not restricted to MYCN status in this panel (although broader validation with additional lines would be required to make a definitive MYCN-based conclusion). A notable finding is that SG suppression persisted even when SG formation was driven by sodium arsenite, a canonical inducer. This pattern supports the idea that cisplatin acts upstream of, or at the level of, SG nucleation/assembly, rather than merely changing baseline SG abundance. Mechanistically, cisplatin's effects are likely multifactorial. Cisplatin has been reported to perturb RNA biology and translation control pathways that are central to SG formation, including steps in translation initiation and mRNA–protein interactions required for SG nucleation[9, 10]. One plausible model is that cisplatin induces a cellular state in which mRNAs and SG-nucleating proteins (e.g., G3BP1

complexes) are no longer available or competent to undergo the dynamic interactions needed for robust SG assembly. Under this model, SA exposure after cisplatin cannot fully restore canonical SG formation, consistent with the strong reduction observed in the Cis plus SA condition. The SK-N-AS response highlights an important difference. SK-N-AS displayed punctate G3BP1 structures after cisplatin alone, yet cisplatin still strongly suppressed SA-induced SG assembly. This raises the possibility that cisplatin triggers SG-like condensates that are compositionally incomplete or functionally distinct from canonical arsenite-induced SGs, consistent with prior reports describing cisplatin-induced "SG-like" assemblies that lack key SG components[13]. In this interpretation, the puncta observed in SK-N-AS under cisplatin may represent non-canonical condensates (or partially assembled granules) that do not reflect intact SG biology, and cisplatin may still compromise the cell's ability to assemble canonical SGs when challenged with SA. This distinction is important because SG function depends not only on puncta morphology but also on recruitment of core factors and RNAs[7, 12]. Cell viability and the potential confounding effects of cell death are important considerations when interpreting SG quantification. Although cisplatin treatment at IC_{50} concentration induces approximately 50% cell death, we took specific measures to ensure our observations were restricted to the viable cell population. All SG counts were normalized to the total number of intact DAPI-stained nuclei. Importantly, at the time of analysis, cisplatin-treated cells exhibited no morphological hallmarks of apoptosis, such as nuclear fragmentation or chromatin condensation. Therefore, the observed reduction in SG formation cannot be attributed to nonspecific effects of cellular degradation or impending cell death. The intact, viable cells in the cisplatin-treated groups exhibited a complete failure to form SGs upon SA induction, in stark contrast to the robust SG formation seen in the SA-only control. This strongly indicates that the inhibitory effect of cisplatin on SG assembly is a specific disruption of the SG assembly pathway, rather than a consequence of cell death. A limitation of our study is the reliance on G3BP1 as the sole marker for SG identification. Given that cisplatin may induce non-canonical condensates, G3BP1 alone may not capture the full spectrum of SG-like structures, particularly in the context of cisplatin treatment. To address this limitation, future studies should incorporate additional SG markers, such as TIA-1 and eIF4G, for co-localization analysis, to better define the identity of the condensates observed. Furthermore, the use of fixed-cell immunofluorescence (IF) at a single timepoint introduces the limitation that we cannot differentiate between SG non-formation and rapid SG disassembly, which may occur in cisplatin-treated cells. Rapid disassembly could contribute to the observed reduction in SGs, rather than a complete inhibition of SG formation. While we focused on fixed-cell analysis to establish a general effect of cisplatin on SG assembly, live-cell imaging could provide more dynamic, real-time insights into SG formation and disassembly. Although live-cell imaging is a powerful technique, it would require significant changes to the experimental setup and was beyond the scope of this study. Nonetheless, we propose that future studies employ live-cell imaging to explore the dynamics of SG formation and disassembly in greater detail. From a translational perspective, these data suggest that cisplatin may undermine a major stress-adaptation pathway in neuroblastoma cells. If SG formation supports survival under chemotherapy, then cisplatin-mediated suppression of SG assembly could contribute to cytotoxic efficacy.

Conversely, if some cells evade cisplatin-induced SG suppression (or form non-canonical condensates that preserve survival functions), SG biology may still represent a leverage point for overcoming chemoresistance. Future work should test these possibilities by linking SG suppression to cell-fate and stress-signaling pathways. Key next steps include: (i) validating condensate identity using additional SG markers (e.g., TIA-1, eIF3b) and colocalization, (ii) measuring translation status (e.g., puromycin incorporation or polysome profiling) and stress signaling (e.g., p-eIF2α), and (iii) assessing whether SG suppression correlates with apoptosis/viability under matched conditions. In summary, cisplatin reduces stress granule assembly capacity in neuroblastoma cells, evidenced by strong suppression of SA-induced G3BP1-positive SG burden after cisplatin pretreatment across both MYCN-amplified and non-amplified lines. The SK-N-AS line shows cisplatin-induced puncta but still exhibits marked inhibition of subsequent SA-induced SG formation, consistent with the possibility that cisplatin can promote non-canonical, incomplete SG-like assemblies while impairing formation of canonical SGs. These findings provide a foundation for mechanistic studies on how cisplatin perturbs SG biology and whether SG suppression contributes to therapeutic response or can be exploited to address chemoresistance in high-risk neuroblastoma.

References

1. Pinto, N.R., et al., Advances in Risk Classification and Treatment Strategies for Neuroblastoma. J Clin Oncol, 2015. 33(27): p. 3008-17.
2. Maris, J.M., Recent advances in neuroblastoma. N Engl J Med, 2010. 362(23): p. 2202-11.
3. Xu, Y., et al., LINC00460 promotes neuroblastoma tumorigenesis and cisplatin resistance by targeting miR-149-5p/DLL1 axis and activating Notch pathway in vitro and in vivo. Drug Deliv Transl Res, 2024. 14(7): p. 2003-2018.
4. Rosenberg, B., et al., Platinum compounds: a new class of potent antitumour agents. Nature, 1969. 222(5191): p. 385-6.
5. Makovec, T., Cisplatin and beyond: molecular mechanisms of action and drug resistance development in cancer chemotherapy. Radiol Oncol, 2019. 53(2): p. 148-158.
6. Adams, M.N., et al., Mechanisms of cisplatin resistance: DNA repair and cellular implications. 2014. p. 1-37.
7. Kedersha, N., P. Ivanov, and P. Anderson, Stress granules and cell signaling: more than just a passing phase? Trends Biochem Sci, 2013. 38(10): p. 494-506.
8. Buchan, J.R., Stress granule and P-body clearance: Seeking coherence in acts of disappearance. Semin Cell Dev Biol, 2024. 159-160: p. 10-26.
9. Li, T., et al., Role of stress granules in tumorigenesis and cancer therapy. Biochim Biophys Acta Rev Cancer, 2023. 1878(6): p. 189006.
10. Eum, H., et al., ATP-driven reactions are required for the assembly of large stress granules. Biochem Biophys Res Commun, 2020. 521(1): p. 238-244.
11. Weng, C.H., et al., Cisplatin-Induced Giant Cells Formation Is Involved in Chemoresistance of Melanoma Cells. Int J Mol Sci, 2020. 21(21).
12. Zhou, H., et al., Stress granules: functions and mechanisms in cancer. Cell Biosci, 2023. 13(1): p. 86.
13. Pietras, P., et al., Translation inhibition and suppression of stress granules formation by cisplatin. Biomed Pharmacother, 2022. 145: p. 112382.

Antiproliferative Activity of the PARP Inhibitor Olaparib in Cholangiocarcinoma Cells via G2/M Cell Cycle Arrest and Suppressed Rad51 DNA Repair

Wachirawit Siripattarapaisan[1], Karnchanok Kaimuangpak[1, 2], Piman Pocasap[1, 2], Auemduan Prawan[1, 2], Laddawan Senggunprai[1, 2], Rattanaporn Jaidee[1], Naruemon Busadee[1], Sarinya Kongpetch[1, 2, *]

[1] Department of Pharmacology, Faculty of medicine, Khon Kaen University, Khon Kaen 40002, Thailand
[2] Cholangiocarcinoma Research Institute, Khon Kaen University, Khon Kaen 40002, Thailand

Abstract

Cholangiocarcinoma (CCA) is an aggressive biliary tract malignancy characterized by poor clinical outcomes and limited responsiveness to standard chemotherapy. Recent genomic studies have identified DNA damage response (DDR) alterations in a significant subset of CCA patients, suggesting a potential vulnerability to poly(ADP-ribose) polymerase inhibitors (PARPi). This study investigated the antitumor effects and underlying mechanisms of the PARPi olaparib in CCA cell lines. Our results demonstrate that olaparib reduces cell viability in a dose-dependent manner, with the KKU-023 cell line exhibiting marked sensitivity (IC_{50} 11.0 μM) compared to the insensitive KKU-097 cells. A long-term proliferation assay confirmed that olaparib significantly suppresses colony-forming capacity in CCA cells. Mechanistically, while olaparib induced only modest levels of apoptosis, flow cytometric analysis revealed a robust, dose-dependent accumulation of cells in the G2/M phase. This cell cycle arrest was further supported by the upregulation of the cyclin-dependent kinase inhibitor p21 and the downregulation of G2/M regulatory proteins, specifically Cyclin A and Cyclin B1. Furthermore, high-dose olaparib treatment suppressed RAD51 expression, indicating impaired homologous recombination repair (HRR) and an accumulation of unrepaired DNA damage. Collectively, these findings suggest that olaparib exerts its antitumor effects in CCA primarily through the induction of G2/M arrest and the disruption of DNA repair mechanisms. This study provides a rational basis for the potential therapeutic application of PARPi in CCA harboring DDR vulnerabilities.

Keywords: Cholangiocarcinoma, PARP inhibitor, DNA damage repair, homologous recombination, cell-cycle arrest

Introduction

Cholangiocarcinoma (CCA) is an aggressive biliary tract malignancy characterized by chemoresistance and poor clinical prognosis. The current standard-of-care first-line therapy, gemcitabine plus cisplatin, yields only modest survival benefits, underscoring the imperative for novel targeted interventions.[1] Genomic profiling has identified significant genomic instability in CCA, with approximately 29% of patients harboring alterations in DNA damage response (DDR) genes.[2-4] These molecular signatures suggest a potential therapeutic vulnerability within the DNA repair machinery.

PARP is essential for the repair of single-strand DNA breaks (SSBs). PARPi exert antitumor activity by inhibiting PARylation and promoting PARP-DNA trapping, which ultimately leads to replication fork collapse and the accumulation of lethal double-strand breaks (DSBs).[5, 6] In tumors with homologous recombination repair (HRR) deficiency, specifically those with BRCA1/2 mutations, this unrepaired damage triggers synthetic lethality.[7]

The clinical utility of PARPi is well-established across various HRR-deficient malignancies. Olaparib first gained approval for germline BRCA-mutated ovarian cancer following evidence of superior progression-free survival (PFS) in platinum-sensitive disease, while rucaparib and veliparib have exhibited similar efficacy.[7-10] In breast cancer, talazoparib significantly improved PFS in patients with HER2-negative metastatic disease and germline *BRCA* mutations.[11] Furthermore, PARPi has expanded the therapeutic landscape for prostate cancer, where BRCA and other DDR alterations serve as predictive biomarkers.[12] Preclinical evidence in pancreatic cancer models with BRCA1 and ATM mutations further supports the ability of PARPi to disrupt DNA repair and induce apoptosis.[13] Despite these advancements, the clinical application of PARPi in CCA remains unapproved.

Given the prevalence of DDR alterations in biliary tract cancers and the established success of PARPi in other HRR-deficient tumors, targeting PARP represents a rational therapeutic strategy for CCA. However, the exact antitumor mechanisms and cellular responses to PARP inhibition in this context remain poorly characterized. In this study, we investigated the impact of PARPi on cell proliferation, apoptosis, and cell cycle dynamics in CCA cell lines to evaluate its potential as a targeted therapy.

Methods

Chemicals and reagents

Ham's F12 medium and 0.25 % trypsin-EDTA were purchased from Gibco BRL Life Technologies (Grand Island, NY, USA). Fetal bovine serum (FBS) and penicillin-streptomycin solution were purchased from Cytiva HyClone (Kremplstrasse, Pasching, Austria). Cell Counting Kit-8 (CCK-8) kit was purchased from TargetMol (Boston, MA, USA). Halt™ protease and phosphatase inhibitor cocktail and RIPA lysis buffer were purchased from Thermo Scientific™ (Waltham, MA, USA). FITC Annexin V apoptosis detection kit (556547) was obtained from BD Pharmigen™ (San Jose, California, USA). Bovine serum albumin (BSA) was obtained from Capricorn Scientific (Ebsdorfergrund, Hesse, Germany). Polyvinylidene fluoride (PVDF) membranes and Luminata™ Forte Western HRP substrates were obtained from Merck Millipore Corporation (Billerica, MA, USA). Mouse anti-Cyclin B1 monoclonal antibody (sc-245), rabbit anti-Cyclin A monoclonal antibody (sc-751), and mouse HRP-conjugated anti-β-Actin antibody (sc-47778) were obtained from Santa Cruz Biotechnology (Dallas, Texas, USA). Rabbit anti-RAD51 polyclonal antibody (DF8066) was obtained from Affinity Biosciences (Cincinnati, Ohio, USA) and Mouse anti-p21 monoclonal antibody (2946S) was obtained from Cell Signaling Technology (Danvers, Massachusetts, USA).

Cell culture

CCA cell lines KKU-023 and KKU-097, which are *BRCA1*-deficient, were established at the Cholangiocarcinoma Research Institute (CARI), Khon Kaen University, as previously reported.[14] The cells were cultured in Ham's F12 nutrient mixture supplemented with 10% (v/v) FBS, 10 mM HEPES (pH 7.4), 100 μg/mL streptomycin, and 100 U/mL penicillin. All CCA cell lines were maintained at 37°C in a humidified incubator with 5% CO_2. Cells were routinely passaged upon reaching 70–80% confluence using 0.25% trypsin-EDTA.

Cell Viability Assay (CCK-8)

The effects of olaparib on cell viability were evaluated using the CCK-8 assay. CCA cells were seeded into 96-well plates at about 7,500-10,000 cells and allowed to adhere overnight. Cells were then treated with various concentrations of olaparib (0, 0.2, 2, 20 and 40 μM for KKU-023 and 0, 0.2, 2, 4, 8, 16 and 32 μM for KKU-097 cells) for 72 hours. Following treatment, 10 μL of CCK-8 reagent diluted in 100 μL of serum-free medium was added to each well. The plates were incubated at 37°C for 1–3 hours to allow viable cells to reduce the WST-8 substrate into a water-soluble formazan dye. Absorbance was measured at 450 nm using a microplate reader. Cell viability in each treatment group was calculated as a percentage relative to the untreated control.

Clonogenic Assay

The clonogenic assay was performed to assess the long-term survival and proliferative capacity of CCA following olaparib treatment. Cells were seeded at a low density (50–200 cells per well) in 6-well plates and incubated overnight to allow attachment. Cells were treated with olaparib for 72 hours. After that, the medium was replaced with fresh drug-free medium, and cells were maintained for 14 days to allow colony formation, with medium changes every 2–3 days. At the end of the incubation period, colonies were fixed with absolute methanol at 4°C for 10 minutes, then stained with 0.5% crystal violet for 10 minutes. Excess stain was removed by washing with tap water, and plates were air-dried overnight. Colonies were imaged and quantified using ImageJ software.

Apoptosis Analysis (annexin V-FITC/PI staining)

Apoptosis was analyzed using Annexin V and propidium iodide (PI) staining followed by flow cytometry. CCA were seeded in 6-well plates (2.5×10^5 cells/well) and treated with olaparib for 72 hours. Cells were harvested, washed with cold PBS, and resuspended in 1x binding buffer. Cells were stained with annexin V-FITC/PI, then incubated at room temperature in the dark for 0.5-1 hour and diluted with 1x binding buffer for analysis. Samples were kept on ice and analyzed by flow cytometry to quantify viable, early apoptotic, late apoptotic, and necrotic cell populations.

Cell Cycle Analysis (PI staining)

Cell cycle distribution was determined by PI staining and flow cytometry. Cells were seeded in 6-well plates (2.5×10^5 cells/well) and treated with olaparib for 72 hours. Cells were collected, washed with cold PBS, and fixed in 70% ethanol at 4°C. After fixation, cells were washed and incubated with PI staining solution containing RNase A and Triton X-100 for 1 h at 4°C in the dark. The DNA content was analyzed by flow cytometry, and the percentages of cells in sub G1, G0/G1, S, and G2/M phases were quantified.

Western blot analysis

Following treatment with olaparib (0, 5, 10, and 20 μM) for 72 h, cells were harvested and lysed in ice-cold RIPA buffer supplemented with protease inhibitor cocktail. Cell lysates were incubated on ice for 30 min and centrifuged at 12,000 rpm for 20–30 min at 4 °C to remove cell debris. Protein concentrations were determined using a Bradford assay. Equal amounts of protein (20–30 μg per lane) were separated on 10% SDS–polyacrylamide gels and subsequently transferred onto PVDF membranes. Membranes were blocked with 5% non-fat milk in TBST for 2 h at room temperature, then incubated overnight at 4 °C with primary antibodies against Cyclin A, Cyclin B1, p21, RAD51, and β-actin. After washing with TBST, membranes were incubated with horseradish peroxidase–conjugated secondary antibodies for 1–2 hours at room temperature. Protein bands were visualized using enhanced chemiluminescence reagents and detected. β-actin was used as a loading control. Representative results from at least three independent experiments are shown.

Results

To evaluate the sensitivity of cholangiocarcinoma (CCA) to PARP inhibition, the effect of olaparib on cell viability was investigated in KKU-023 and KKU-097 cell lines. Olaparib treatment induced a robust, dose-dependent reduction in the viability of KKU-023 cells, with survival decreasing to approximately 30% at a concentration of 40 μM. The calculated half-maximal inhibitory concentration (IC50) for KKU-023 was 11.0 ± 1.03 μM (**Figure 1A**). In contrast, KKU-097 cells exhibited a markedly less sensitive phenotype; cell viability remained high (75–80%) even at the maximum tested concentrations **(Figure 1B)**. These data indicate a significant disparity in cytotoxic responsiveness to olaparib between the two CCA models despite their shared molecular backgrounds.

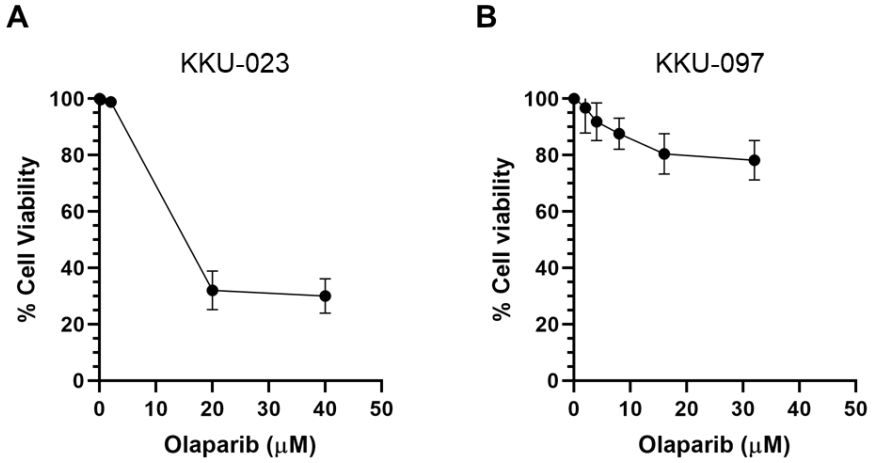

Figure 1. Effect of olaparib on cell viability in CCA cells. (A) KKU-023 and (B) KKU-097 cells were treated with various concentrations of olaparib for 72 hours, and cell viability was measured by CCK-8 assay. The quantitative plots were expressed as mean ± SD (n=3).

Given their marked sensitivity to olaparib, KKU-023 cells were prioritized for downstream investigation. The long-term impact of olaparib on cell survival was quantified via clonogenic assay, which revealed a dose-dependent decline in colony-forming ability

(**Figure 2A-B**). Specifically, treatment with 5 and 10 μM olaparib significantly reduced colony survival to approximately 60% and 40%, respectively, relative to the control group. Although a modest increase in colony formation was noted at lower concentrations (0.5–1.0 μM), the overall findings support a potent, concentration-dependent suppression of CCA cell proliferation following PARP inhibition.

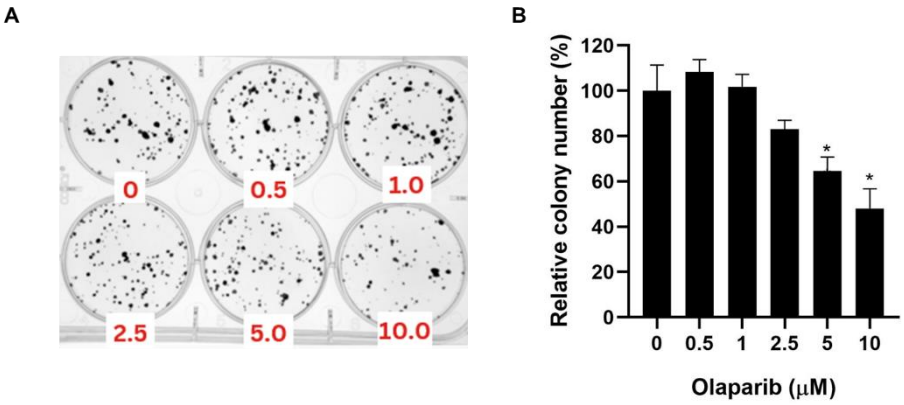

Figure 2. Effect of olaparib on colony formation in KKU-023 cells. (A) Crystal violet staining of KKU-023 treated with olaparib at 0, 0.5, 1, 2.5, 5, and 10 μM for 14 days. (B) Quantification of colony formation, expressed as mean ± SD (n=3). *$p < 0.05$ compared to untreated control.

To evaluate the pro-apoptotic potential of PARP inhibition, KKU-023 cells were treated with escalating concentrations of olaparib, followed by flow cytometric analysis. Exposure to 5 and 10 μM olaparib failed to induce significant apoptosis; however, treatment with 20 μM olaparib resulted in a statistically significant increase in apoptotic cell death, albeit at a relatively low level of approximately 10% (**Figure 3A-B**). These observations suggest that while olaparib can trigger cytotoxic effects, apoptotic induction may not represent the primary mechanism underlying its gro*WT*h-suppressive effects in CCA cells.

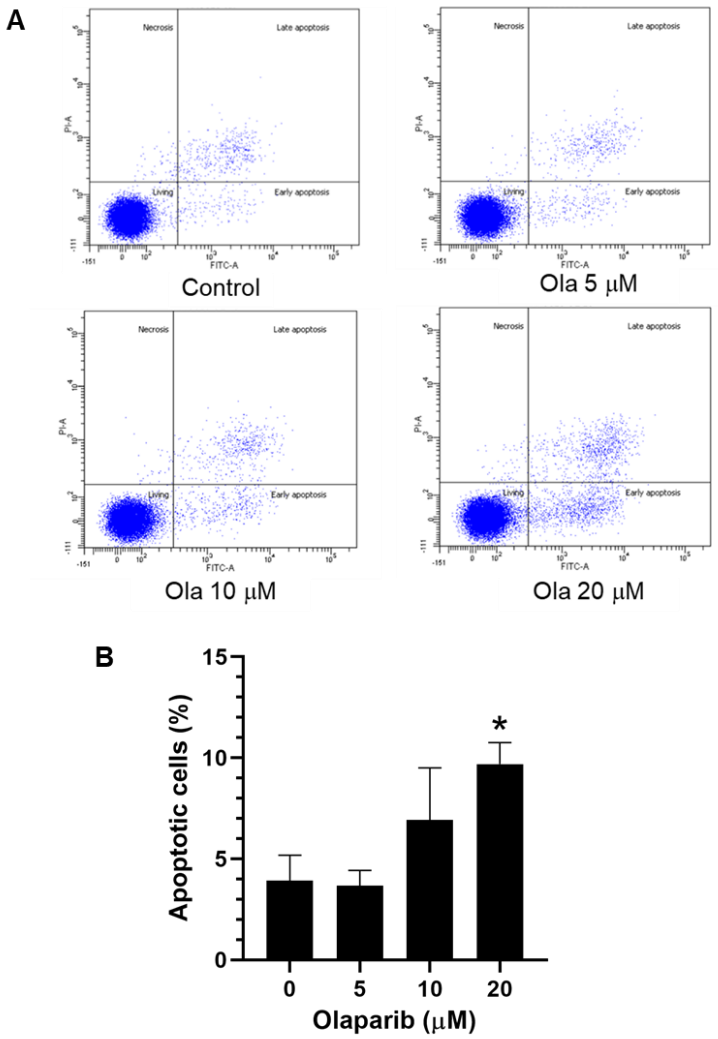

Figure 3. Effect of olaparib (Ola) on apoptotic cell death in KKU-023 cells. (A) Apoptosis was quantified by flow cytometry using annexin V-FITC/PI staining. (B) The bar graph shows the proportion of apoptotic cells after olaparib treatment, expressed as mean ± SD (n=3). *p < 0.05 compared to untreated control.

To further elucidate the mechanistic basis of olaparib-mediated gro*WT*h inhibition in CCA, cell cycle distribution was analyzed in KKU-023 cells using flow cytometry. Treatment with olaparib resulted in concentration-dependent shifts in the cell cycle profile (**Figure 4A-B**). Specifically, compared to untreated controls, olaparib exposure led to a progressive reduction in the G1 phase population, which was characterized by a concomitant and significant accumulation of cells in the G2/M phase. This G2/M fraction increased to approximately 20% and 30% following treatment with 10 µM and 20 µM olaparib, respectively. Notably, while a modest increase in the sub-G1 population, indicative of cell death was observed at the 20 µM dose, the proportion of cells in the S-phase remained largely unchanged across all treatment groups. These findings suggest that olaparib primarily exerts its antiproliferative effects in CCA cells by triggering robust G2/M phase arrest.

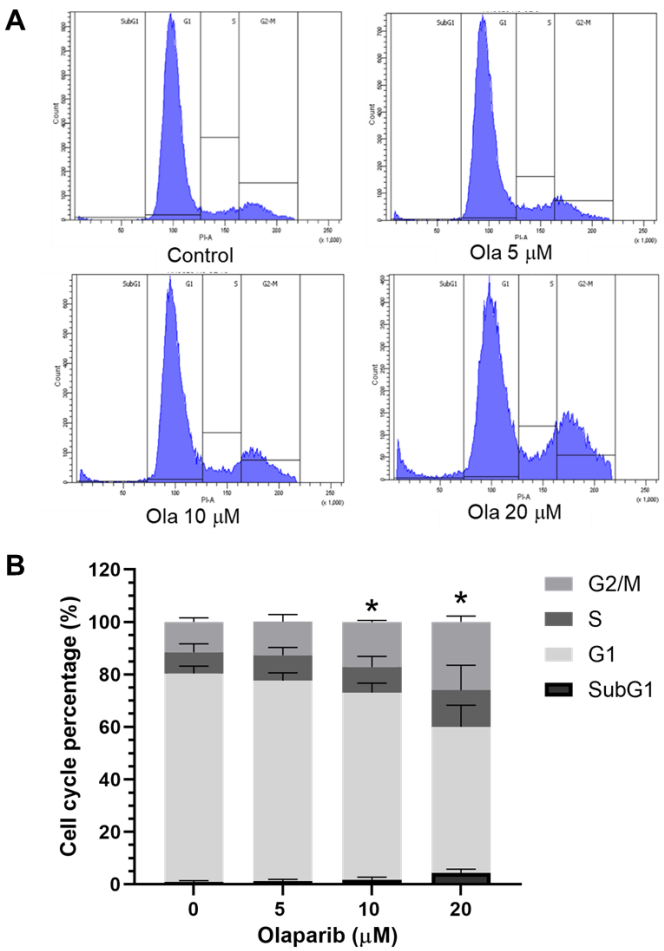

Figure 4. The effect of olaparib (Ola) on cell-cycle progression in KKU-023 cells. (A) Histogram plots show cell cycle analysis and the percentage of cells in each phase (SubG1, G1, S, G2/M). (B) The bar graph presented quantitative analysis of the cell cycle, as mean ± SD (n=3). *$p < 0.05$ versus untreated control.

To validate the cell cycle arrest observed via flow cytometry, we analyzed the expression of key regulatory proteins Cyclin A, Cyclin B1, and p21, using immunoblotting. At a concentration of 20 μM, olaparib markedly suppressed the expression of Cyclin A and Cyclin B1. Interestingly, p21 levels were consistently upregulated across all tested concentrations, suggesting a robust activation of the p21-mediated DNA damage checkpoint (**Figure 5**). These molecular alterations confirm a disruption of G2/M transition, consistent with the observed arrest in cell cycle progression.

Furthermore, we assessed the impact of olaparib on RAD51, a central mediator of HRR. While low-dose olaparib (5 and 10 μM) induced a modest increase in RAD51 expression, potentially reflecting a compensatory cellular response to accumulated DNA damage, the 20 μM dose resulted in a notable reduction of RAD51 (**Figure 5**). This concentration-dependent suppression highlights an eventual collapse of the DNA repair machinery, reinforcing the antiproliferative activity of olaparib in CCA.

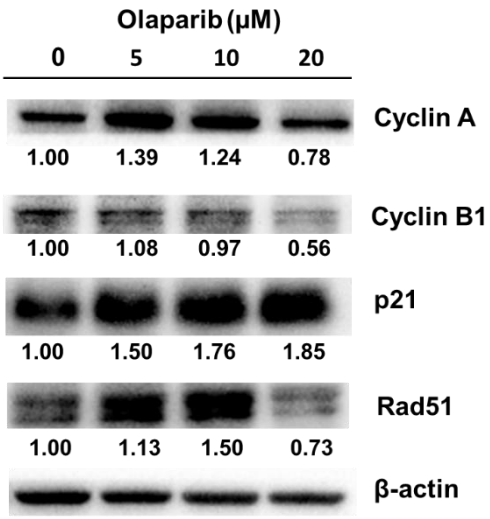

Figure 5. Effects of olaparib on protein-related cell cycle and DNA repair. Representative western blots show expression of key cell cycle regulatory proteins: cyclin A, cyclin B1, p21, and DNA repair protein Rad51, following olaparib treatment. The relative expression levels of a specific protein compared to β-actin from three independent experiments.

Discussion

PARPi represent a sophisticated class of targeted therapy designed to exploit deficiencies in the DNA damage response (DDR) machinery. While PARPi have gained regulatory approval for various BRCA1/2-mutated malignancies, their therapeutic potential in cholangiocarcinoma (CCA) remains under-investigated despite a subset of patients harboring similar genomic vulnerabilities. This study aimed to bridge this gap by characterizing the impact of the PARPi olaparib on cell proliferation, apoptotic induction, and cell cycle dynamics in CCA cell models.

In the principle of synthetic lethality, tumors with homologous recombination deficiency (HRD) are more susceptible to PARP inhibition.[7] Previous studies using patient-derived organoids have demonstrated that mutations in *BRCA1/2* and other DDR genes, such as *RAD54L*, *BRIP1*, and *ATR*, confer high sensitivity to olaparib.[15] Intriguingly, our results revealed a more nuanced response. Despite both KKU-023 and KKU-097 cell lines harboring the same BRCA1 mutation, they exhibited disparate sensitivities; KKU-023 cells were highly susceptible to olaparib, whereas KKU-097 cells were relatively insensitive. This phenotypic divergence suggests that BRCA status alone may not be a definitive predictor of response in CCA, pointing toward a significant degree of molecular heterogeneity and potentially the existence of BRCA1-independent resistance mechanisms. Nevertheless, in the sensitive KKU-023 cells, clonogenic assays confirmed that olaparib exerted sustained, long-term suppression of proliferative capacity. Similar findings have been reported in *BRCA*-mutant ovarian and breast cancer models treated with PARPi, where persistent DNA damage prevents colony formation.[7, 11, 16]

While apoptosis is a primary pathway of cell death following PARP inhibition, the moderate level of apoptotic induction observed in our CCA models suggests that alternative mechanisms, such as checkpoint-mediated cell cycle arrest, may also contribute.

Mechanistically, PARPi promote PARP trapping and the accumulation of replication-associated double-strand breaks (DSBs).[5, 6] When these lesions remain unrepaired due to HRD, they trigger substantial replication stress and activate the G2/M DNA damage checkpoint.[6]

In this study, olaparib treatment led to a significant G2/M phase accumulation in KKU-023 cells, characterized by the downregulation of Cyclin A and Cyclin B1 and the concomitant upregulation of the cyclin-dependent kinase inhibitor p21. This molecular profile is a hallmark of impaired G2/M transition and has been similarly observed in triple-negative breast cancer cell lines (MDA-MB-231 and CAL51) treated with olaparib.[16] Our findings therefore support the notion that DNA damage checkpoint activation constitutes a primary mechanism governing the gro*WT*h-suppressive efficacy of olaparib in CCA.

The role of RAD51 is critical in this context, as it is a key mediator of genomic stability through the HRR pathway.[17] Suppression of RAD51 can sensitize cells to PARPi by effectively inducing a "BRCA-ness" phenotype, thereby amplifying synthetic lethality.[7] For example, RAD51C deficiency has been proposed as a predictive biomarker for olaparib sensitivity in the gastric cancer-xenograft model.[18] Our results demonstrate a dose-dependent response in RAD51 expression: lower concentrations of olaparib appeared to trigger a compensatory increase in RAD51, likely as a survival response to repair emerging DNA damage. However, high-dose olaparib treatment successfully suppressed RAD51 expression, suggesting a threshold at which the HRR machinery is overwhelmed, thereby enhancing cytotoxicity. This observation is consistent with previous reports showing that while olaparib alone may induce RAD51 foci formation, combination therapies (e.g., with carboplatin) or high-dose regimens can abrogate this response, leading to a profound loss of repair capacity.[16]

Conclusion

Our findings underscore the therapeutic potential of olaparib in cholangiocarcinoma, characterized by significant antiproliferative effects and the suppression of clonogenic survival. We showed that PARP inhibition triggers robust G2/M arrest via the modulation of Cyclin A, Cyclin B1, and p21, while simultaneously impairing DNA repair through the downregulation of RAD51. These results suggest that targeting the DNA damage response is a viable strategy in CCA, providing a clear rationale for further investigation into personalized PARPi-based interventions for patients harboring DNA repair deficiencies.

Acknowledgement

This study was funded by the Fundamental Fund of KKU from National Science, Research and Innovation Fund (NSRF), Thailand. Wachirawit Siripattarapaisan received additional support through the Postgraduate Study Support Grant from the Faculty of Medicine, KKU.

References

1. Valle J, Wasan H, Palmer DH, Cunningham D, Anthoney A, Maraveyas A, Madhusudan S, Iveson T, Hughes S, Pereira SP, Roughton M, Bridgewater J, Investigators ABCT. Cisplatin plus gemcitabine versus gemcitabine for biliary tract cancer. N Engl J Med. 2010;362(14):1273-81.
2. Chae H, Kim D, Yoo C, Kim KP, Jeong JH, Chang HM, Lee SS, Park DH, Song TJ, Hwang S, Kim KH, Song GW, Ahn CS, Lee JH, Hwang DW, Kim SC, Jang SJ, Hong SM, Kim TW, Ryoo BY. Therapeutic relevance of targeted sequencing in management of patients with advanced biliary tract cancer: DNA damage repair gene mutations as a predictive biomarker. Eur J Cancer. 2019;120:31-9.
3. Lin J, Shi J, Guo H, Yang X, Jiang Y, Long J, Bai Y, Wang D, Yang X, Wan X, Zhang L, Pan J, Hu K, Guan M, Huo L, Sang X, Wang K, Zhao H. Alterations in DNA Damage Repair Genes in Primary Liver Cancer. Clin Cancer Res. 2019;25(15):4701-11.
4. Yu H, Xu Y, Gao W, Li M, He J, Deng X, Xing W. Comprehensive germline and somatic genomic profiles of Chinese patients with biliary tract cancer. Front Oncol. 2022;12:930611.
5. Murai J, Huang SY, Das BB, Renaud A, Zhang Y, Doroshow JH, Ji J, Takeda S, Pommier Y. Trapping of PARP1 and PARP2 by Clinical PARP Inhibitors. Cancer Res. 2012;72(21):5588-99.
6. Rose M, Burgess JT, O'Byrne K, Richard DJ, Bolderson E. PARP Inhibitors: Clinical Relevance, Mechanisms of Action and Tumor Resistance. Front Cell Dev Biol. 2020;8:564601.
7. Lord CJ, Ashworth A. PARP inhibitors: Synthetic lethality in the clinic. Science. 2017;355(6330):1152-8.
8. Ledermann J, Harter P, Gourley C, Friedlander M, Vergote I, Rustin G, Scott C, Meier W, Shapira-Frommer R, Safra T, Matei D, Macpherson E, Watkins C, Carmichael J, Matulonis U. Olaparib maintenance therapy in platinum-sensitive relapsed ovarian cancer. N Engl J Med. 2012;366(15):1382-92.
9. Oza AM, Tinker AV, Oaknin A, Shapira-Frommer R, McNeish IA, Swisher EM, Ray-Coquard I, Bell-McGuinn K, Coleman RL, O'Malley DM, Leary A, Chen LM, Provencher D, Ma L, Brenton JD, Konecny GE, Castro CM, Giordano H, Maloney L, Goble S, Lin KK, Sun J, Raponi M, Rolfe L, Kristeleit RS. Antitumor activity and safety of the PARP inhibitor rucaparib in patients with high-grade ovarian carcinoma and a germline or somatic BRCA1 or BRCA2 mutation: Integrated analysis of data from Study 10 and ARIEL2. Gynecol Oncol. 2017;147(2):267-75.
10. Coleman RL, Fleming GF, Brady MF, Swisher EM, Steffensen KD, Friedlander M, Okamoto A, Moore KN, Efrat Ben-Baruch N, Werner TL, Cloven NG, Oaknin A, DiSilvestro PA, Morgan MA, Nam JH, Leath CA, 3rd, Nicum S, Hagemann AR, Littell RD, Cella D, Baron-Hay S, Garcia-Donas J, Mizuno M, Bell-McGuinn K, Sullivan DM, Bach BA, Bhattacharya S, Ratajczak CK, Ansell PJ, Dinh MH, Aghajanian C, Bookman MA. Veliparib with First-Line Chemotherapy and as Maintenance Therapy in Ovarian Cancer. N Engl J Med. 2019;381(25):2403-15.
11. Litton JK, Rugo HS, Ettl J, Hurvitz SA, Goncalves A, Lee KH, Fehrenbacher L, Yerushalmi R, Mina LA, Martin M, Roche H, Im YH, Quek RGW, Markova D, Tudor IC, Hannah AL, Eiermann W, Blum JL. Talazoparib in Patients with Advanced Breast Cancer and a Germline BRCA Mutation. N Engl J Med. 2018;379(8):753-63.
12. Zhang Z, Diao L, Zhang C, Wang F, Guan X, Yao X. Use of PARP inhibitors in prostate cancer: from specific to broader application. Front Endocrinol (Lausanne). 2023;14:1164067.
13. Gout J, Perkhofer L, Morawe M, Arnold F, Ihle M, Biber S, Lange S, Roger E, Kraus JM, Stifter K, Hahn SA, Zamperone A, Engleitner T, Muller M, Walter K, Rodriguez-Aznar E, Sainz B, Jr., Hermann PC, Hessmann E, Muller S, Azoitei N, Lechel A, Liebau S, Wagner M, Simeone DM, Kestler HA, Seufferlein T, Wiesmuller L, Rad R, Frappart PO, Kleger A.

Synergistic targeting and resistance to PARP inhibition in DNA damage repair-deficient pancreatic cancer. Gut. 2021;70(4):743-60.
14. Jaidee R, Jusakul A, Pocasap P, Kukongviriyapan V, Senggunprai L, Prawan A, Loilome W, Titapun A, Jareanrat A, Thanasukarn V, Khuntikeo N, Namwat N, Chamgramol Y, Thanee M, Wichian P, Hong JH, Guan P, Heng HL, Pairojkul C, Teh BT, Kongpetch S. Establishment and genomic profiling of cholangiocarcinoma cells with functional characterization. Sci Rep. 2025;15(1):8621.
15. Li Y, Tang S, Wang H, Zhu H, Lu Y, Zhang Y, Guo S, He J, Li Y, Zhang Y, Shi X, Miao Y, Zhong C, Zhu Y, Ju Y, Liu Y, Sun M, Wang Y, Chen L, Zhou H, Jin G, Gao D. A pancreatic cancer organoid biobank links multi-omics signatures to therapeutic response and clinical evaluation of statin combination therapy. Cell Stem Cell. 2025;32(9):1369-89 e14.
16. Zhao H, Yang Q, Hu Y, Zhang J. Antitumor effects and mechanisms of olaparib in combination with carboplatin and BKM120 on human triple-negative breast cancer cells. Oncol Rep. 2018;40(6):3223-34.
17. Laurini E, Marson D, Fermeglia A, Aulic S, Fermeglia M, Pricl S. Role of Rad51 and DNA repair in cancer: A molecular perspective. Pharmacol Ther. 2020;208:107492.
18. Min A, Im SA, Yoon YK, Song SH, Nam HJ, Hur HS, Kim HP, Lee KH, Han SW, Oh DY, Kim TY, O'Connor MJ, Kim WH, Bang YJ. RAD51C-deficient cancer cells are highly sensitive to the PARP inhibitor olaparib. Mol Cancer Ther. 2013;12(6):865-77.

Investigation of the Genotoxic Effects of Anti-Hepatitis B Virus Drugs and the Involvement of BRCA1 in DNA Damage Repair Pathways

Sathida Liekwannacharoen[1] , Rakkreat Wikiniyadhanee[1] , Tassanee Lerksuthirat[2] , Sermsiri Chitphuk[2] , Donniphat Dejsuphong[1*]

[1]Program in Translational Medicine, Faculty of Medicine Ramathibodi Hospital, Mahidol University, Bangkok, Thailand xxxxxxxxxxxxxxxxxxxxxxxxxxxrt 5555555555d33g4n t+
[2]Research Center, Faculty of Medicine Ramathibodi Hospital, Mahidol University, Bangkok, Thailand

Abstract

Hepatitis B virus (HBV) infection remains a major global health concern, and nucleos(t)ide analogues (NAs) are widely used for long-term suppression of HBV replication. FDA-approved NAs for HBV treatment includes entecavir (ETV), adefovir dipivoxil (ADV), lamivudine (3TC), telbivudine (TBV), and tenofovir disoproxil fumarate (TDF). However, their potential genotoxic effects and the role of the DNA repair pathway in responding to druginduced damage remain incompletely understood. This study aimed to investigate the genotoxic effects of ETV, ADV, 3TC and TBV and to evaluate the role of BRCA1 in repairing antiviral drug-induced DNA damage. TK6 wild-type (*WT*) and breast cancer type 1 susceptibility protein conditional knockout (BRCA1$^{AID/AID}$) cells were used to assess cell viability and DNA damage response following drug treatment. Cytotoxic effects were determined by IC50 analysis, while DNA damage was evaluated by immunofluorescence staining of γ-H2AX , a marker of DNA double-strand breaks (DSBs), together with geminin as a marker of S/G2-phase cells. ETV and ADV reduced cell viability in a dose-dependent manner, with BRCA1$^{AID/AID}$ cells exhibiting greater sensitivity than *WT* cells, whereas 3TC and TBV did not show detectable cytotoxicity under the tested conditions. Notably, ADV exhibited greater toxicity than ETV, as reflected by lower IC50 values and higher γ-H2AX levels. BRCA1$^{AID/AID}$ cells also showed an increased rate of γ-H2AX foci formation following ETV and ADV treatment. In addition, γ-H2AX signals were more persistent in BRCA1$^{AID/AID}$ cells than in *WT* cells, indicating delayed resolution of ETV- and ADV-induced DNA damage. Overall, these findings suggest that BRCA1 plays an important role in facilitating recovery from ETV- and ADV-induced DNA DSBs and that BRCA1 deficiency increases cellular sensitivity to ETV and ADV. This study provides insight into the differential cellular response to NAs and highlights the importance of BRCA1 repair pathway in maintaining genomic stability during antiviral-HBV treatment.

Keywords: Nucleos(t)ide analogues, Antiviral drugs, HBV, DNA damage, DNA repair, BRCA1

Introduction

Hepatitis B virus (HBV) infection remains a major global health concern, affecting hundreds of millions of people worldwide[1] and contributing to the development of chronic liver disease cirrhosis, and hepatocellular carcinoma[2]. Antiviral therapy using nucleos(t)ide analogues (NAs) is a key strategy in the treatment of HBV, as these agents effectively suppress viral replication. Clinically approved NAs include entecavir (ETV), adefovir dipivoxil (ADV), lamivudine (3TC), telbivudine (TBV), and tenofovir disoproxil fumarate (TDF)[3]. Although these drugs are generally considered safe, their effects on host DNA damage responses and the involvement of DNA repair pathways in resolving antiviral drug-induced DNA damage remain unclear.

NAs function by mimicking natural nucleotides and inhibiting viral reverse transcriptase, thereby interfering with viral DNA synthesis. After intracellular phosphorylation to their active forms, these compounds compete with endogenous deoxynucleoside triphosphates (dNTPs) and may be incorporated into viral DNA, leading to chain termination[4]. Genotoxic stress can arise from various types of DNA lesions, including single-strand breaks (SSBs) and double-strand breaks (DSBs), which may result from exposure to genotoxic agents or replication-associated stress. If such DNA damage is unrepaired or not properly repaired, it can lead to genomic instability[5]. BRCA1 is a key DNA repair protein that plays a central role in homologous recombination (HR), a high-fidelity pathway required for the repair of DSBs and maintenance of genome integrity[6]. One of the earliest markers of DSBs signaling is the phosphorylation of histone variant H2AX (γ -H2AX), which occurs rapidly at sites of DSBs[7]. γ -H2AX plays a crucial role in recruiting and activating DNA repair proteins at sites of damage[8]. Efficient resolution of DNA damage is essential to maintain genomic stability, and defects in DNA repair pathways can increase cellular sensitivity to genotoxic stress. Liu H et al. reported that antiviral drug namely ADV[9], which is widely used in the treatment of HBV infection, induced genotoxic effects in both TK6 wild type (*WT*) and DT40 cell lines, including *WT* and breast cancer type 1 susceptibility protein knockout (BRCA1$^{-/-}$) cell. DNA damage was assessed using cell viability assays, chromosome aberration analysis and immunofluorescence detection of γ-H2AX foci as a marker of DNA DSBs. Their results demonstrated that ADV significantly increased DNA DSBs and chromosomal abnormalities. Moreover, DT40 BRCA1$^{-/-}$ cells exhibited enhanced sensitivity to ADV compared with *WT* cells, indicating the critical role of BRCA1 in repairing ADV-induced damage. Similarly, ETV has also been reported to induce DNA damage[10], particularly in DNA repair-deficient cell lines such as PARP1 knockout (PARP1$^{-/-}$), BRCA1$^{-/-}$, RAD18 knockout (RAD18$^{-/-}$). These findings suggest that certain anti-HBV NAs may exert genotoxic effects in vitro, particularly under conditions of impaired DNA repair capacity. While TBV and 3TC have been associated with mitochondrial DNA depletion[11, 12]. In contrast, TDF has shown a comparatively lower level of reported genotoxicity. In this study, we focused on four NAs commonly used for the treatment of HBV infection: ETV, ADV, 3TC, and TBV. We aimed to investigate the genotoxic effects of these agents and to determine whether BRCA1 deficiency influences cellular tolerance to antiviral NAs drug-induced DNA damage. Initially, we assessed cytotoxicity in *WT* and breast cancer

type 1 susceptibility protein conditional knockout (BRCA1$^{AID/AID}$) cells by determining their IC_{50} values. We then performed immunofluorescence analysis using γ-H2AX to evaluate DNA DSBs and its repair kinetics. Comparative analysis of *WT* and BRCA1$^{AID/AID}$ provides mechanistic insight into the role of BRCA1 in DNA damage response and repair pathways involved in NAs-induced DNA damage.

Methods

1. Drugs

ADV, 3TC and TBV were purchased from the MedChemExpress, ADV (cat. no. HYB0255), 3TC (cat. no. HY-B0017), and TBV (cat. no. HY-B0250). ETV was purchased from Sigma-Aldrich (cat no. SML1103-10MG). All drugs were dissolved in dimethyl sulfoxide (DMSO).

2. Cell lines and cell culture

Human lymphoblastoid TK6-derived *WT* and BRCA1$^{AID/AID}$ cells were provided by Professor Shunichi Takeda (Department of Radiation Genetics, Graduate School of Medicine, Kyoto University). Cells were cultured in RPMI-1640 medium (cat no. SH3002702; HyClone) supplemented with 5 % horse serum (cat no. 1TFS-1RS-16050122; Gibco), 200mg/ml sodium pyruvate (cat no. SIA-S8636-100ML; Sigma-Aldrich), and 100U/ml penicillin/streptomycin (cat no. SIA-P0781-100mL; Sigma-Aldrich). Cells were maintained in suspension culture at 37°C in a humidified incubator with 5 % CO_2. The BRCA1$^{AID/AID}$ cells line was engineered by tagging the miniauxin-induced degron (mAID) into the C-terminal end of the BRCA1 gene[13]. To conditionally disrupt BRCA1 gene expression for in vitro experiments, BRCA1$^{AID/AID}$ cells were cultured in the medium containing 250 μM 3-indoleacetic acid (auxin, cat. no. SIA-I2886- sG; Sigma-Aldrich) for 2 hr before exposing to drugs and for entire experiments.

3. Cell viability assay

Cell viability was quantified using CellTiter-Glo® Luminescent Cell Viability Assay (cat. no. G7572; Promega). *WT* were seeded in 96-well plates at a density of 2,500 cells/well in 200 μL and BRCA1$^{AID/AID}$ cells using 10,000 cells/well in 200 μL. Cells were treated with ADV, ETV, TBV, and 3TC at the indicated concentrations for 72 hr. Luminescence data were measured using a microplate reader and dose-response curves were analyzed using GraphPad prism version 10.2.3. Dose-response curves were fitted using nonlinear regression with an inhibitor vs. normalized response with variable slope model to calculate IC_{50} values. The 50 % inhibitory concentration (IC_{50}) values of each drug were calculated and compared between *WT* and BRCA1$^{AID/AID}$ cells. Data are presented as the mean ± standard deviation of at least three independent replicates. For a two-fold serial dilution of ADV, the final concentrations were 0, 0.5, 1, 2, 4, 8, 16, and 32 μM. For ETV, a four-fold serial dilution was performed with final concentrations of 0, 0.25, 1, 4, 16, 64, and 256 μM. In contrast, 3TC and TBV were tested at a maximum concentration of 500 μM. The final concentration of DMSO in all treatments did not exceed 0.1 %.

4. Immunofluorescence assay

WT and BRCA1$^{AID/AID}$ cells were seeded at a density of 5x10^5 cells/mL and were pulsed with 100 μM ETV for 10 min, washed, and incubated in fresh medium. Cells were collected at the indicated time points for immunofluorescence analysis. Following treatment, cells were harvested onto glass slides using a cytospin at 600 rpm for 5 min. After centrifugation, the cells were fixed with 4 % paraformaldehyde for 10 min at room temperature, followed by two washes with PBS. The fixed cells were permeabilized with 0.5 % Triton X-100 in PBS for 10 min at room temperature and washed again with PBS. Following permeabilization, the cells were blocked with InterceptÒ Blocking Buffer for 1 hr. Primary antibody incubation was performed overnight at 4°C using rabbit polyclonal anti-Geminin (cat no. 10802-1-AP; 1:500 dilution, Proteintech) and mouse monoclonal anti-γ-H2AX (D7T2V; 1:1,000 dilution, CST). After incubation, the cells were washed with Tween-PBS (TPBS) for 5 min, four times. Secondary antibody incubation was carried out for 1 hr at room temperature using Alexa Flour 488 Donkey Anti-Rabbit IgG (HL) (cat no. 1IVM-A21206; 1:500 dilution, Invitrogen) and Alexa Flour 647 Donkey Anti-Mouse IgG (HL) (cat no. 1IVM-A31571; 1:500 dilution, Invitrogen), followed by TPBS washes. The nuclei were stained with Hoechst 33342 (cat no. 1IVM-H3570; 1:2000 dilution, Thermo Fisher Scientific) for 5 min and washed again with TPBS. Finally, the slides were mounted using MowiolÒ 4-88 (cat no. 9002-89-5; SigmaAldrich).

4.1 Image processing method for quantification of γ-H2AX foci images

Fluorescence images were acquired using a Zeiss Axio Imager M2 microscope. All images were captured using the same exposure settings within each experiment and analyzed using manual counting in combination with ImageJ software to quantify the number of γ-H2AX foci. Nuclear regions were identified and segmentation using ImageJ software (version. Java 1.8.0_381, Wayne Rasband and contributors, National Institutes of Health, USA).

γ-H2AX foci were quantified through manual counting. To enhance foci visibility and ensure consistent scoring, γ-H2AX images were processed in ImageJ using the same settings across at each time points.

Counting criteria: (1) A minimum of 150 cells per condition per replicate were scored. (2) Number of foci more than five foci per cells were counted as positive cells. (3) Pan-nuclear γ-H2AX staining (uniform bright nuclear signal without discrete foci) was recorded as pan nuclear.

5. Statistical analysis

Data are presented as mean ± standard deviation. Statistical analysis was performed using GraphPad prism version 10.2.3. Comparison of IC50 values and γ-H2AX foci formation between *WT* and BRCA1$^{AID/AID}$ cells were performed using a Student's t-test, with $p < 0.05$ considered statistically significant. Two-way ANOVA followed by Tukey's post hoc multiple comparisons test was used to evaluate the effects of cell lines (*WT* and

BRCA1$^{AID/AID}$ cells) and drug concentrations on cell viability. All data were obtained from three independent biological replicates.

Results

1. Cell viability of ETV in TK6 cell lines both in WT and BRCA1$^{AID/AID}$

The cytotoxic effect of ETV was assessed in *WT* and BRCA1$^{AID/AID}$ cells using a cell viability assay. Cells were treated with ETV at concentrations of 0, 0.25, 1, 4, 16, 64, and 256 μM for 72 hr. The results demonstrated that ETV significantly reduced cell viability in both *WT* and BRCA1$^{AID/AID}$ cells in a dose-dependent manner (Figure 1A). The IC50 of ETV in *WT* cells was 11.43 ± 1.997 μM, whereas BRCA1$^{AID/AID}$ cells exhibited a lower IC50 of 7.916 ± 0.7048 μM, with a statistically significant difference ($p = 0.0455$) (Figure 1B). These results indicate that BRCA1 deficiency increases cellular susceptibility to ETV treatment. Moreover, the findings suggest that BRCA1 is involved in repairing DNA lesions induced by ETV. Thus, BRCA1$^{AID/AID}$ cells exhibit hypersensitivity to ETV compared with *WT* cells.

To further assess the effects of BRCA1 deficiency and drug concentration on cell viability following ETV treatment, two-way ANOVA was performed. Post hoc analysis showed significant differences between *WT* and BRCA1$^{AID/AID}$ cells at 0.25 μM ($p = 0.0098$), 1 μM ($p < 0.0001$), and 4 μM ($p < 0.0001$) (Figure 1A). These findings suggest that BRCA1 deficiency may sensitize TK6 cells to ETV at certain concentrations, highlighting the potential involvement of DNA repair pathways in cellular responses to ETV treatment.

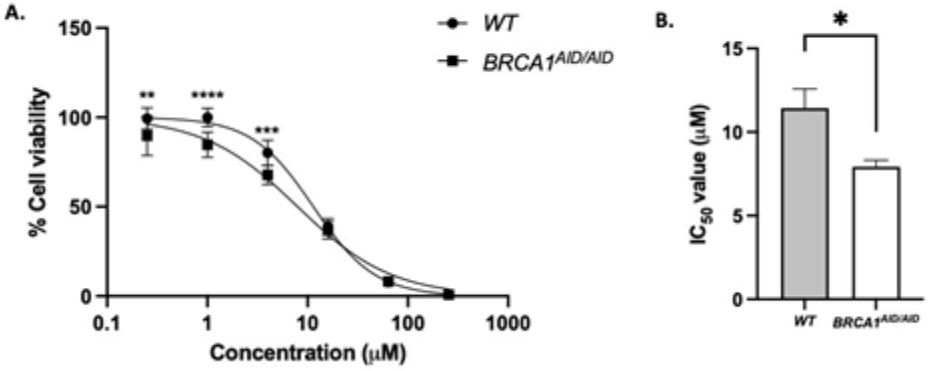

Figure 1. ETV reduces cell viability in *WT* and BRCA1$^{AID/AID}$ cells. Cells were treated with the indicated concentrations of ETV for 72 hr. Dose-response curves showing the effects of ETV on cell viability in *WT* and BRCA1$^{AID/AID}$ cells. Post hoc analysis revealed significance differences between *WT* and BRCA1$^{AID/AID}$ cells at 0.25 μM ($p = 0.0098$), 1 μM ($p < 0.0001$), and 4 μM ($p < 0.0001$) (A). The IC50 of ETV in *WT* was 11.43 μM and BRCA1$^{AID/AID}$ cells showed an IC50 of 7.916 μM, with a statistically significant difference ($p = 0.0455$) (B). Data are presented as the mean ± standard deviation of at least three independent replicates. *$p < 0.05$, **$p < 0.01$, ***$p < 0.001$, and ****$p < 0.0001$.

2. Cell viability of ADV in TK6 cell lines both in WT and BRCA1$^{AID/AID}$

The cytotoxic effect of ADV was assessed in *WT* and BRCA1$^{AID/AID}$ cells using a cell viability assay. Cells were treated with ADV at concentrations of 0, 0.5, 1, 2, 4, 8, 16, and 32 μM for 72 hr. The results demonstrated that ADV significantly reduced cell survival in both *WT* and BRCA1$^{AID/AID}$ in TK6 cells in a dose-dependent manner (Figure 2A). The IC50 of ADV in *WT* cells was 3.594 ± 0.5425 μM, whereas BRCA1$^{AID/AID}$ cells exhibited a lower IC50 of 2.458 ± 0.5196 μM. Although this difference did not reach statistical significance ($p = 0.0589$) (Figure 2B), the trend suggests increased sensitivity of BRCA1-deficient cells to ADV treatment. To further assess the effects of BRCA1 deficiency and drug concentration on cell viability, a two-way ANOVA was performed. Post hoc analysis showed significant differences in cell viability between *WT* and BRCA1$^{AID/AID}$ cells at 0.5 μM ($p = 0.0063$), 2 μM ($p = 0.0018$), and 4 μM ($p = 0.0010$) (Figure 2A). These findings suggest that BRCA1 deficiency may sensitize TK6 cells to ADV at certain concentrations, highlighting the potential involvement of DNA repair pathways in cellular responses to this antiviral drug.

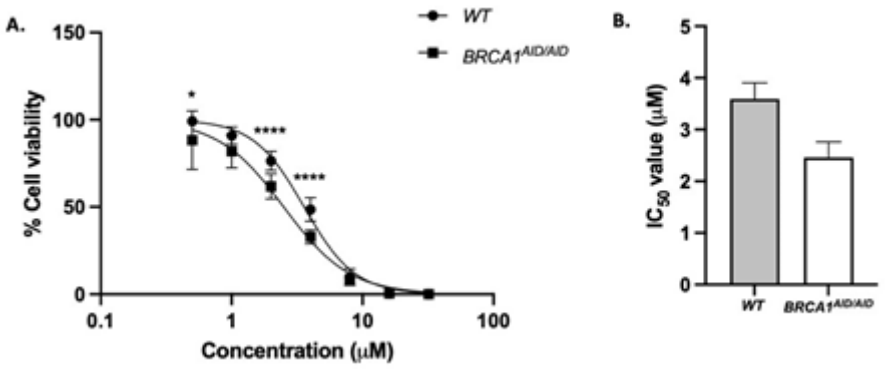

Figure 2. ADV reduces cell viability in *WT* and BRCA1$^{AID/AID}$ cells. Cells were treated with the indicated concentrations of ADV for 72 hr. Dose-response curves showing the effects of ADV on cell viability in *WT* and BRCA1$^{AID/AID}$ cells. Post hoc analysis revealed significant differences in cell viability between *WT* and BRCA1$^{AID/AID}$ cells at 0.5 μM ($p = 0.0063$), 2 μM ($p = 0.0018$), and 4 μM ($p = 0.0010$) (A). The IC50 of ADV in *WT* cells was 3.594 μM and BRCA1$^{AID/AID}$ cells showed an IC50 of 2.458 μM ($p = 0.0589$) (B). Data are presented as the mean ± standard deviation of at least three independent replicates. *$p < 0.05$ and ****$p < 0.0001$.

3. Cell viability of TBV and 3TC in TK6 cell lines both in WT and BRCA1$^{AID/AID}$

The cytotoxic effect of TBV and 3TC was assessed in *WT* and BRCA1$^{AID/AID}$ cells using a cell viability assay. Cells were treated with TBV and 3TC at concentrations of 0, 7.8125, 15.625, 31.25, 62.5, 125, 250, and 500 μM for 72 hr. The results demonstrated that both of TBV and 3TC did not significantly reduce cell viability in *WT* and BRCA1$^{AID/AID}$ cells under tested conditions (Figure 3).

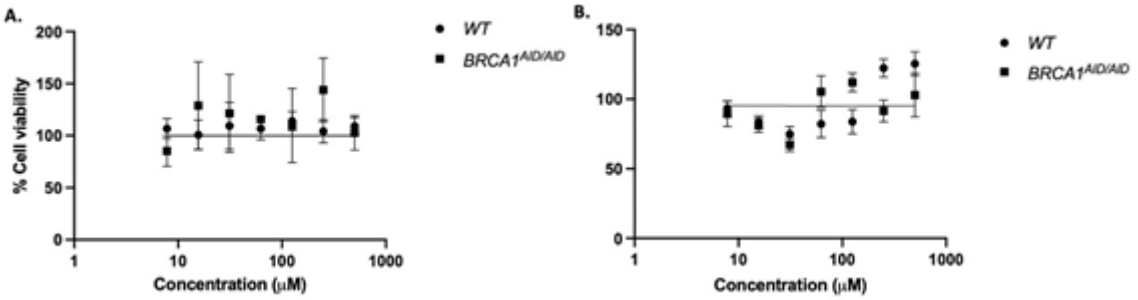

Figure 3. TBV (A) and 3TC (B) did not show cytotoxic effect under tested conditions both in *WT* and BRCA1$^{AID/AID}$.

4. Immunofluorescence analysis following ETV treatment in TK6 cell lines both in WT and BRCA1$^{AID/AID}$

To investigate ETV-induced DNA DSBs, immunofluorescence staining was performed to evaluate γ-H2AX foci formation following ETV treatment in *WT* and BRCA1$^{AID/AID}$ cells. Co-analysis of geminin and γ-H2AX was performed to determine whether DNA DSBs foci were present in S/G2-phase cells. The percentage of γ-H2AX positive among geminin positive cells increased following ETV treatment in both *WT* and BRCA1$^{AID/AID}$ cells (Figure 4A and 5). In both *WT* and BRCA1$^{AID/AID}$ cells, the percentage of γ-H2AX positive among geminin positive cells peaked at 6 hr, which was used as the normalization reference point for comparison of damage resolution kinetics. In *WT* cells, the normalized percentage of γ-H2AX levels decreased over time until 9 hr, indicating progressive recovery from ETV-induced DNA DSBs. In contrast, BRCA1$^{AID/AID}$ cells showed only a slight reduction in γ-H2AX levels, which remained consistently higher than those observed in *WT* cells at 7, 8, and 9 hr ($p = 0.006$, $p < 0.001$, and $p < 0.0143$, respectively). The slower decline in γ-H2AX foci in BRCA1$^{AID/AID}$ cells suggests delayed resolution of DNA DSBs in the absence of functional BRCA1.

Pan-nuclear γ-H2AX staining was also quantified and expressed as the percentage of total pan-nuclear (Figure 4B). In BRCA1$^{AID/AID}$ cells, the percentage of pan-nuclear showed highest levels than in *WT* with a significance difference at 6, 7, 8, and 9 hr ($p = 0.0266$, $p = 0.0154$, $p = 0.0057$ and $p = 0.0097$, respectively). The trend in pan-nuclear staining corresponded with the increase in γ-H2AX -positive cells, suggesting that BRCA1-deficient cells accumulate more extensive DNA DSBs following treatment.

The percentage of geminin positive cells was used to assess the proportion of cells in the S/G2 phase following ETV treatment (Figure 4C). Approximately 60 % of both *WT* and BRCA1$^{AID/AID}$ cells were geminin positive under untreated conditions. In *WT* cells, a significant increase was observed at 8 and 9 hr compared with untreated controls ($p = 0.0261$, and $p = 0.0212$, respectively). In contrast, BRCA1$^{AID/AID}$ cells showed a significant increase at 6, 7, 8, and 9 hr ($p = 0.0272$, $p = 0.0388$, $p = 0.0377$, and $p = 0.0270$, respectively). These findings indicate that ETV treatment increased the proportion of cells in the S/G2 phase, with an earlier and more sustained accumulation of geminin positive in BRCA1$^{AID/AID}$ cells. In addition, ETV treatment may reflect delayed cell cycle progression.

The percentage of micronucleus was similar between *WT* and BRCA1$^{AID/AID}$ cells, remaining below 2 % across all time points, suggesting no substantial chromosome damage under these conditions (Figure 4D).

Figure 5 summarizes the accumulation of γ-H2AX foci in nuclei of *WT* and BRCA1$^{AID/AID}$ following ETV treatment. The highest increase in γ-H2AX foci was observed at the 6 hr time point in *WT* and BRCA1$^{AID/AID}$. Notably, BRCA1$^{AID/AID}$ cells showed delayed resolution rate of γ-H2AX foci compared in *WT* cells. Loss of BRCA1 may lead to accumulation of unrepaired DNA DSBs and BRCA1 might play a role in ETV-induced DNA DSBs.

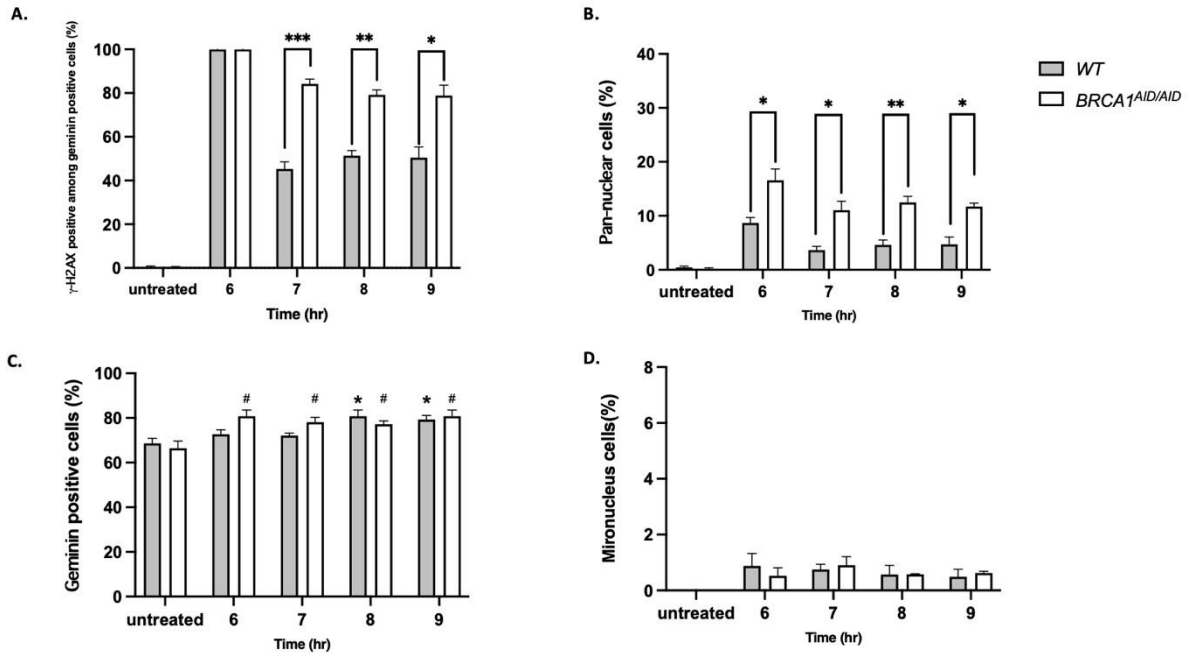

Figure 4. BRCA1 deficiency is associated with delays resolution of ETV-induced DNA DSBs repair. Cells were pulsed with 100 μM ETV for 10 min, washed, and incubated in fresh medium. Cells were collected at the indicated time points for immunofluorescence analysis. Normalized percentage of γ-H2AX positive among geminin positive cells following ETV treatment (A). Percentage of pan-nuclear (B). Percentage of geminin positive (C). Percentage of micronucleus (D). Data are presented as the mean ± standard deviation. Statistical analysis was performed using Student's t-test. For panels (A) and (B), *p < 0.05, **p < 0.01, ***p < 0.001 vs. *WT* group. For panel (C), *p < 0.05, vs. *WT* untreated; # p < 0.05 vs. BRCA1$^{AID/AID}$ untreated.

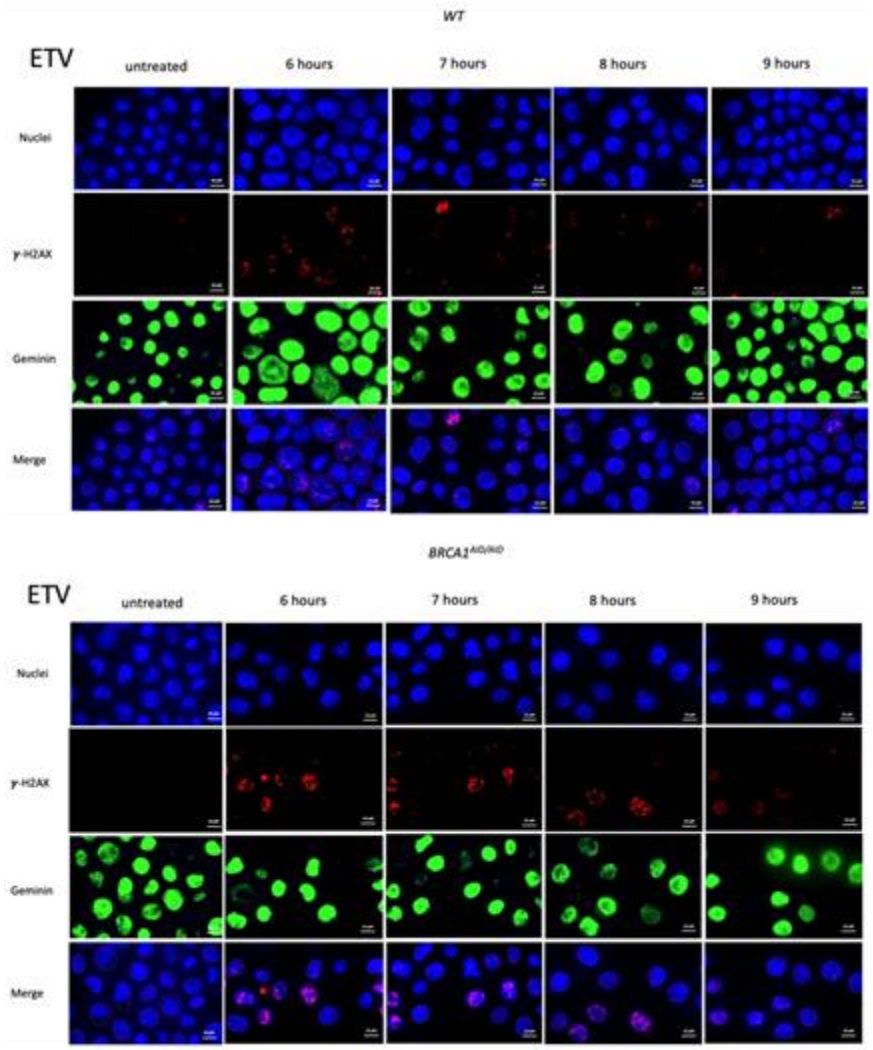

Figure 5. Representative immunofluorescence images showed γ-H2AX formation in *WT* and BRCA1$^{AID/AID}$ cells following ETV treatment. In the merged images, geminin positive cells are outlined with a red border. Cells were pulsed with 100 μM ETV for 10 min, washed, and incubated in fresh medium, then collected at indicated time point (scale bar, 10 μM; magnification, x100).

5. Immunofluorescence analysis following ADV treatment in TK6 cell lines both in WT and BRCA1$^{AID/AID}$

To investigate ADV-induced DNA DSBs, immunofluorescence analysis was performed to evaluate γ-H2AX foci formation following ADV treatment in *WT* and BRCA1$^{AID/AID}$ cells. Co-analysis of geminin and γ-H2AX was performed to determine whether DNA DSBs foci were present in S/G2-phase cells. The percentage of γ-H2AX positive among geminin cells increased following ADV treatment in both *WT* and BRCA1$^{AID/AID}$ cells (Figure 6A and 7). In both *WT* and BRCA1$^{AID/AID}$ cells, the percentage of γ-H2AX positive among geminin positive cells peaked at 6 hr, which was used as the normalization reference point for comparison of damage resolution kinetics. In *WT* cells, percentage of γ-H2A levels decreased over time until 9 hr, indicating progressive recovery from ADV-induced DNA DSBs. In contrast, BRCA1$^{AID/AID}$ cells showed only a slight

reduction in γ-H2AX levels, which remained consistently higher than those observed in *WT* cells at 7 hr ($p = 0.0435$). However, the differences in γ-H2AX foci levels between *WT* and BRCA1$^{AID/AID}$ cells at 8 and 9 hr were not statistically significant ($p = 0.1992$ and $p = 0.1678$, respectively). The slower decline in gH2AX foci in BRCA1$^{AID/AID}$ cells suggested that BRCA1 deficiency causes a transient delay resolution of ADV-induced DNA DSBs, rather than sustained persistence of DSBs over time point.

Pan-nuclear γ-H2AX staining was also quantified and expressed as the percentage of total pan-nuclear, approximately 20 % at 6 hr, then gradually decreased over time in both *WT* and BRCA1$^{AID/AID}$ cells (Figure 6B). In BRCA1$^{AID/AID}$ cells, the percentage of pan-nuclear showed highest levels than in *WT* with a significance difference at 7 and 8 hr ($p = 0.0293$ and $p = 0.0045$, respectively). The trend in pan-nuclear staining corresponded with the increase in γ-H2AX -positive cells, suggesting that BRCA1-deficient cells accumulate more extensive DNA damage following treatment.

The percentage of geminin positive cells was used to assess the proportion of cells in the S/G2 phase following ADV treatment (Figure 6C). Approximately 80 % of both *WT* and BRCA1$^{AID/AID}$ cells were geminin positive under untreated conditions. In *WT* cells, a significant increase was observed at 6 - 9 hr compared with untreated controls ($p = 0.0151$, $p = 0.0005$, $p = 0.0139$ and $p = 0.0056$, respectively). Meanwhile, BRCA1$^{AID/AID}$ cells showed a significant increase at 6 - 9 hr ($p < 0.0001$, $p = 0.0053$, $p = 0.0007$ and $p = 0.0051$, respectively). These findings indicate that ADV treatment increased the proportion of cells in the S/G2 phase, with an earlier and more sustained accumulation of geminin positive in BRCA1$^{AID/AID}$ cells. In addition, ADV treatment may reflect delayed cell cycle progression.

The percentage of micronucleus was similar between *WT* and BRCA1$^{AID/AID}$ cells approximately 2 % suggesting no substantial chromosome damage under these conditions (Figure 6D).

Figure 7 summarizes the accumulation of γ-H2AX foci in nuclei of *WT* and BRCA1$^{AID/AID}$ following ADV treatment. The highest increase in γ-H2AX foci was observed at the 6 hr time point in *WT* and BRCA1$^{AID/AID}$. Notably, the levels of γ-H2AX foci were higher in BRCA1-deficient cells than in *WT* cells. Loss of BRCA1 may lead to accumulation of unrepaired DNA DSBs and BRCA1 might play a role in ADV-induced DNA DSBs.

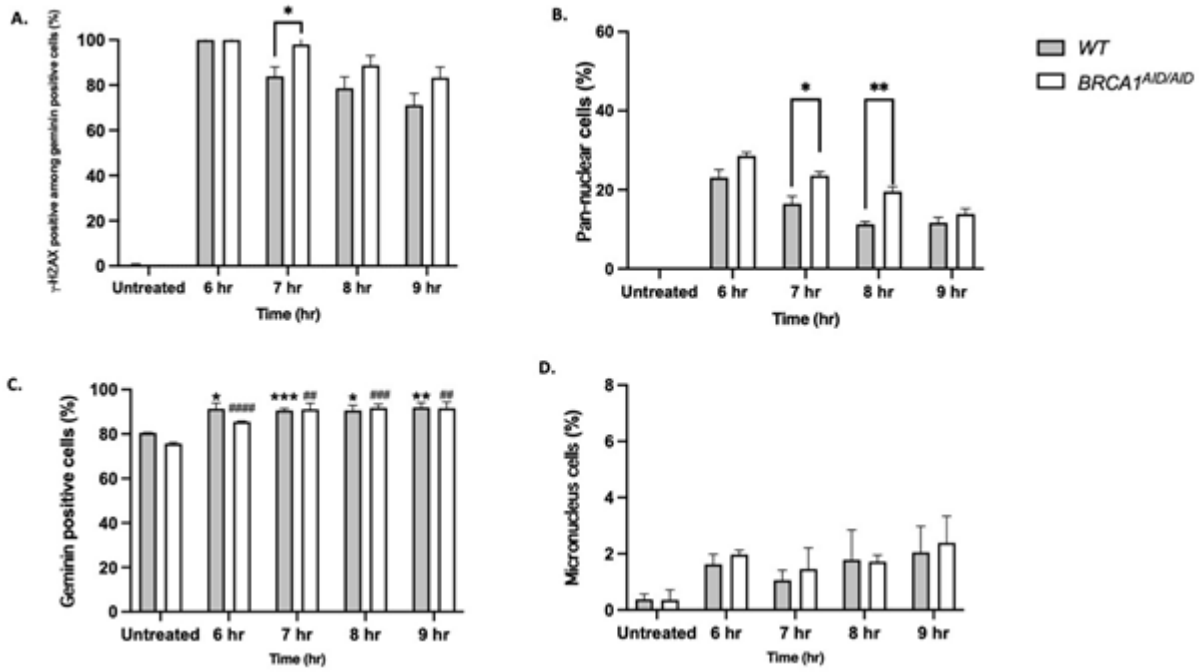

Figure 6. BRCA1 deficiency is associated with delays resolution of ADV-induced DNA DSBs repair. Cells were pulsed with 100 μM ADV for 10 min, washed, and incubated in fresh medium. Cells were collected at the indicated time points for immunofluorescence analysis. Normalized percentage of γ-H2AX positive among geminin positive cells following ADV treatment (A). Percentage of pan-nuclear (B). Percentage of geminin positive (C). Percentage of micronucleus (D). Data are presented as the mean ± standard deviation. Statistical analysis was performed using Student's t-test. For panels (A) and (B), *p < 0.05, **p < 0.01 vs. *WT* group. For panel (C), *p < 0.05, **p < 0.01, ***p < 0.001 vs. *WT* untreated; # p < 0.05, ##p < 0.01, ###p < 0.001, #### p < 0.0001 vs. BRCA1$^{AID/AID}$ untreated.

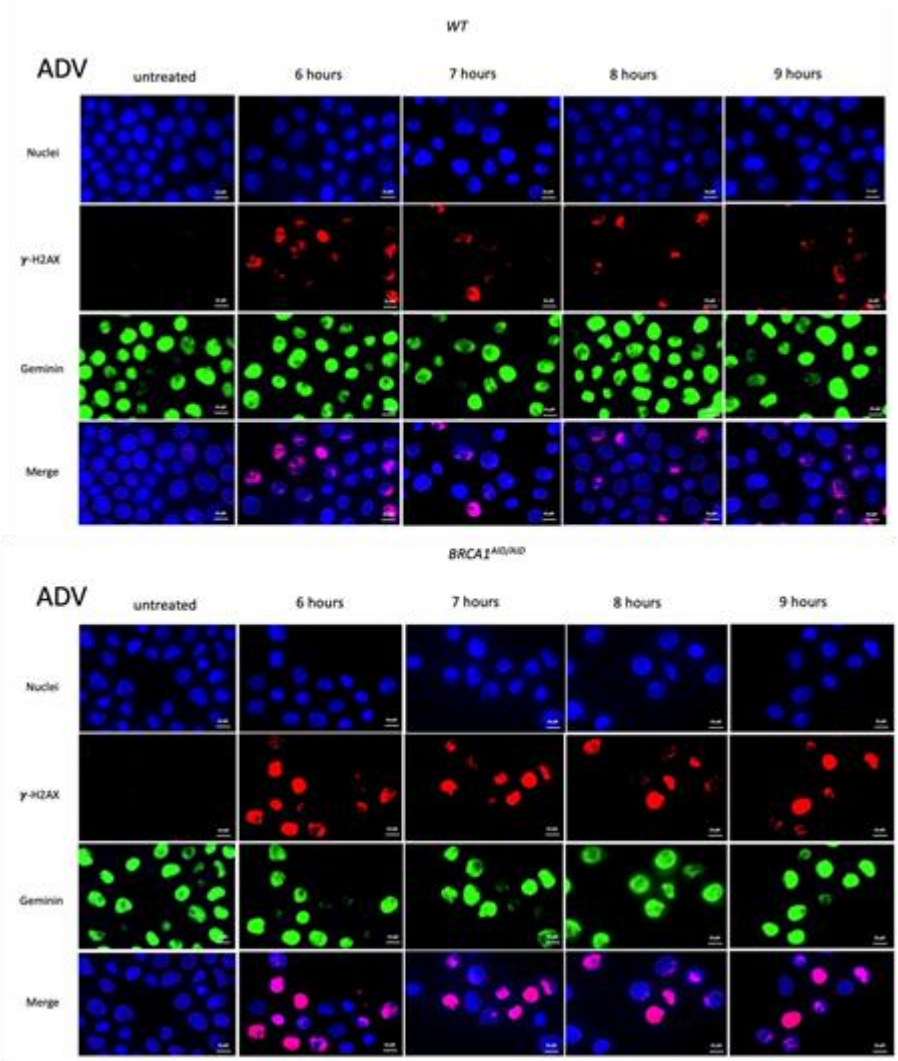

Figure 7. Representative immunofluorescence images showed γ-H2AX formation in *WT* and BRCA1*AID/AID* cells following ADV treatment. In the merged images, geminin positive cells are outlined with a red border. Cells were pulsed with 100 μM ADV for 10 min, washed, and incubated in fresh medium, then collected at indicated time point (scale bar, 10 μM; magnification, x100).

Discussion

The hypersensitivity of BRCA1*AID/AID* cells to ETV and ADV treatment, relative to *WT* cells was supported by the lower IC50 values observed in BRCA1*AID/AID* cells compared with *WT* cells. These findings suggest that BRCA1 deficiency increases cellular sensitivity to ETV and ADV exposure. BRCA1 plays a critical role in maintaining genomic stability through HR repair, replication fork protection, and cellular stress response pathways[14, 15]. In the absence of functional BRCA1, cells may be less capable of resolving replication-associated stress and maintaining efficient DNA repair during cell division. Persistent cellular stress may subsequently promote cell death, thereby reducing overall cell viability. Consequently, loss of BRCA1 may decrease the ability of cells to tolerate ETV- and ADV-induced stress, leading to reduced survival at lower drug concentrations. In contrast, *WT* cells retain functional BRCA1- dependent pathways, allowing them to better

tolerate and recover from ETV and ADV treatment, thereby requiring higher concentrations to achieve the same inhibitory effects. These findings indicate that BRCA1 deficiency compromises cellular defense mechanisms, resulting in increased sensitivity to ETV and ADV treatment.

However, 3TC and TBV did not significantly reduce cell viability in both *WT* and BRCA1$^{AID/AID}$ cells under the tested conditions and were therefore excluded from subsequent immunofluorescence analysis. A possible explanation for their lower cytotoxicity is that their L-enantiomer stereochemistry may be less efficiently recognized by host DNA polymerases than natural D-nucleosides, thereby reducing off-target incorporation into host DNA[16, 17]. Consequently, these structural features may minimize off-target effects and preserve cell viability.

To investigate the involvement of BRCA1-mediated repair in the response to ETV- and ADV-induced DSBs, we evaluated the dynamics of γ-H2AX foci formation following ETV and ADV treatment. The 6 hr time point was used as the normalization reference to compare the subsequent decline in γ-H2AX levels between *WT* and BRCA1$^{AID/AID}$ cells. Subsequently, the resolution of γ-H2AX foci was delayed in the BRCA1$^{AID/AID}$ cells compared with *WT* cells. This prolonged persistence of γ-H2AX levels suggests impaired recovery from ETV- and ADV-induced DSBs in the absence of functional BRCA1.

DSBs can be repaired through two major pathways: non-homologous end joining (NHEJ) and HR. NHEJ repaired DSBs by directly ligating the two broken DNA ends without the requirement for a homologous template. This pathway is active throughout the cell cycle and is relatively fast but can be error-prone[18]. In contrast, HR uses the intact sister chromatid as a homologous template to accurately restore the damaged DNA sequence. As a result, HR is considered a high-fidelity repair mechanism and predominantly occurs during the S and G2 phases[19]. BRCA1 protein is responsible for repairing DNA damage, particularly through the HR during the repair of DSBs. BRCA1 acts as an early responder that helps recruit and coordinate other proteins at damage sites. When functioning correctly, the BRCA1 protein contributes to maintaining genomic stability by facilitate accurate DNA repair processes. In BRCA1-deficient cells, impaired HR may lead to inefficient repair of DSBs, contributing to the persistence of γ-H2AX signals observed in BRCA1$^{AID/AID}$ cells. Supporting this interpretation, previous studies have shown that NHEJ-deficient cells, such as Ku70$^{-/-}$ or 53BP1-deficient cells, do not exhibit increased sensitivity to ADV compared with *WT* cells, suggesting that NHEJ may not play a major role in repairing ADV-induced DNA DSBs[9]. In contrast, *WT* cells retain functional HR pathways, allowing more accurate and efficient resolution of DNA damage, as reflected by the more rapid decline in γ-H2AX levels. Collectively, these findings support an important role for BRCA1 in promoting recovery from ETV- and ADV-induced DNA damage.

Although BRCA1$^{AID/AID}$ cells exhibited higher and more persistent γ-H2AX levels than *WT* cells following ETV and ADV treatment, micronucleus did not differ significantly between the two cell lines. γ-H2AX is a sensitive and early marker of DSBs[7], which can be rapidly induced following DNA lesions. In contrast, micronucleus formation reflects a later chromosomal outcome that occurs after cell division, arising from chromosome fragments

or mis-segregation during mitosis[20]. Consequently, increased γ-H2AX does not necessarily result in immediate micronucleus formation within short observation periods in this study. It is possible that DNA damage induced by ETV and ADV triggered damage signaling but was repaired before progressing into chromosome abnormalities prior to mitotic entry. Moreover, the percentage of micronucleus remained low (< 2 %), suggesting that a larger number of cells may be required to detect subtle differences. This may also reflect the limitation of the study to early time points, which may not allow sufficient time for chromosomal abnormalities. Additionally, although differences in DNA damage resolution were observed, the relative contribution of HR and NHEJ was not directly assessed. Therefore, the proposed shift in DNA repair pathway usage remains inferential. Direct evaluation using pathway-specific markers, such as RAD51 for HR and 53BP1 for NHEJ[21, 22], would be required to confirm the underlying repair mechanism.

In addition, a pulse-treatment protocol was used, in which cells were exposed to drug for 10 min followed by washing, to allow rapid induction of DNA damage and subsequent analysis of DNA repair kinetics. Continuous treatment was not used because prolonged exposure caused excessive cell death and extensive pan-nuclear γ-H2AX staining, which was not suitable for evaluating DNA repair kinetics.

Based on these findings, we suggest that BRCA1 plays an important role in the repair of ETV- and ADV-induced DSBs. Loss of BRCA1 function may lead to the accumulation of unrepaired DNA lesions, resulting in delayed resolution of DNA DSBs.

Conclusion

This study investigated the potential genotoxic effects of ETV, ADV, 3TC, and TBV and the role of BRCA1 in the repair of ETV- and ADV-induced DNA damage. Our results demonstrated that ETV and ADV reduced cell viability, whereas 3TC and TBV did not show a detectable reduction in cell viability under the tested conditions. Notably, ADV exhibited greater toxicity than ETV, as reflected by lower IC50 values and higher γ-H2AX levels. BRCA1$^{AID/AID}$ cells showed increased sensitivity to ETV and ADV, as indicated by lower IC50 values and more persistent γ-H2AX signals compared with *WT* cells. These findings suggest that BRCA1 plays an important role in facilitating recovery from ETV- and ADV-induced DNA DSBs.

Acknowledgement

We sincerely thank Professor Shunichi Takeda for providing the BRCA1 conditional knockout cell lines used in this study. We also gratefully acknowledge the BioImaging Facility from Research Center, Faculty of Medicine, Ramathibodi Hospital, Mahidol University for training and support in immunofluorescence image acquisition. Sathida Liekwannacharoen received financial support from the Faculty of Graduate Studies through a graduate scholarship.

References

1. Wong GL-H, Lemoine M. The 2024 updated WHO guidelines for the prevention and management of chronic hepatitis B: Main changes and potential implications for the next major liver society clinical practice guidelines. J Hepatol. 2025;82(5):918-25.
2. Liaw Y-F, Chu C-M. Hepatitis B virus infection. The Lancet. 2009;373(9663):582- 92.
3. Tsai E. Review of Current and Potential Treatments for Chronic Hepatitis B Virus Infection. Gastroenterol Hepatol (N Y). 2021;17(8):367-76.
4. Ewald B, Sampath D, Plunkett W. Nucleoside analogs: molecular mechanisms signaling cell death. Oncogene. 2008;27(50):6522-37.
5. Németh E, Szüts D. The mutagenic consequences of defective DNA repair. DNA Repair. 2024;139:103694.
6. Liu Y, Lu L-Y. BRCA1: a key player at multiple stages of homologous recombination in DNA double-strand break repair. Genome Instability & Disease. 2021;2(3):164-74.
7. Rahmanian N, Shokrzadeh M, Eskandani M. Recent advances in γH2AX biomarkerbased genotoxicity assays: A marker of DNA damage and repair. DNA Repair (Amst). 2021;108:103243.
8. Prabhu KS, Kuttikrishnan S, Ahmad N, Habeeba U, Mariyam Z, Suleman M, et al. H2AX: A key player in DNA damage response and a promising target for cancer therapy. Biomed Pharmacother. 2024;175:116663.
9. Liu H, Wu Y, He F, Cheng Z, Zhao Z, Xiang C, et al. Brca1 is involved in tolerance to adefovir dipivoxil-induced DNA damage. Int J Mol Med. 2019;43(6):2491-8.
10. Jiang L, Wu X, He F, Liu Y, Hu X, Takeda S, et al. Genetic Evidence for Genotoxic Effect of Entecavir, an Anti-Hepatitis B Virus Nucleotide Analog. PLoS One. 2016;11(1):e0147440.
11. Fujii T, Takase KI, Honda H, Kawamura N, Yamasaki R, Urata M, et al. Toxic myopathy with multiple deletions in mitochondrial DNA associated with long-term use of oral anti-viral drugs for hepatitis B: A case study. Neuropathology. 2019;39(2):162-7.
12. Kim JW, Park SH, Louie SG. Telbivudine: a novel nucleoside analog for chronic hepatitis B. Ann Pharmacother. 2006;40(3):472-8.
13. Phanindhar K, Mishra RK. Auxin-Inducible Degron System: An Efficient Protein Degradation Tool to Study Protein Function. Biotechniques. 2023;74(4):186-98.
14. Jang ER, Lee JS. DNA damage response mediated through BRCA1. Cancer Res Treat. 2004;36(4):214-21.
15. Fu X, Tan W, Song Q, Pei H, Li J. BRCA1 and Breast Cancer: Molecular Mechanisms and Therapeutic Strategies. Front Cell Dev Biol. 2022;10:813457.
16. Ruiz FX, Hoang A, Dilmore CR, DeStefano JJ, Arnold E. Structural basis of HIV inhibition by L-nucleosides: Opportunities for drug development and repurposing. Drug Discov Today. 2022;27(7):1832-46.
17. Brown JA, Pack LR, Fowler JD, Suo Z. Presteady state kinetic investigation of the incorporation of anti-hepatitis B nucleotide analogues catalyzed by noncanonical human DNA polymerases. Chem Res Toxicol. 2012;25(1):225-33.
18. Mao Z, Bozzella M, Seluanov A, Gorbunova V. Comparison of nonhomologous end joining and homologous recombination in human cells. DNA Repair. 2008;7(10):1765-71.
19. Ackerson SM, Romney C, Schuck PL, Stewart JA. To Join or Not to Join: Decision Points Along the Pathway to Double-Strand Break Repair vs. Chromosome End Protection. Frontiers in Cell and Developmental Biology. 2021;9.
20. Duan H, Peng X, Qin S, Zhou Y, Xiao D, Tao Y, et al. Micronuclei: origins, assays, mechanisms, diseases and treatments. Signal Transduction and Targeted Therapy. 2026;11(1):114.
21. Wassing IE, Esashi F. RAD51: Beyond the break. Semin Cell Dev Biol. 2021;113:38- 46.

22. Garabedian MV, Zhang T, Datta A, Wang W, Wadley M, Greenberg RA, et al. 53BP1 condensates function as bioreactors for NHEJ directed DNA repair and insulators to determine pathway choice. bioRxiv. 2025:2025.12.19.695596.

Investigate the effect of *Centella asiatica* (ECa233) on pancreatic iron overload and oxidative stress in beta-thalassemia mice.

Natthakarn Tubthong[1], Paranee Yatmark[2], Pimtip Sanvarinda[1], Noppawan Phumala Morales[1*]

[1]Deparment of Pharmacology, Faculty of Science, Mahidol University, 272 Rama VI Road, Ratchathewi District, Bangkok 10400, Thailand
[2]Department of Preclinic and Applied Animal Science, Faculty of Veterinary Science, Mahidol University, Phuttamonthon 4 Road, Salaya, Phuttamonthon District, Nakhon Pathom 73170, Thailand

Abstract

Beta-thalassemia patients require regular blood transfusions to prevent ineffective erythropoiesis and anaemia, though the long-term effects of receiving blood transfusions cause excess iron accumulation or iron overload. The excess of iron that accumulates in the circulation can be deposits to several organs, including the pancreas. The extract of Centella asiatica (ECa233) provides anti-inflammation and antioxidants, which may improve iron accumulation and oxidative stress conditions. The aim is to investigate the effect of Eca233 on iron overload, lipid peroxidation, and antioxidant activity in the pancreatic tissue of beta-thalassemia mice. The twelve-month-old C57BL7 wild-type (WT) and β-globin knockout (BKO) were used in this study. BKO mice received 20 mg/kg of iron dextran for 5 days, stop for 3 days, were followed by 80 mg/kg of deferiprone or 70 mg/kg of Ecav233 or combination for 14 days via oral gavage. The iron content in pancreatic tissue was assessed by the ferrozine method. The lipid peroxidation and antioxidant activity were evaluated by the thiobarbituric acid reactive substances (TBARS) assay, total glutathione (GSH) and glutathione peroxidase (GPx), respectively. The results demonstrated that coadministration of deferiprone and ECa233 likely decreased the iron level and lipid peroxidation level but did not increase the antioxidant activity in BKO with iron overload mice. A positive correlation between iron and TBARS level was shown (r = 0.6715, p <0.001), and a negative correlation was shown between iron and lipid peroxidation (r = -0.4989, p <0.05). The findings suggested that the coadministration may help to reduce the iron and lipid peroxidation in pancreatic tissues in BKO mice with an iron overload condition.

Keywords: Beta-thalassemia, Iron overload, oxidative stress, *C. asiatica*

Introduction

Thalassemias are considered an autosomal recessive disorder, which are distinguished by the impairment of haemoglobin production or destruction of the haemoglobin and lead to red blood cell destruction, as a result of ineffective erythropoiesis and anaemia [1, 2]. The most common type of thalassemia is β-thalassemia. This is caused by the mutation of the β-globin gene and leads to ineffective production or absence of the β-globin chain [3, 4]. Blood transfusion is frequently required for the patient with thalassemia[5].

The patients who receive blood transfusions may be associated with iron overload, which can damage several organs such as the liver, pancreas, parathyroid gland, thyroid gland, and heart. Pancreatic iron overload and diabetes mellitus (DM) are common in thalassemia major, and there are more than 10% of children with thalassemia major have been diagnostic with DM [6, 7]. Noetzil et al[7] studied the association between pancreatic iron and glucose tolerance in thalassemia patients who received long-term blood transfusion treatment. The evidence reported that insulin release and sensitivity had a significant decrease in diabetes and impaired glucose tolerance with thalassemia. This suggested that pancreatic iron causes β-cell toxicity.

Iron accumulation causes ferroptosis in the β-cell function and leads to cell death by lipid oxidation from the reduction of glutathione and consequently inhibits the glutathione peroxidase-4 (GPX4) [8]. This consequence continuously causes pancreatic β-cell dysfunction and impaired insulin secretion. As a result of high blood glucose in thalassemia with blood transfusion. In addition, prolonged high blood glucose and inability to secrete insulin properly to maintain blood glucose levels also led to a diabetic condition. Also, iron can be deposited in the liver, which causes the development of non-alcoholic fatty liver disease (NAFLD) by ROS [9], which may increase the risk of diabetes and worsen the patient's life.

Centella asiatica (CA) is widely used as a treatment for many diseases, for example, neurodegenerative disorders, skin disease, and metabolic disorders, due to its containing several bioactive compounds such as triterpenes, flavonoids, phytosterols, and phenolic acids that have therapeutic effects [10]. The most crucial components in CA are pentacyclic triterpenes, including asiaticoside, asiatic acid, madecassoside, and madecassic acid[11]. In vitro study, CA extract has established glucose uptake activity [12]. CA extract also enhances the antioxidant activity by increasing the ability of ferric reducing and peroxidase activity, improving glutathione S-transferase activity and reducing glutathione levels [13]. Additionally, Yatmark et al [14] has shown that a standard extract of CA (ECa 233) reduced iron deposition and restored the brain function of β-thalassemia mice. These findings suggest that CA extract may provide a therapeutic effect on improving iron accumulation, antioxidant and anti-inflammatory properties in the pancreatic β-cell function of β-thalassemia mice.

This study aims to investigate the effect of Centella asiatica (Eca 233) on improving lipid peroxidation and antioxidant activity in the β-thalassemia mice model, which may provide a beneficial effect on enhancing the quality of the β-thalassemia patients with pancreatic dysfunction conditions.

Methods

1. *Animal model*

Twelve-month-old male wild-type (WT) and heterozygous β-globin knockout ($^{mu}\beta^{th3/+}$) C57BL/6 mice were obtained from the Thalassemia Research Centre, Institute of Molecular Biosciences, Mahidol University, Thailand. The temperature and humidity of the room were controlled (12/12 h light/dark cycle, 22°C ± 1°C). All BKO mice received a standard diet and *ad libitum*.

2. *Experimental design*

12-month-old WT mice received normal saline treatment (WN), and BKO mice were divided into 5 groups: β-globin knockout with normal saline treatment (BN), iron overload (BI), iron overload with deferiprone treatment (BIL), iron overload with Eca233 treatment (BIE), and iron overload with co-administration of deferiprone and Eca233. BI mice were orally administered 20 mg/kg of iron dextran (Sigma, St. Louis, MO) for 5 days. BIL and BILE received 80 mg/kg of deferiprone and 70 mg/kg of Eca233 by oral gavage for 14 days. After the treatment, all mice were euthanised with pentobarbital (50-60 mg/kg) via intraperitoneal (i.p.) injection. The fresh pancreatic tissue was collected for the determination of iron content and antioxidant activity.

3. Determination of iron content in the pancreatic tissue

The pancreatic tissues were homogenised by a bead mill (HT lysing homogeniser, Ohaus, Parsippany, NJ) with 0.1 M phosphate-buffered saline (PBS), pH 7.4. The non-heme content was measured by the modified ferrozine method that was described by Foy [15]. The procedure details were provided by Yatmak et al. [16]. The ferrozine-iron complex was measured at 526 nm by a microplate reader (Varioskan™ Flash, Thermo Scientific, Vantaa, Finland).

4. Determination of lipid peroxidation and antioxidant activity in the pancreatic tissue

The lipid peroxidation activity in the pancreatic tissues was determined by the thiobarbituric acid reactive substances (TBARS) assay. To measure the fatty acid oxidation, which is a byproduct also known as malondialdehyde (MDA). The pink colour is due to the interaction of thiobarbituric acid and MDA.

The homogenates from pancreatic tissues were centrifuged at 9,200 × g for 10 min (Spectrafuge 24D, Labnet International, Inc., Woodbridge, NJ). The supernatant was collected to determine the levels of total glutathione (GSH) and glutathione peroxidase (GPx) by the method from Kondo and Sawada [17] and Takahashi K [18].

5. Statistical analysis

Statistical analysis was performed using GraphPad Prism 9.00 (GraphPad Software, San Diego, CA, United States). The data analysis was represented as mean ± SD. Significant differences among the five treatment groups were analysed by using one-way analysis of variance (ANOVA), Kruskal-Wallis test. The correlation of iron content and TBARS was analysed and interpreted via Pearson's correlation coefficient ®. p-value < 0.05 was represent significant difference.

Results

The determination of pancreatic iron was measured by the iron ferrozine method (Figure 1.A). Lipid peroxidation and antioxidant activity were assessed by the method from Kondo and Sawada [17] and Takahashi K [18] (Figure 1.B-D). The control of WN and BN groups demonstrated low levels of iron content but did not reach significantly different levels when compared to the BI group. There was no significant difference between BI among treatment groups (fig 1.A). The BI group demonstrated a significantly increased lipid peroxidation level when compared to the control WN group (Fig 1.B). The treatment of deferiprone, Eca233 or co-administration tends to decrease lipid peroxidation level when compared to the BI group(Fig 1.B). The administration of deferiprone, Eca233 or

co-administration of deferiprone and Eca233 did not show an improvement in total GSH level in iron overload mice (fig 1.C). The GPx level was significantly increased in the BN group when compared to the BI group. The treatment of both deferiprone and Eca233 alone or co-administered groups did not elevate GPx activity (fig 1.D).

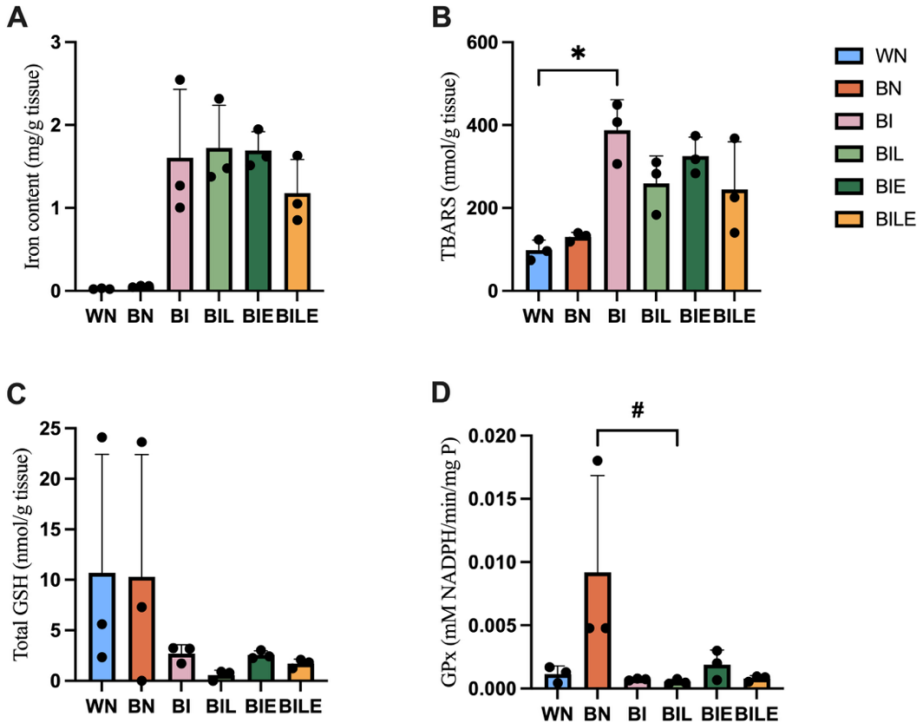

Figure 1. Determination of lipid peroxidation in the pancreatic tissue of 12-month-old C57BL6 β-thalassemia mice. A) Iron content. B) Lipid peroxidation. C) Total GSH level. D) GPx level. The values were expressed as mean ± SD (n=3). * p-value < 0.05 when compared to the control WT or BN group. # p-value < 0.05 when compared to the treatment groups. Abbreviations: TBARS, thiobarbituric acid reactive substances; GSH, total glutathione; GPx, glutathione peroxidase.

The correlation of iron and TBARS, total GSH and GPx were illustrated below (**Figure 2. A-C**). The correlation between iron and TBARS shown significant difference (r = 0.6715, p <0.001) (fig 2.A). Additionally, the correlation between iron and total GSH level shown significant difference (r = -0.4989, p <0.05) (fig 2.B). There was no significant correlation between iron and GPx level (r = -0.4079, p = 0.0929).

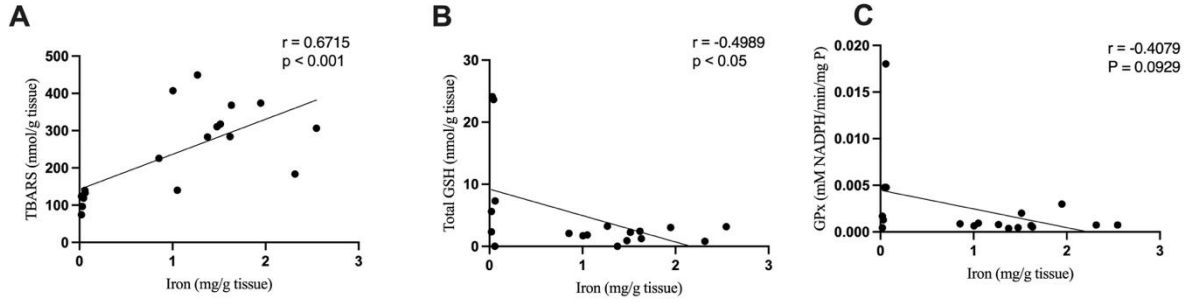

Figure 2. **The correlation between pancreatic iron and lipid peroxidation and antioxidant in 12-month-old C57BL6 β-thalassemia mice.** A) Correlation between iron and TBARS. B) Correlation between iron and total GSH level C) Correlation between iron and GPx level. Abbreviations: TBARS, thiobarbituric acid reactive substances; GSH, total glutathione; GPx, glutathione peroxidase.

Discussion

Tian et al [19] have demonstrated that pancreatic iron is deposited in WT mice with iron overload after being injected with 120 mg/kg of iron dextran for 12 weeks. The present study found that administered iron increased iron content levels in the pancreatic tissue of BKO mice with iron overload. This result suggested that the administration of 20 mg/kg iron dextran for 5 days may induce pancreatic injury.

In the previous study, Yatmark et al [14] had shown a significant reduction in iron deposition in the brain of BKO mice with iron overload after administration of 20 mg/kg/day of ECa 233 for 5 days. In addition, a study from Oyenihi et al [13] demonstrated that the CA extract reduced lipid peroxidation level and increased antioxidant activity, including GSH level. Our finding has been shown that the coadministration of deferiprone and Eca233 is prone to reduced iron level but did not reach a significant difference. The lipid peroxidation tends to decrease the lipid peroxidation level in derferiprone, ECa233 or coadministration of derferiprone and ECa233. However, the treatment groups did not alleviate GPx activity when compared to the BKO with iron overload group. Moreover, the correlation between iron content, TBARS and Total GSH demonstrated significant differences (r = 0.6715, p <0.001) and (r = -0.4989, p <0.05), respectively. There was no significant difference between the iron content and GPx level.

The limitations of this study were a small sample size and a variation in individual mice, which may not have represented a significant difference in iron content, lipid peroxidation, and antioxidant activity in β-thalassemia mice.

Conclusion

In conclusion, the co-administration of deferiprone and ECa233 may reduce iron levels and lipid peroxidation levels in the pancreatic tissue of BKO mice with iron overload. However, the co-administration may not enhance antioxidant activity in β-thalassemia mice. A further investigation of the effect of ECa233 or the co-administration of deferiprone and ECa233 in histological analysis, gene and protein expression needs to be evaluated.

Acknowledgement

This study was financially supported by the Fundamental Fund (FF) from Mahidol University in Fiscal Year 2026 by the National Science Research and Innovation Fund (NSRF), Thailand.

References

1. Rund D, Rachmilewitz E. β-Thalassemia. New England Journal of Medicine. 2005;353(11):1135-46.
2. Benz EJ, Jr. Introduction to the Thalassemia Syndromes: Molecular Medicine’s Index Case. Hematology/Oncology Clinics. 2023;37(2):245-59.

3. Shang X, Xu X. Update in the genetics of thalassemia: What clinicians need to know. Best Practice & Research Clinical Obstetrics & Gynaecology. 2017;39:3-15.
4. Modell B, Darlison M. Global epidemiology of haemoglobin disorders and derived service indicators. Bull World Health Organ. 2008;86(6):480-7.
5. Yutarti C, Susilowati I. Hubungan Kadar Feritin Serum dengan Tes Fungsi Hati pada Pasien Thalasemia Mayor. Jurnal Kesehatan. 2023;14:42-8.
6. Carsote M, Vasiliu C, Trandafir AI, Albu SE, Dumitrascu MC, Popa A, et al. New Entity-Thalassemic Endocrine Disease: Major Beta-Thalassemia and Endocrine Involvement. Diagnostics (Basel). 2022;12(8).
7. Noetzli LJ, Mittelman SD, Watanabe RM, Coates TD, Wood JC. Pancreatic iron and glucose dysregulation in thalassemia major. Am J Hematol. 2012;87(2):155-60.
8. Hansen JB, Dos Santos LRB, Liu Y, Prentice KJ, Teudt F, Tonnesen M, et al. Glucolipotoxic conditions induce β-cell iron import, cytosolic ROS formation and apoptosis. Journal of Molecular Endocrinology. 2018;61(2):69-77.
9. Altamura S, Müdder K, Schlotterer A, Fleming T, Heidenreich E, Qiu R, et al. Iron aggravates hepatic insulin resistance in the absence of inflammation in a novel db/db mouse model with iron overload. Molecular Metabolism. 2021;51.
10. Samananda Singh L, Singh S. Centella asiatica and its bioactive compounds: a comprehensive approach to managing hyperglycemia and associated disorders. Discover Plants. 2024;1.
11. Bansal K, Bhati H, Vanshita, Bajpai M. Recent insights into therapeutic potential and nanostructured carrier systems of Centella asiatica: An evidence-based review. Pharmacological Research - Modern Chinese Medicine. 2024;10:100403.
12. Park DW, Jeon H, So R, Kang SC. Centella asiatica extract prevents visual impairment by promoting the production of rhodopsin in the retina. Nutr Res Pract. 2020;14(3):203-17.
13. Oyenihi AB, Chegou NN, Oguntibeju OO, Masola B. Centella asiatica enhances hepatic antioxidant status and regulates hepatic inflammatory cytokines in type 2 diabetic rats. Pharm Biol. 2017;55(1):1671-8.
14. Yatmark P, Anutagerngkun P, Huaijantug S, Tantisira MH, Ngampramuan S, Svasti S, Morales NP. A standardized extract of Centella asiatica (ECa 233) alleviates brain injury and improves brain function in β-thalassemia mice with iron overload. BMC Complement Med Ther. 2025;25(1):412.
15. Foy AL, Williams HL, Cortell S, Conrad ME. A modified procedure for the determination of nonheme iron in tissue. Analytical Biochemistry. 1967;18(3):559-63.
16. Yatmark P, Morales NP, Chaisri U, Wichaiyo S, Hemstapat W, Srichairatanakool S, et al. Iron distribution and histopathological study of the effects of deferoxamine and deferiprone in the kidneys of iron overloaded β-thalassemic mice. Exp Toxicol Pathol. 2016;68(8):427-34.
17. Kondo T, Sawada F. Glutathione (oxidized and reduced form): assay mixture and measurement. In: Taniguchi N, Gutteridge JMC, editors. Experimental protocols for reactive oxygen and nitrogen species: Oxford University Press; 2000. p. 0.
18. Takahashi K. Glutathione peroxidase: coupled enzyme assay. 2000. p. 79-80.
19. Tian C, Zhao J, Xiong Q, Yu H, Du H. Secondary iron overload induces chronic pancreatitis and ferroptosis of acinar cells in mice. Int J Mol Med. 2023;51(1).

Anti-inflammatory Effects of *Rhinacanthus nasutus* Leaf Extract in TNF-α/IFN-γ–Stimulated HaCaT Keratinocytes

Sornmanee Chokthienanun[1], Narongrit Sritana[1,*], Anyamanee Chatsirisupachai[1], Piyakan Limtanyakul[1]

[1] Princess Srisavangavadhana Faculty of Medicine, Chulabhorn Royal Academy, Bangkok, Thailand

Abstract

Chronic inflammatory skin diseases such as atopic dermatitis are characterized by dysregulated immune responses and increased production of inflammatory mediators in the skin. Keratinocytes play an important role in cutaneous inflammation by producing chemokines that recruit immune cells to the site of inflammation. Among these mediators, CCL5 (RANTES) contributes to the recruitment of inflammatory cells and the persistence of skin inflammation. *Rhinacanthus nasutus* is a medicinal plant traditionally used in Southeast Asia for the treatment of inflammatory skin diseases and has been reported to possess anti-inflammatory and immunomodulatory activities. The objective of this study was to investigate the anti-inflammatory effects of *R. nasutus* leaf extract in TNF-α/IFN-γ–stimulated HaCaT keratinocytes. HaCaT cells were treated with serial dilutions of *R. nasutus* extract to determine non-cytotoxic concentrations using the PrestoBlue™ cell viability assay. Cells were then stimulated with TNF-α and IFN-γ (10 ng/mL each) and co-treated with non-toxic concentrations of the extract. CCL5 production in culture supernatants was measured using ELISA. High concentrations of the extract reduced cell viability, whereas dilutions ≥1:100 maintained viability comparable to untreated controls. Under inflammatory conditions, TNF-α/IFN-γ stimulation decreased cell viability after 48 h, whereas treatment with *R. nasutus* extract preserved keratinocyte viability, particularly at the 1:100 and 1:250 dilutions. In addition, the extract reduced CCL5 production in stimulated cells, with the 1:250 dilution showing a significant inhibitory effect compared with the stimulated control. These findings suggest that *R. nasutus* leaf extract may exert anti-inflammatory effects by modulating chemokine production and maintaining keratinocyte viability under inflammatory conditions. Further studies are required to elucidate the molecular mechanisms underlying its anti-inflammatory activity.

Keywords: *Rhinacanthus nasutus*, HaCaT keratinocytes, CCL5 (RANTES), inflammation, atopic dermatitis

Introduction

Chronic inflammatory skin diseases, such as atopic dermatitis (AD), are common conditions with complex pathogenesis involving immune dysregulation, cutaneous inflammation, and impairment of the skin barrier, which significantly affect patients' quality of life.[1] A key mechanism underlying disease development involves the activation of epidermal keratinocytes by multiple cytokines, leading to the release of inflammatory

mediators and chemokines that recruit immune cells into the skin and perpetuate chronic inflammation.[2]

Among the cytokines involved in cutaneous inflammation, tumor necrosis factor-alpha (TNF-α) and interferon-gamma (IFN-γ) play important roles in activating keratinocytes and promoting intracellular inflammatory signaling pathways.[3] This activation leads to increased expression and secretion of various pro-inflammatory chemokines, including regulated upon activation, normal T-cell expressed and secreted (RANTES/CCL5).[4] RANTES facilitates the recruitment of T cells, eosinophils, and macrophages into lesional skin, thereby contributing to the maintenance of chronic inflammatory infiltrates in AD.[5] Consequently, stimulation of keratinocytes with TNF-α and IFN-γ is widely used as a standard in vitro model to mimic inflammatory skin conditions and evaluate potential anti-inflammatory agents through inhibition of chemokine production.[4, 6]

Although current treatments for inflammatory skin diseases, including topical corticosteroids, calcineurin inhibitors, and biologic agents, are effective in controlling inflammation, their long-term use may be limited by adverse effects, high cost, and the need for prolonged therapy.[7] Therefore, increasing attention has been directed toward natural compounds with anti-inflammatory properties that may serve as safer alternatives or adjunctive treatments. Medicinal plants containing bioactive phytochemicals such as polyphenols, flavonoids, and naphthoquinones have been reported to reduce oxidative stress and inhibit inflammatory signaling pathways.[8]

Rhinacanthus nasutus (L.) Kurz, commonly known as "Thong Pan Chang," is a medicinal plant in the family Acanthaceae that has long been used in Southeast Asian traditional medicine for the treatment of inflammatory skin diseases and pruritic conditions.[9, 10] Phytochemical studies have identified several bioactive compounds in the leaves, including naphthoquinone derivatives such as rhinacanthin-C, rhinacanthin-D, and rhinacanthin-N, as well as flavonoids, phenolic compounds, steroids, triterpenoids, saponins, and tannins. These compounds have been associated with antioxidant, antimicrobial, and anti-inflammatory activities.[9, 11]

Previous studies have reported anti-inflammatory and immunomodulatory activities of *Rhinacanthus nasutus*. Preclinical studies demonstrated that standardized extracts rich in rhinacanthins can reduce both acute and chronic inflammation in animal models, including carrageenan-induced paw edema and cotton pellet-induced granuloma formation.[12] In cellular models, *R. nasutus* extracts have also been shown to improve keratinocyte survival under TNF-α/IFN-γ–induced inflammatory stress.[13] In addition, isolated rhinacanthins have demonstrated inhibitory effects on mast cell degranulation and pro-inflammatory cytokine production, suggesting potential anti-allergic and immunomodulatory properties.[14, 15] These findings support the biological plausibility of the anti-inflammatory effects observed in the present study.

However, information regarding the effects of *R. nasutus* extracts on the regulation of pro-inflammatory chemokine production in keratinocytes, particularly RANTES, remains limited. Therefore, the present study aimed to investigate the anti-inflammatory potential of *R. nasutus* leaf extract in TNF-α/IFN-γ–stimulated HaCaT keratinocytes by evaluating its effects on cell viability and CCL5 production.

Methods

Cell Culture

Human keratinocyte HaCaT cells were cultured in Dulbecco's Modified Eagle Medium (DMEM) supplemented with 10% fetal bovine serum and 1% penicillin–streptomycin. Cells were maintained at 37 °C in a humidified incubator with 5% CO_2 and subcultured when reaching approximately 70–80% confluence.

Rhinacanthus nasutus leaf extract

R. nasutus leaf extract was obtained as a commercial preparation (Dainty Spure Extract, WS-DAI). The extract was stored at 4 °C and diluted in culture medium to the indicated concentrations before use.

Cell Viability Assay

To determine the cytotoxicity of *R. nasutus* leaf extract, HaCaT cells were seeded into 96-well plates at a density of 3×10^4 cells per well and incubated overnight. Cells were then treated with serial dilutions of the extract (1:5, 1:10, 1:25, 1:50, 1:100, 1:250, 1:500, and 1:1000, v/v) for 24 and 48 h. Cell viability was assessed using the PrestoBlue™ cell viability assay according to the manufacturer's instructions. Fluorescence was measured using a microplate reader, and cell viability was expressed as a percentage relative to untreated control cells.

Cell viability under inflammatory conditions

To evaluate the effect of *R. nasutus* leaf extract on cell viability under inflammatory conditions, HaCaT cells were stimulated with tumor necrosis factor-α (TNF-α) and interferon-γ (IFN-γ) (10 ng/mL each). Cells were treated with non-toxic concentrations of *R. nasutus* leaf extract (1:100, 1:250, and 1:500, v/v), hydrocortisone as a positive anti-inflammatory control, or propylene glycol (PG) as the vehicle control.

After incubation for 24 and 48 hours, cell viability was measured using the PrestoBlue™ cell viability assay according to the manufacturer's protocol. Fluorescence was measured using a microplate reader, and cell viability was expressed as a percentage relative to the untreated medium control.

Measurement of CCL5 production

The anti-inflammatory activity of *R. nasutus* leaf extract was evaluated by measuring CCL5 (RANTES) secretion. HaCaT cells were seeded into 6-well plates at a density of 5×10^5 cells/well and allowed to adhere overnight. Cells were then stimulated with TNF-α and IFN-γ (10 ng/mL each) and co-treated with *R. nasutus* extract (1:100, 1:250, and 1:500, v/v), hydrocortisone, or vehicle control for 24 h. After incubation, culture supernatants were collected, and CCL5 levels were quantified using a LEGEND MAX™ Human CCL5 (RANTES) ELISA Kit (BioLegend, San Diego, CA, USA) according to the manufacturer's instructions.

Statistical analysis

Data are presented as mean ± standard deviation (SD) from three independent experiments ($n = 3$). Statistical analysis was performed using one-way analysis of variance (ANOVA) followed by Dunnett's multiple comparison test. A p-value < 0.05 was considered statistically significant.

Results

Effect of Rhinacanthus nasutus extract on HaCaT cell viability

The cytotoxicity of *R. nasutus* leaf extract was evaluated in HaCaT keratinocytes using the PrestoBlue™ cell viability assay. Cells were treated with serial dilutions of the

extract in culture medium (1:5 – 1:1000, v/v) for 24 and 48 h. As shown in **Figure 1**, high concentrations of the extract (1:5 and 1:10) significantly reduced cell viability after 24 h compared with the medium control. After 48 h, significant reductions in viability were observed at concentrations ranging from 1:5 to 1:50. Cell viability gradually increased with decreasing extract concentrations, and dilutions ≥1:100 maintained viability close to the control level. Therefore, dilutions of 1:100, 1:250, and 1:500 were selected as non-cytotoxic concentrations for subsequent experiments.

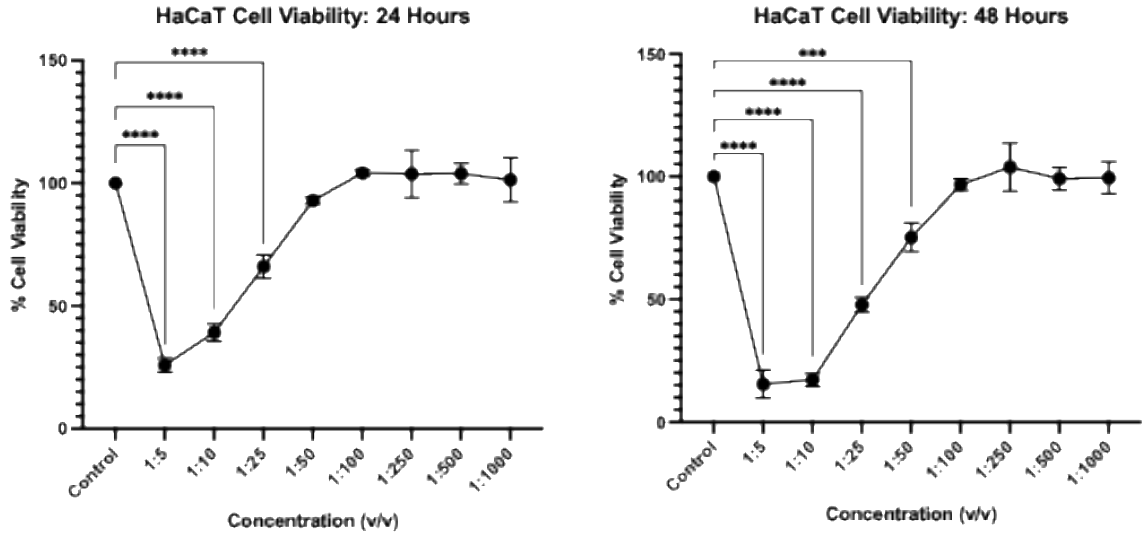

Figure 1. Effect of *R. nasutus* leaf extract on HaCaT cell viability. HaCaT keratinocytes were treated with serial dilutions of R. nasutus leaf extract (1:5–1:1000, v/v) for 24 and 48 h. Data are presented as mean ± SD (n = 3). Statistical analysis was performed using one-way ANOVA followed by Dunnett's multiple comparison test. *p < 0.05, **p < 0.01, ***p < 0.001 vs medium control.

Effect of Rhinacanthus nasutus leaf extract on HaCaT cell viability under inflammatory conditions

To evaluate the effect of *R. nasutus* extract under inflammatory conditions, HaCaT cells were co-treated with TNF-α and IFN-γ (10 ng/mL each) and non-toxic dilutions of the extract. As shown in **Figure 2**, cell viability remained above 90% across all treatment groups after 24 h, with no significant reduction compared with the medium control.

After 48 h, stimulation with TNF-α/IFN-γ alone resulted in a significant decrease in cell viability to approximately 77% ($p < 0.05$) compared with the medium control, indicating inflammatory stress. Cells treated with *R. nasutus* extract at dilutions of 1:100 and 1:250 maintained viability levels comparable to the untreated control. In contrast, the vehicle control (propylene glycol; PG) at dilutions of 1:250 and 1:500 showed a greater reduction in viability ($p < 0.0001$). These findings indicate that *R. nasutus* extract does not exhibit cytotoxic effects in TNF-α/IFN-γ–stimulated HaCaT cells and may help maintain cell viability under inflammatory conditions.

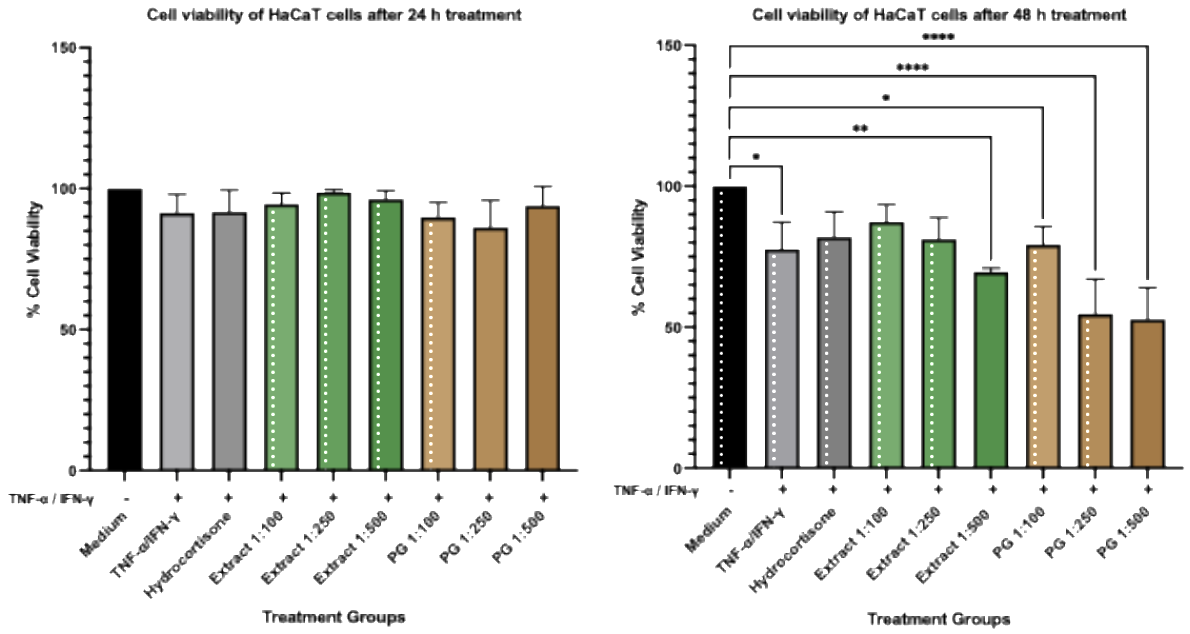

Figure 2. Cell viability of HaCaT cells after treatment with *R. nasutus* leaf extract in the presence of TNF-α/IFN-γ (TI). HaCaT keratinocytes were treated with non-toxic dilutions of *R. nasutus* leaf extract (1:100, 1:250, 1:500, v/v), vehicle control (propylene glycol; PG), or hydrocortisone in the presence of TNF-α/IFN-γ (TI; 10 ng/mL each) for 24 and 48 h. Data are presented as mean ± SD (n = 3). Statistical analysis was performed using one-way ANOVA followed by Dunnett's multiple comparison test. *p < 0.05, **p < 0.01, ***p < 0.001, ****p < 0.0001 vs medium control.

Inhibitory Effect of R. nasutus Extract on CCL5 Production

To evaluate the anti-inflammatory activity of *R. nasutus* extract, CCL5 production was measured in TNF-α/IFN-γ–stimulated HaCaT cells. As shown in **Figure 3**, stimulation with TNF-α/IFN-γ markedly increased CCL5 production compared with the medium control ($p < 0.001$). Treatment with hydrocortisone (positive control) significantly suppressed CCL5 levels compared with the stimulated control ($p< 0.01$), confirming the responsiveness of the inflammatory model.

Treatment with *R. nasutus* extract reduced CCL5 production in stimulated HaCaT cells, with the 1:250 dilution showing a significant reduction compared with the stimulated control ($p < 0.05$). Other extract concentrations showed a trend toward decreased CCL5 levels but did not reach statistical significance. In contrast, vehicle control groups containing propylene glycol (PG) showed higher CCL5 levels. These findings suggest that *R. nasutus* extract may modulate inflammatory chemokine production in keratinocytes under inflammatory conditions.

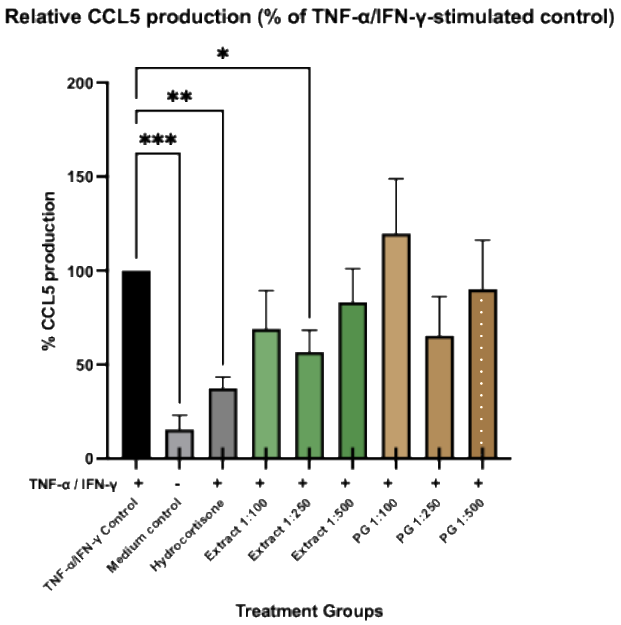

Figure 3. Relative CCL5 production (% of TNF-α/IFN-γ-stimulated control). HaCaT cells were stimulated with TNF-α and IFN-γ (10 ng/mL each) and treated with *R. nasutus* extract (1:100, 1:250, 1:500), hydrocortisone, or propylene glycol (PG) as the vehicle control at the indicated concentrations. CCL5 levels in culture supernatants were measured by ELISA. Results are expressed as relative CCL5 production (% of TNF-α/IFN-γ–stimulated control). Data are presented as mean ± SD (n = 3). Statistical analysis was performed using one-way ANOVA followed by Dunnett's multiple comparisons test. *p < 0.05, **p < 0.01, ***p < 0.001 vs stimulated control.

Discussion

Chronic inflammatory skin diseases such as atopic dermatitis involve persistent activation of keratinocytes and the production of chemokines that drive immune cell recruitment and sustain cutaneous inflammation.[3] The management of inflammatory skin conditions therefore requires a balance between protecting the integrity of the epidermis and modulating the local immune response.[2, 7] In this study, we investigated the dual role of *Rhinacanthus nasutus* leaf extract in supporting HaCaT keratinocyte survival and inhibiting the production of a key inflammatory chemokine, CCL5. Our findings suggest that the extract not only helps maintain cell viability under stress but also actively interferes with the signaling pathways that drive skin inflammation.

Our initial evaluation of cell viability under inflammatory conditions over 24 and 48 h revealed that the *R. nasutus* extract is non-toxic at the tested dilutions and, more importantly, provides a potential protective effect against cytokine-induced damage. The significant reduction in viability observed in the TNF-α/IFN-γ–stimulated group at 48 h confirms the success of our inflammatory model. By contrast, the preservation of cell health in the extract-treated groups indicates that *R. nasutus* may help stabilize keratinocytes against the apoptotic signals typically triggered by these pro-inflammatory cytokines. It is also notable that the vehicle control, propylene glycol (PG), exhibited its own level of toxicity at higher concentrations, which further validates that the survival-enhancing effects observed are specifically attributable to the plant extract itself.

Beyond simple cell survival, the ability of a topical agent to reduce leukocyte recruitment is critical for treating chronic skin inflammation. Keratinocytes are known to secrete CCL5 (RANTES) in response to TNF-α and IFN-γ, a process that recruits T cells and eosinophils to the skin.[4] In our ELISA results, the *R. nasutus* extract effectively suppressed relative CCL5 production compared with the stimulated control. The significant inhibition observed at the 1:250 dilution suggests that the extract can modulate the secretory profile of keratinocytes even under inflammatory conditions. While hydrocortisone showed a more potent reduction, the extract's performance is encouraging, especially considering the potential for fewer long-term side effects compared with traditional corticosteroids.

Future investigations should focus on exploring a broader range of chemokines relevant to inflammatory skin diseases to fully characterize the extract's inhibitory profile. In addition, identifying the specific active phytochemical compounds and their concentrations within the extract will be important for understanding its bioactivity. Further studies investigating molecular targets, such as the NF-κB or JAK/STAT signaling pathways, will also be necessary to elucidate the mechanisms underlying the observed anti-inflammatory and cytoprotective properties.

Conclusion

In conclusion, *Rhinacanthus nasutus* leaf extract showed no cytotoxic effects on HaCaT keratinocytes at appropriate dilutions and maintained cell viability under TNF-α/IFN-γ–induced inflammatory conditions. The extract also significantly reduced CCL5 production in stimulated keratinocytes, suggesting potential anti-inflammatory activity. These findings support further investigation of *R. nasutus* as a candidate for managing inflammatory skin conditions.

Acknowledgement

This research was supported by a research grant from Chulabhorn Royal Academy, Bangkok, Thailand.

References

1. Kim J, Kim BE, Leung DYM. Pathophysiology of atopic dermatitis: Clinical implications. Allergy Asthma Proc. 2019;40(2):84-92.
2. Tsakok T, Woolf R, Smith CH, Weidinger S, Flohr C. Atopic dermatitis: the skin barrier and beyond. Br J Dermatol. 2019;180(3):464-74.
3. Fania L, Moretta G, Antonelli F, Scala E, Abeni D, Albanesi C, et al. Multiple Roles for Cytokines in Atopic Dermatitis: From Pathogenic Mediators to Endotype-Specific Biomarkers to Therapeutic Targets. Int J Mol Sci. 2022;23(5).
4. Wakugawa M, Nakamura K, Akatsuka M, Nakagawa H, Tamaki K. Interferon-gamma-induced RANTES production by human keratinocytes is enhanced by IL-1beta, TNF-alpha, IL-4 and IL-13 and is inhibited by dexamethasone and tacrolimus. Dermatology. 2001;202(3):239-45.
5. Pivarcsi A, Homey B. Chemokine networks in atopic dermatitis: traffic signals of disease. Curr Allergy Asthma Rep. 2005;5(4):284-90.
6. Dong L, Lee H, Liu Z, Woo ER, Lee DS. Anti-Inflammatory Activity of Compounds Isolated from Digitalis purpurea L. in TNF-α/IFN-γ-Induced HaCaT Keratinocytes and a Three-Dimensionally Reconstructed Human Skin Model. Int J Mol Sci. 2025;26(16).
7. Sidbury R, Alikhan A, Bercovitch L, Cohen DE, Darr JM, Drucker AM, et al. Guidelines of care for the management of atopic dermatitis in adults with topical therapies. J Am Acad Dermatol. 2023;89(1):e1-e20.

8. Arora P, Bhatia S, Garg M, Kumari S, Goyal A. Curative Potency of Medicinal Plants in Management of Eczema: A Conservative Approach. Phytomedicine Plus. 2022;2:100256.
9. Brimson JM, Prasanth MI, Malar DS, Brimson S, Tencomnao T. Rhinacanthus nasutus "Tea" Infusions and the Medicinal Benefits of the Constituent Phytochemicals. Nutrients. 2020;12(12):3776.
10. Brimson JM, Tencomnao T. Medicinal herbs and antioxidants: potential of Rhinacanthus nasutus for disease treatment? Phytochemistry Reviews. 2014;13(3):643-51.
11. Sivagnanam S, Ranganathan V, Subban P. Qualitative Phytochemical analysis of Rhinacanthus nasutus. The Journal of Phytopharmacology. 2021;10:316-8.
12. Bhusal N, Panichayupakaranant P, Reanmongkol W. In vivo analgesic and anti-inflammatory activities of a standardized Rhinacanthus nasutus leaf extract in comparison with its major active constituent rhinacanthin-C. Songklanakarin Journal of Science and Technology. 2014;36:325-31.
13. Thongrakard V, Tencomnao T. Modulatory effects of Thai medicinal plant extract on proinflammatory cytokines-induced apoptosis in human keratinocyte HaCaT cells. African Journal of Biotechnology. 2010;9:4999-5003.
14. Tewtrakul S, Tansakul P, Panichayupakaranant P. Anti-allergic principles of Rhinacanthus nasutus leaves. Phytomedicine. 2009;16(10):929-34.
15. Dahima R. Inhibition of Innate Immune Responses of Polymorphonuclear Leucocytes and Monocytes by Rhinacanthin-C. Journal of Drug Delivery and Therapeutics. 2019;9:40-2.

Panduratin A Induces Apoptosis and Cell Cycle Arrest Mediated by AMPK in Diffuse Large B-cell Lymphoma

Jiranan Janpattanapichai[1], Piyanuch Wonganan[2], Kran Suknuntha[3,4], Pornpun Vivithanaporn[3,4], Suttinee Phuagkhaopong[2,*]

[1] Interdisciplinary Program in Pharmacology, College of Interdisciplinary and Integrative Studies, Chulalongkorn University, Bangkok, Thailand.
[2]Department of Pharmacology, Faculty of Medicine, Chulalongkorn University, Bangkok, Thailand.
[3]Chakri Naruebodindra Medical Institute, Faculty of Medicine Ramathibodi Hospital, Mahidol University, Samut Prakan, Thailand.
[4]Ramathibodi Medical School, Faculty of Medicine Ramathibodi Hospital, Mahidol University, Samut Prakan, Thailand.

Abstract

Diffuse large B-cell lymphoma (DLBCL) is an aggressive B-cell malignancy. Although a R-CHOP regimen remains the standard treatment, 30–40% of patients develop relapsed or refractory disease. Reduced AMP-activated protein kinase (AMPK) activity has been observed in DLBCL and may contribute to disease pathogenesis and progression. Panduratin A (Pan A), a cyclohexanyl chalcone derived from *Boesenbergia rotunda* or fingerroot, has shown anti-cancer effects through activation of AMPK in melanoma. In our study, human DLBCL cell lines were selected and treated with Pan A to detect its anti-cancer effects on the proliferation, apoptosis, and AMPK signaling pathway. Pfeiffer and Toledo cells was cultured and treated with different Pan A concentrations for 24 hours followed by measuring the changes of cell proliferation activity and cell cycle by 3-(4,5-dimethylthiazol-2-yl)-2,5-diphenyltetrazolium bromide (MTT) assay and flow cytometry, respectively. Protein expressions of Cyclin-dependent kinase (CDK) 4, Cyclin D1, B-cell lymphoma-extra large (Bcl-xL), Bcl-2 homologous antagonist/killer (Bak), Poly (ADP-ribose) polymerase (PARP), and topoisomerase II were tested by Western blot, and the level of AMP-activated protein kinase (AMPK) was also detected. Different concentrations of Pan A inhibited cell proliferation in a dose-dependent manner. The proportion of cells in the G0/G1 phase markedly increased, while the proportions of cells in the S and G2/M phases decreased after 24 hours of treatment with Pan A at concentrations of 5 and 10 μM. In addition, Pan A with a concentration of 10 μM further induced apoptotic cell death. Western blot results reveal a reduction in CDK4, Cyclin D1, topoisomerase II, and Bcl-xL protein expression, together with an increase in Bak, cleaved PARP, and AMPK protein levels. In addition, inhibiting AMPK activity by its specific inhibitor abolished Pan A-induced apoptotic cell death. Taken together, these results suggest that Pan A induces G0/G1 phase arrest, apoptosis, and activates the AMPK pathway in human DLBCL.

Keywords: Panduratin A, AMPK activator, DLBCL, G0/G1 arrest, mitochondrial pathway

Introduction

Diffuse large B cell lymphoma (DLBCL) is the most common aggressive B-cell lymphoma subtype in Thailand and worldwide[1]. A standard regimen for DLBCL treatment is R-CHOP which combines rituximab with cyclophosphamide, doxorubicin, vincristine, and prednisolone[2]. However, only half of patients treated with R-CHOP achieve long-term clinical benefits since 10% to 15% of patients have primary refractory disease after 6 months, and 20% to 25% of patients have a relapse within 2 years after initial chemotherapy[3]. Currently, there is no standard treatment for relapses/refractory DLBCL.

Panduratin A (Pan A) is a cyclohexanol chalcone found in rhizome extract of *Boesenbergia rotunda* or fingerroot[4]. Pan A has been well reported to possess anti-metabolic effects, anti-inflammatory effects, and anti-viral effects[4]. Moreover, Pan A has shown anti-cancer effects in various cancer cell types such as breast cancer[5], lung cancer[6], colon cancer[7], and melanoma[8]. Pan A interferes with cancer-promoting signaling through activation of AMP-activated protein kinase (AMPK) and inhibition of mechanistic target of rapamycin (mTOR) pathways[9]. Recent study by our group has demonstrated that Pan A exerts anti-cancer effects in leukemia and lymphoma, with the Forkhead box O (FOXO) 3 pathway identified by transcriptomics as a potential underlying mechanism[10].

AMPK signaling pathway is involved in regulating various cellular processes, such as cell survival and cell death, through mechanistic target of rapamycin complex (mTORC) 1 inhibition[9] and FOXO3a activation[10]. In cancer, AMPK pathway plays a dual role in the progression of tumor cells by either suppressing or promoting cancer development, depending on several factors. Evidence suggests that AMPK activators have potential therapeutic efficacy in the treatment of lymphoma[11]. Therefore, this study aims to investigate the role of AMPK pathway in the anticancer effects of Pan A in DLBCL.

Methods

Cell culture

Pfeiffer and Toledo were cultured in Iscove's Modified Dulbecco's Medium (IMDM) supplemented with 10% (v/v) fetal bovine serum and 1% (v/v) penicillin-streptomycin. The cells were maintained in a humidified atmosphere with 5% CO_2 at 37°C.

3-(4,5-dimethylthiazol-2-yl)-2,5-diphenyltetrazolium bromide (MTT) cell viability assay

After 24 hours of Pan A treatment, with or without 2 hours of AMPK inhibitor pretreatment, cells were incubated with MTT solution for 3 hours, and dimethyl sulfoxide (DMSO) was subsequently added to dissolve the insoluble formazan crystals. Absorbance was measured at 570 and 650 nm using a microplate reader. The IC_{50} values were calculated.

bromodeoxyuridine (BrdU) cell proliferation assay

After 24 hours of Pan A treatment, cells were labeled with BrdU solution for 24 hours, followed by anti-BrdU-fluorescein isothiocyanate (FITC) conjugated antibody staining. The fluorescence signal was analyzed using a flow cytometer.

Annexin V–FITC and Propidium Iodide (PI) cell apoptosis assay

After 24 hours of Pan A treatment, with or without 2 hours of AMPK inhibitor pretreatment, cells were stained with Annexin V-FITC for 1 hour, followed by PI staining for 15 minutes. The fluorescence signal was analyzed using a flow cytometer.

Western immunoblotting

After 24 hours of Pan A treatment, cells were lysed to extract total cellular proteins. The protein samples were separated by sodium dodecyl sulfate–polyacrylamide gel electrophoresis and transferred onto a nitrocellulose membrane. The membranes were probed with specific primary antibodies against Bcl-2 homologous antagonist/killer (Bak), B-cell lymphoma-extra large (Bcl-xL), Poly (ADP-ribose) polymerase (PARP) 1, cleaved PARP, topoisomerase II, Cyclin-dependent kinase (CDK) 4, Cyclin D1, phosphorylated AMPK (p-AMPK), total AMPK (AMPK), and β-actin. Protein bands were detected using a chemiluminescence method.

Statistical analysis

All data presented as mean ± standard error of the mean (SEM). Statistical comparisons were performed using one-way ANOVA followed by Tukey's test ($p < 0.05$) using GraphPad Prism version 11.0.

Results

Pan A exhibited cytotoxic effects on DLBCL cells.

Pan A decreased cell viability of DLBCL in a dose-dependent manner. At 24 hours, the IC_{50} values of Pan A in Pfeiffer and Toledo cells were 8.08 ± 1.05 μM and 9.66 ± 1.09 μM, respectively (**Figure 1**). Pan A at 5 and 10 μM exerted anti-proliferative effects, as evidenced by an increased proportion of cells in the G0/G1 phase and a reduced proportion of cells in the S and G2/M phases. Next, to elucidate the underlying molecular mechanisms, the expression of key cell cycle–regulatory proteins were examined. Western blot analysis revealed a significant reduction in the expression of CDK4 and Cyclin D1 (**Figure 2**). These findings suggest that Pan A inhibited cell proliferation through the suppression of key regulatory proteins involved in the G0/G1-to-S phase transition.

In contrast, treatment with 10 μM Pan A, but not 5 μM, induced apoptotic cell death and modulated mitochondrial-apoptotic protein expression, as evidenced by decreased levels of the anti-apoptotic protein Bcl-xL and increased levels of the pro-apoptotic protein Bak and cleaved PARP. Furthermore, a marked reduction in topoisomerase II expression was observed following exposure to 10 μM of Pan A, suggesting a potential mechanism by which Pan A induced apoptosis (**Figure 3**).

Pan A exhibited cytotoxic effects on DLBCL cells through AMPK pathway.

To further investigate the role of AMPK pathway in the anticancer effects of Pan A in DLBCL. We evaluated the expression of p-AMPK and AMPK by Western Blotting. Pan A increased p-AMPK/AMPK expression ratio in both cell types (**Figure 4**). In addition, a specific AMPK inhibitor, dorsomorphin, was employed to investigate whether Pan A induces cell death through regulation of the AMPK signaling pathway. The results demonstrated that pretreatment with dorsomorphin attenuated Pan A-induced cell death, as determined by the MTT assay. Notably, this effect was more pronounced when dorsomorphin was combined with a low dose of Pan A (**Figure 5**). This may be because,

at higher concentrations, the inhibitor itself can induce cytotoxicity, potentially leading to enhanced cell death. In addition to the cell viability assay, the percentage of apoptotic cells was assessed by flow cytometry. Consistently, Pan A significantly increased apoptotic cell populations, whereas this effect was tended to attenuate by dorsomorphin treatment (**Figure 6**).

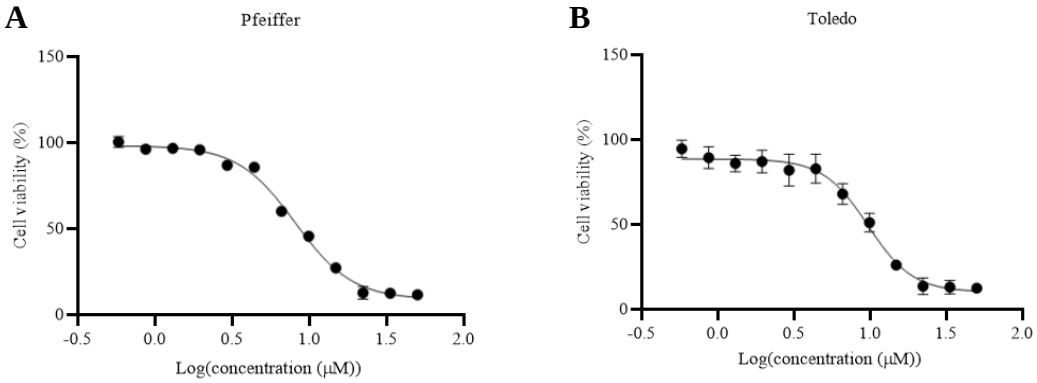

Figure 1. Pan A decreased cell viability of Pfeiffer (A) and Toledo (B) in a dose-dependent manner. Data presented mean ± SEM.

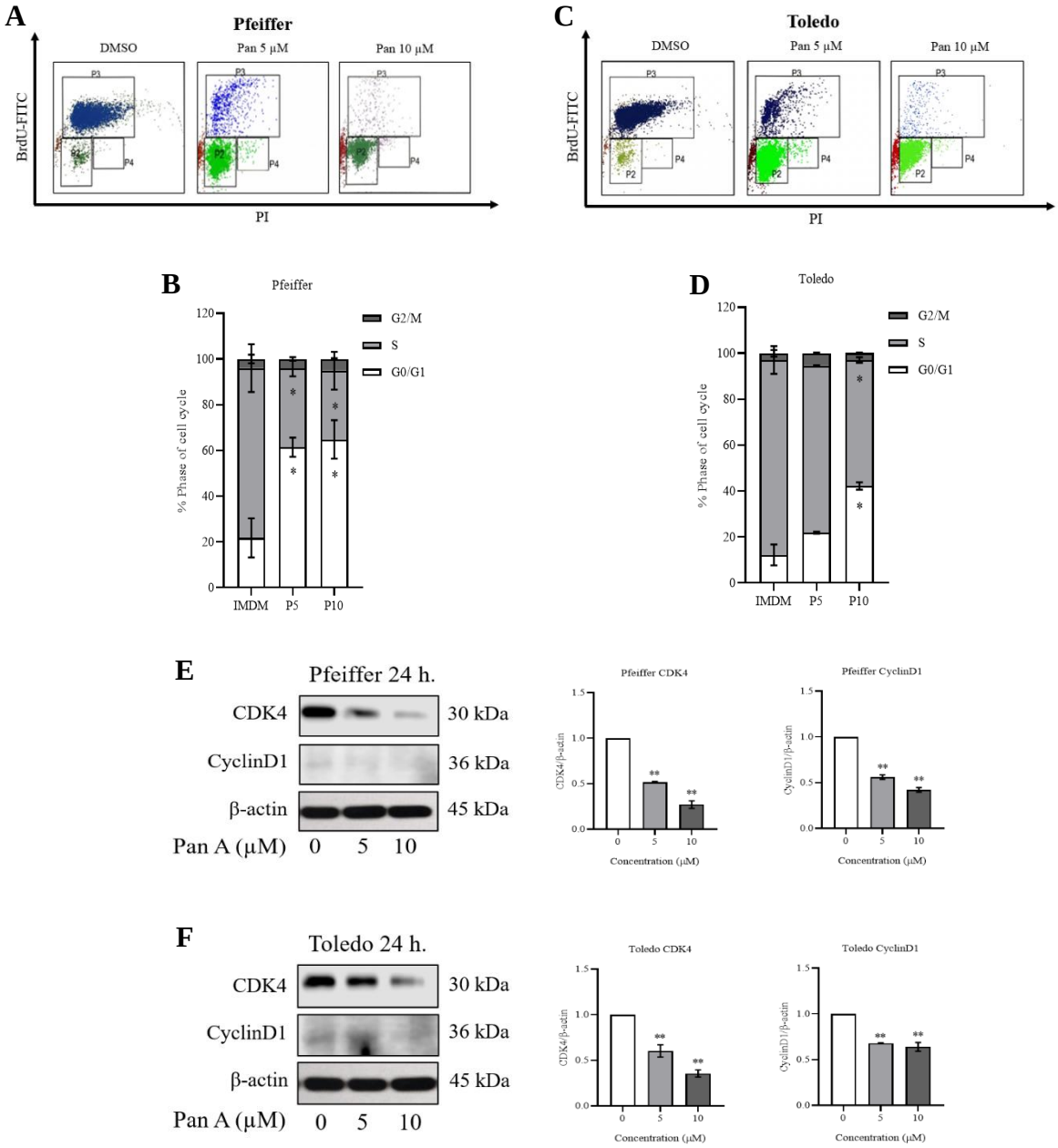

Figure 2. Pan A inhibited cell progression of Pfeiffer (A-B) and Toledo (C-D) from G0/G1 phase to S phase by modulating cell cycle-related protein expression, including CDK4 and Cyclin D1 (E-F). Data presented mean ± SEM. *p≤0.05 and **p≤0.01, when compared to PanA-treated cells with mock-treated cells (0.01%DMSO).

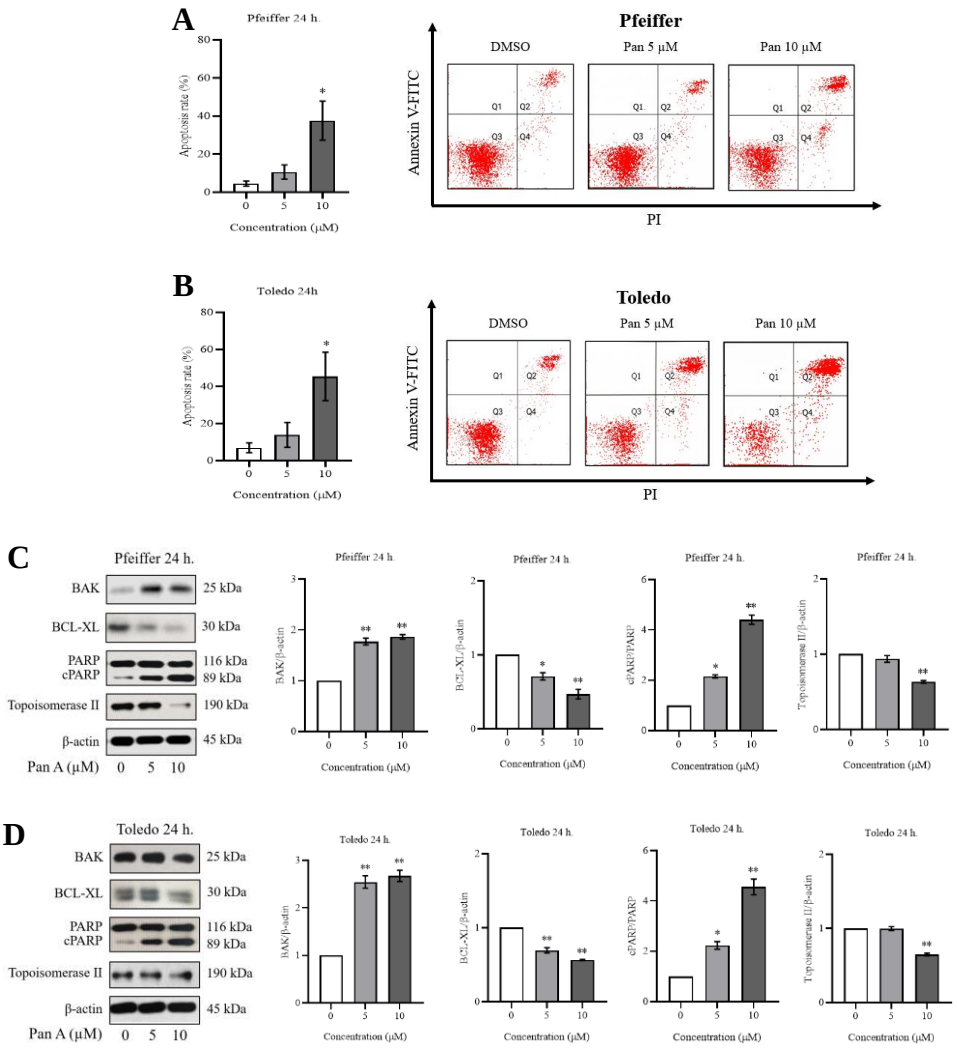

Figure 3. Pan A induced apoptotic cell death in Pfeiffer (A) and Toledo (B) via activation of the mitochondrial apoptotic pathway, as evidenced by reduced expression of Bcl-xL and topoisomerase II, along with increased levels of BAK and cleaved PARP, respectively (C-D). Data presented mean ± SEM. *p≤0.05 and **p≤0.01, when compared to PanA-treated cells with mock-treated cells (0.01%DMSO).

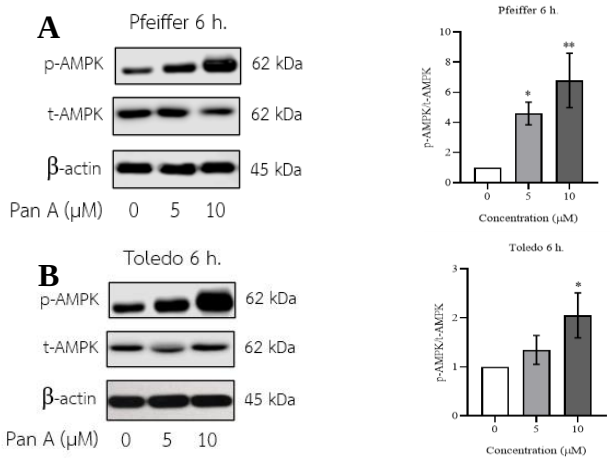

Figure 4. Pan A increased p-AMPK/AMPK expression ratio in Pfeiffer (A) and Toledo (B). Data presented mean ± SEM. *p≤0.05 and **p≤0.01, when compared to PanA-treated cells with mock-treated cells (0.01%DMSO).

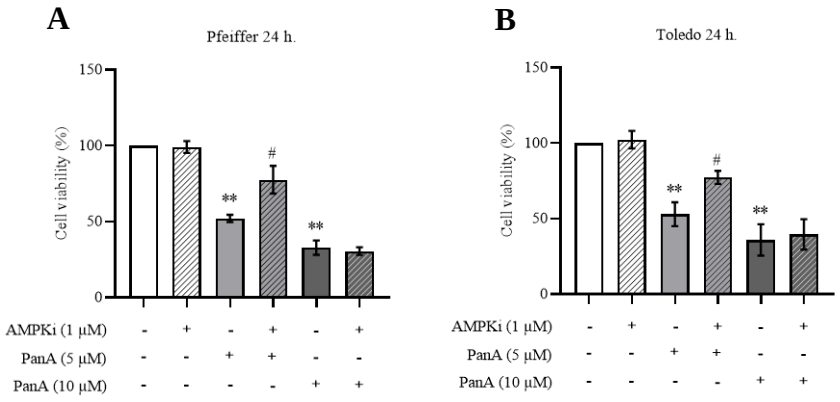

Figure 5. Pretreatment with a specific AMPK inhibitor attenuated Pan A-induced cell death in Pfeiffer (A) and Toledo (B). Data presented mean ± SEM. *p≤0.05 and **p≤0.01, when compared to PanA-treated cells with mock-treated cells (0.01%DMSO). #p≤0.05, when compared between Pan A-treated cells with and without a specific AMPK inhibitor.

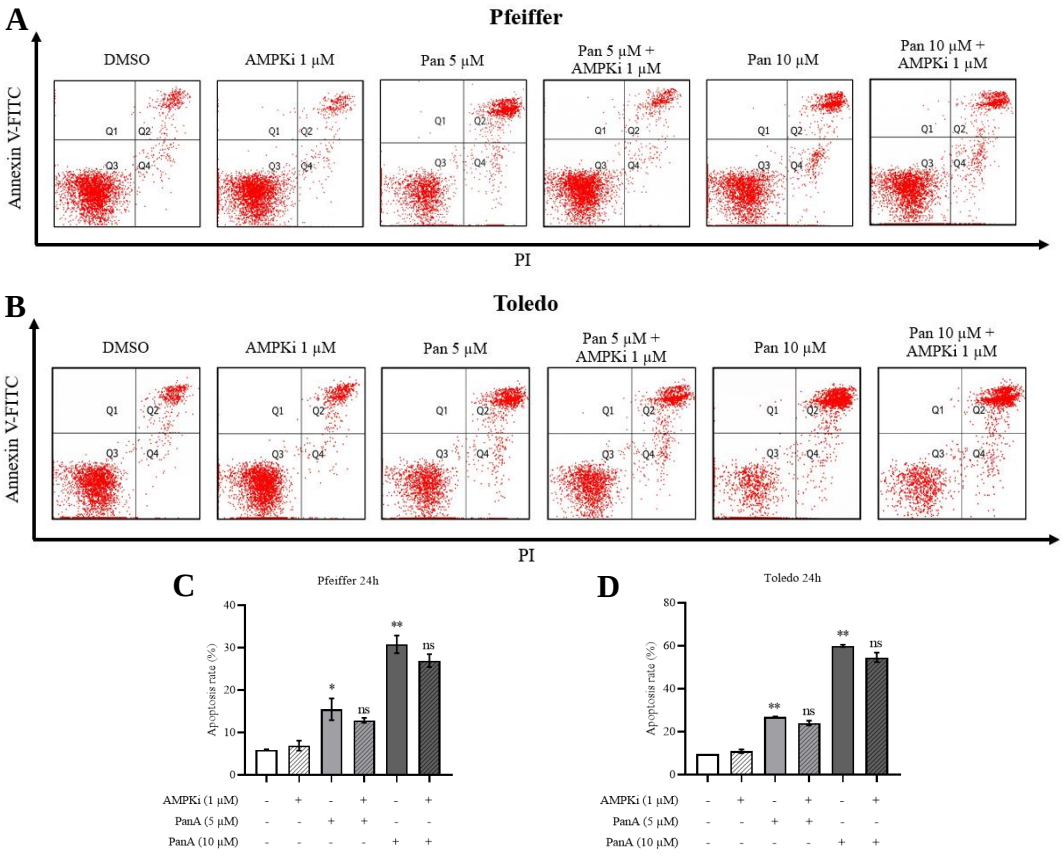

Figure 6. Inhibiting AMPK activity by a specific AMPK inhibitor abolished Pan A-induced apoptotic cell death in Pfeiffer (A, C) and Toledo (B, D). Data presented mean ± SEM. *p≤0.05 and **p≤0.01, when compared to PanA-treated cells with mock-treated cells (0.01%DMSO). ns, when no statistically significant difference was observed between Pan A-treated cells with and without a specific AMPK inhibitor.

Discussion

Pan A inhibits G0/G1 cell progression and induces apoptosis in DLBCL. This process is characterized by the significant reduction in CDK4 and Cyclin D1 expression. Since the Cyclin D1/CDK4 complex is essential for the transition from G1 to S phase, its downregulation effectively halts DNA synthesis and cellular division. These findings are consistent with the study by Phuagkhaopong *et al.*[10], which reported that Pan A at 10 µM increases the number of cells in G0/G1 phase in leukemia and lymphoma cells. Similarly, Liu *et al.*[5] found that Pan A promotes G0/G1 arrest in human breast cancer cells (MCF7 and T47D) through the downregulation of Cyclin D1/CDK4 and upregulation of p21/p27. Moreover, we found that Pan A, a potent AMPK activator, showed comparable results to commercial AMPK activators such as metformin and 5-Aminoimidazole-4-carboxamide ribonucleoside (AICAR) across various solid[12-14] and hematological malignancies[11, 15, 16], which also promotes cell death by mitochondria-apoptotic cell death through the upregulation of pro-apoptotic proteins, such as Bak and cleaved PARP,

alongside the downregulation of the anti-apoptotic protein Bcl-xL. This mechanism is strongly supported by research in other models. For instance, Yun *et al.*[7] Pan A induced apoptosis in colon cancer cells (HT29) via Caspase-3/PARP cascade. Liu *et al.*[5] demonstrated that in breast cancer cells, Pan A modulates cytochrome c, Bax, and B-cell lymphoma-2 (Bcl-2). The consistent involvement of the Bcl-2 family across these diverse models highlights the mitochondrial pathway as a central target for Pan A-mediated cytotoxicity.

Anti-tumor effects in DLBCL are mediated through the activation of AMPK. AMPK acts as a master regulator of cellular energy homeostasis, exerting pleiotropic effects on metabolism and cell growth. Elevated AMPK activity modulates several downstream pathways, including the suppression of fatty acid synthesis[17, 18]. Crucially, AMPK regulates mTORC1[20, 21], thereby promoting apoptosis and restricting proliferation. This aligns with reports in Jurkat cells, which suggested that AMPK inhibition abrogated the effects of metformin[11]. Studies also elicited that Pan A inhibited cancer cell growth by complex crosstalk of multi-pathways[6, 22]. For instance, Eiamart et al. reported that Pan A induces apoptosis in non-small cell lung cancer (NSCLC) cell lines (A549 and H1975) by inhibiting the epidermal growth factor receptor/ signal transducer and activator of transcription 3/ protein kinase B (EGFR/STAT3/AKT) signaling pathways[6].

Despite these significant findings, some limitations remain. Firstly, Pan A acts as a potent AMPK activator; however, further studies are required to fully elucidate its downstream signaling pathways such as mTOR and AKT. Secondly, in terms of the selectivity of Pan A on cancer cells, the cytotoxic effect of Pan A on normal cells, particularly blood cells, should be studied. Lastly, *in vivo* studies are warranted to assess the safety and efficacy of Pan A before transition to clinical evaluation.

Conclusion

In summary, we demonstrated that Pan A suppressed proliferation, regulated G0/G1 phase cell cycle arrest, and induced apoptosis in DLBCL. In addition, Pan A activated the AMPK pathway, which led to the induction of apoptosis through mitochondrial-apoptotic cell death. These findings may lead to a novel area of research into DLBCL treatment.

Acknowledgement

The authors would like to express their gratitude to the Department of Pharmacology, Faculty of Medicine, Chulalongkorn University, for providing the laboratory facilities and scientific equipment used in this study.

References

1. Susanibar-Adaniya S, Barta SK. 2021 Update on Diffuse large B cell lymphoma: A review of current data and potential applications on risk stratification and management. Am J Hematol. 2021;96(5):617-29.

2. Coiffier B, Lepage E, Briere J, Herbrecht R, Tilly H, Bouabdallah R, et al. CHOP chemotherapy plus rituximab compared with CHOP alone in elderly patients with diffuse large-B-cell lymphoma. N Engl J Med. 2002;346(4):235-42.
3. Sehn LH, Salles G. Diffuse Large B-Cell Lymphoma. N Engl J Med. 2021;384(9):842-58.
4. Kim D, Lee MS, Jo K, Lee KE, Hwang JK. Therapeutic potential of panduratin A, LKB1-dependent AMP-activated protein kinase stimulator, with activation of PPARalpha/delta for the treatment of obesity. Diabetes Obes Metab. 2011;13(7):584-93.
5. Liu Q, Cao Y, Zhou P, Gui S, Wu X, Xia Y, et al. Panduratin A Inhibits Cell Proliferation by Inducing G0/G1 Phase Cell Cycle Arrest and Induces Apoptosis in Breast Cancer Cells. Biomol Ther (Seoul). 2018;26(3):328-34.
6. Eiamart W, Wonganan P, Tadtong S, Samee W. Panduratin A from Boesenbergia rotunda Effectively Inhibits EGFR/STAT3/Akt Signaling Pathways, Inducing Apoptosis in NSCLC Cells with Wild-Type and T790M Mutations in EGFR. International Journal of Molecular Sciences. 2025;26(5):2350.
7. Yun JM, Kwon H, Mukhtar H, Hwang JK. Induction of apoptosis by Panduratin A isolated from Kaempferia pandurata in human colon cancer HT-29 cells. Planta Med. 2005;71(6):501-7.
8. Lai SL, Mustafa MR, Wong PF. Panduratin A induces protective autophagy in melanoma via the AMPK and mTOR pathway. Phytomedicine. 2018;42:144-51.
9. Song Y, Zhang P, Sun Y, Li X, Chen L, Xiao Y, et al. AMPK activation-dependent autophagy compromises oleanolic acid-induced cytotoxicity in human bladder cancer cells. Oncotarget. 2017;8(40):67942-54.
10. Phuagkhaopong S, Janpattanapichai J, Sirirak N, Khemawoot P, Vivithanaporn P, Suknuntha K. Transcriptome analysis reveals a role of FOXO3 in antileukemia/lymphoma properties of panduratin A. Sci Rep. 2024;14(1):24795.
11. Shi WY, Xiao D, Wang L, Dong LH, Yan ZX, Shen ZX, et al. Therapeutic metformin/AMPK activation blocked lymphoma cell growth via inhibition of mTOR pathway and induction of autophagy. Cell Death Dis. 2012;3(3):e275.
12. Memmott RM, Mercado JR, Maier CR, Kawabata S, Fox SD, Dennis PA. Metformin prevents tobacco carcinogen--induced lung tumorigenesis. Cancer Prev Res (Phila). 2010;3(9):1066-76.
13. Su CC, Hsieh KL, Liu PL, Yeh HC, Huang SP, Fang SH, et al. AICAR Induces Apoptosis and Inhibits Migration and Invasion in Prostate Cancer Cells Through an AMPK/mTOR-Dependent Pathway. Int J Mol Sci. 2019;20(7).
14. Brown JR, Chan DK, Shank JJ, Griffith KA, Fan H, Szulawski R, et al. Phase II clinical trial of metformin as a cancer stem cell-targeting agent in ovarian cancer. JCI Insight. 2020;5(11).
15. Vakana E, Altman JK, Glaser H, Donato NJ, Platanias LC. Antileukemic effects of AMPK activators on BCR-ABL-expressing cells. Blood. 2011;118(24):6399-402.
16. Green AS, Chapuis N, Maciel TT, Willems L, Lambert M, Arnoult C, et al. The LKB1/AMPK signaling pathway has tumor suppressor activity in acute myeloid leukemia through the repression of mTOR-dependent oncogenic mRNA translation. Blood. 2010;116(20):4262-73.
17. Steinberg GR, Hardie DG. New insights into activation and function of the AMPK. Nat Rev Mol Cell Biol. 2023;24(4):255-72.
18. Herzig S, Shaw RJ. AMPK: guardian of metabolism and mitochondrial homeostasis. Nat Rev Mol Cell Biol. 2018;19(2):121-35.
19. Jang JE, Eom J-I, Jeung H-K, Cheong J-W, Lee JY, Kim JS, et al. AMPK–ULK1-mediated autophagy confers resistance to BET inhibitor JQ1 in acute myeloid leukemia stem cells. Clinical Cancer Research. 2017;23(11):2781-94.
20. Xia YC, Zha JH, Sang YH, Yin H, Xu GQ, Zhen J, et al. AMPK activation by ASP4132 inhibits non-small cell lung cancer cell growth. Cell Death Dis. 2021;12(4):365.
21. Zhong ZT, Wang XY, Pan Y, Zhou K, Chen JH, Gao YQ, et al. AMPK: An energy sensor for non-small cell lung cancer progression and treatment. Pharmacol Res. 2025;212:107592.

22. Sun S, Kim MJ, Omar AM, Phan ND, Awale S. (+)-Panduratin A induces PANC-1 human pancreatic cancer cell death preferentially under nutrient starvation by inhibiting PI3K/Akt/mTOR/autophagy signaling pathway. Phytomedicine plus. 2021;1(4):100101.

Biological effects of iberin on cholangiocarcinoma cells

Nanthawut Buachaban [a], Rattanaporn Jaidee [a], Sarinya Kongpetch [a,b], Auemduan Prawan [a,b], Laddawan Senggunprai [a,b], Karnchanok Kaimuangpak [a,b], Natthida Weerapreeyakul [c], Piman Pocasap [a,b*]

[a] Department of Pharmacology, Faculty of Medicine, Khon Kaen University, Khon Kaen, 40002, Thailand
[b] Cholangiocarcinoma Research Institute, Khon Kaen University, Khon Kaen, 40002, Thailand
[c] Division of Pharmaceutical Chemistry, Faculty of Pharmaceutical Sciences, Khon Kaen University, Khon Kaen, 40002, Thailand

Abstract

Iberin (IBN), a naturally occurring isothiocyanate, has shown anticancer activity in several malignancies, but its effect on cholangiocarcinoma (CCA) remains unclear. This study investigated the anticancer activity of IBN in CCA cells. Cell viability was assessed by sulforhodamine B (SRB) assay in the CCA cell line KKU-452. Cell cycle distribution was analyzed by propidium iodide (PI) staining, apoptosis induction was evaluated by acridine orange/ethidium bromide (AO/EB) and Annexin V/PI staining, and cell migration was examined using a wound healing assay. The results showed that IBN reduced CCA cell viability in a time- and concentration-dependent manner, with potency comparable to sulforaphane (SFN). At lethal concentrations (10 and 25 μM), IBN induced cell cycle arrest, causing S-phase arrest and G1-phase arrest, and also promoted apoptotic cell death. At sub-lethal concentrations (3.12 and 6.25 μM), IBN suppressed cell migration. However, IBN also affected the viability of non-cancerous cells, including MMNK-1 and NRK-52E cells, indicating limited selectivity under the present conditions. Overall, these findings suggest that IBN exerts multiple anticancer effects in CCA cells, including growth inhibition, apoptosis induction, and migration suppression. Given its limited selectivity, sub-lethal concentrations may represent a more suitable condition for further investigation. Further studies are needed to clarify its mechanisms of action and biological relevance in CCA.

Keywords: Iberin, Cholangiocarcinoma, Cell cycle, Apoptosis, Migration

Introduction

Cholangiocarcinoma (CCA) is a rare and heterogeneous group of malignancies arising from the biliary epithelium, particularly in Thailand, where it has the highest incidence and mortality worldwide. According to the pathological area, it is classified into intrahepatic, perihilar, and distal subtypes[1]. Although surgical excision is the preferred treatment for all subtypes, less than 50% of cases are successfully[2]. Radiation and chemotherapy both have limited effectiveness, and resistance is a major problem[3]. As a result, the identification of novel bioactive compounds with potential anticancer effects is of considerable interest.

Isothiocyanates (ITCs), which are naturally occurring compounds produced from glucosinolates in cruciferous vegetables, have been extensively studied, including antioxidant, anti-inflammatory, and anticancer effects. Sulforaphane (SFN) is one of the

most widely investigated. It shows a potential anticancer effect against many types of cancer through mechanisms such as oxidative stress modulation, apoptosis induction, and the inhibition of tumor progression pathways[4]. Besides SFN, several ITCs emerged as promising anticancer agents, although their biological actions are not as thoroughly characterized.

Iberin (IBN), an aliphatic ITC, has been reported to exhibit antitumor activity in several cancer types, including breast, glioblastoma, and liver cancers[5–7]. Previously, IBN has been shown to reduce cancer cell viability and induce apoptosis, potentially through mechanisms involving reactive oxygen species (ROS) generation and disruption of microtubule dynamics[7]. Thereby, IBN could be a bioactive agent of interest for cancer research. However, its biological effects in CCA remain unclear.

Given the aggressive nature of CCA and the limited treatment options. Further investigation into the anticancer potential of IBN is necessary. In the present study, we evaluated the effects of IBN in CCA cells using the KKU-452 cell line. The studies focused on cell viability, cell cycle progression, apoptosis, and migration to provide initial evidence of the biological activity of IBN in CCA cells and to support further investigation into its potential relevance as an anticancer agent.

Methods

Compounds

Iberin (IBN) (purity > 98%, HY-101413) was obtained from MedChemExpress (NJ, USA). Sulforaphane (SFN) (purity ≥98%, ALX-350-232-M025) was obtained from Enzo Life Sciences (NY, USA).

Cell line and Cell culture

The human cholangiocarcinoma cell line (KKU-452)[8]. The human cholangiocyte cell line (MMNK-1) was also purchased from JCRB Cell Bank, and a rat kidney cell line (NRK-1) was purchased from ATCC[9,10]. KKU-452 was cultured in Ham's F-12 medium (#21700-075, Life Technologies, NY, USA). MMNK-1 and NRK-52E were cultured in DEMEM-high glucose (#12800017, Life Technologies, NY, USA). Cells were grown in basal medium supplemented with 10% FBS in a 5% CO_2 humidified incubator at 37°C.

Sulforhodamine B (SRB) Assay

Cells were seeded into a 96-well plate at 7,500 cells per well in complete medium and incubated overnight at 37°C with 5% CO_2. Cells were treated with ITCs at various concentrations (0, 6.25, 12.5, 25, 50, 100 μM) for 24 and 48 h. Then, cells were fixed with 10% TCA at 4 °C, washed, and stained with 0.04% SRB. Excess dye was removed with 1% acetic acid, and plates were air-dried. Bound dye was solubilized in 10 mM Tris base (pH 10.5), and absorbance was measured at 540 nm using a Sunrise ELISA plate reader (Tecan, Austria).

Cell cycle analysis

Cells were seeded in a 6-well plate at $2.5x10^5$ cells per well in complete medium and incubated overnight at 37 °C with 5% CO_2. Cells were treated with 10 μM and 25 μM of IBN for 12 h. Cells were harvested and fixed using cold 70 % ethanol. Fixed cells were washed with 1x cold PBS and incubated with PI/RNase buffer for 1 h in the dark. DNA content was measured via flow cytometry afterward (BD FACS Calibur, San Jose, CA).

Acridine orange/ethidium bromide (AO/EB) staining

Cells were seeded into a 96-well plate at 7,500 cells per well in complete medium and incubated overnight at 37 °C with 5% CO_2. Cells were treated with 10 μM and 25 μM of IBN for 24 and 48 h. Following treatment, cells were stained with a mixture of acridine orange (AO) (10127-02-3) and ethidium bromide (EB) (1239-45-8), which were purchased from Sigma-Aldrich. An inverted phase contrast microscope (Nikon Eclipse TS100, Nikon Instruments Inc., Japan) with a B2A filter at 10× magnification was used to examine morphological changes. Cells were classified as viable, early apoptotic, late apoptotic, or necrotic. When attached to DNA, AO enters both viable and non-viable cells and emits green fluorescence, while EB is only absorbed by cells with damaged membrane integrity and emits orange to red fluorescence.

Annexin V/ PI staining

CCA cells were seeded in 6-well plates and incubated overnight at 37 °C with 5% CO_2. Cells were treated with 10 μM and 25 μM of IBN for 24 and 48 h. Cells were harvested, washed, and resuspended in 1x binding buffer. Subsequently, cell suspensions were incubated with 5 μl of Annexin V/PI at 4 °C in the dark for 15 min, following the protocol provided by the manufacturer's instructions. (BD Pharmingen™, Switzerland). Cell suspensions were analyzed by flow cytometry.

Wound healing assay

CCA cells were seeded in 24-well plates at $3x10^5$ cells per well and incubated overnight at 37 °C with 5% CO_2. A scratch was created using a sterile pipette tip, and the detached cells were washed with 1x PBS. Cells were then treated with 3.125 μM and 6.25 μM of IBN. The wound area was captured at 0 h and 18 h. Wound area was analyzed using the ImageJ plug-in, and percentage wound closure was calculated [11] as follows:

$$\%\,\boldsymbol{Wound\ closure} = \left(\frac{\boldsymbol{A_{t=0} - A_{t=\Delta t}}}{\boldsymbol{A_{t=0}}}\right) \times \mathbf{100}\,\%$$

Statistical analysis

All results are presented as the mean ± SEM. Data were analyzed using one-way ANOVA followed by Tukey's post hoc test using GraphPad Prism 8.0 software. Statistically, $p < 0.05$ was considered significant.

Results

Effect of IBN on cell viability

The effect of iberin (IBN) on CCA cells was initially evaluated using a cell viability assay in the KKU-452 cell line. Sulforaphane (SFN) was included as a reference isothiocyanate (ITC). IBN reduced CCA cell viability in a time- and concentration-dependent manner, with IC_{50} values of 22.51 and 13.67 μM at 24 and 48 h, respectively. Comparable effects were observed for SFN, which showed IC_{50} values of 19.23 and 13.65 μM at 24 and 48 h, respectively (**Figure 1**).

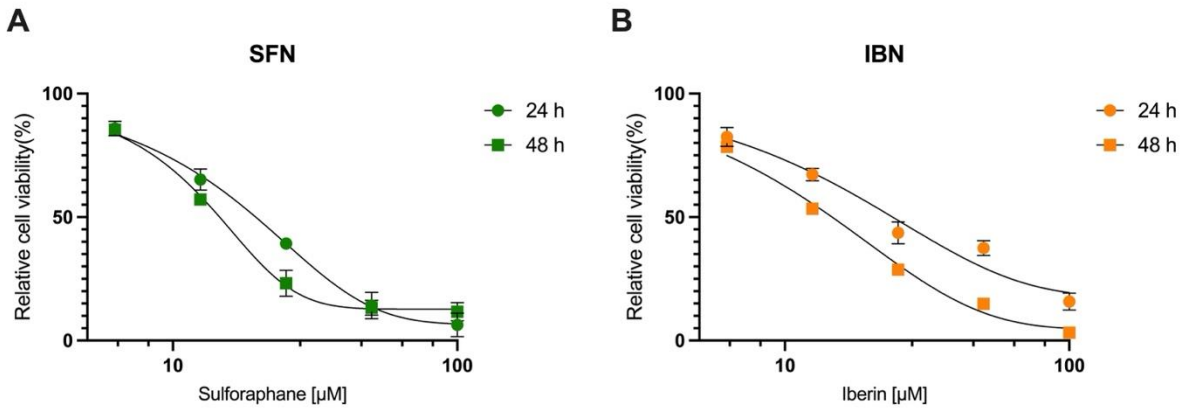

KKU-452	24 h		48 h	
	IC_{50}	Emax	IC_{50}	Emax
SFN	19.23 ± 0.73 μM	92.54 ± 6.09	13.65 ± 0.31 μM	88.60 ± 2.96
IBN	22.51 ± 2.90 μM	93.52 ± 1.47	13.67 ± 0.64 μM	98.66 ± 1.34

Figure 1. Effect of ITCs on cell viability of KKU-452 cell. Cell viability was assessed by SRB assay after 24 h and 48 h of treatment with different concentrations of (A) SFN and (B) IBN. Data were presented as mean ± SEM from independent experiments (n = 3).

The cytotoxic effects of both ITCs were further assessed at 24 h in non-cancerous cell lines, including immortalized cholangiocytes (MMNK-1) and normal rat kidney epithelial cells (NRK-52E). IBN exhibited IC_{50} values of 20.82 μM in MMNK-1 cells and 21.78 μM in NRK-52E cells. In comparison, SFN showed IC_{50} values of 22.01 μM in MMNK-1 cells and 18.14 μM in NRK-52E cells (**Figure 2**).

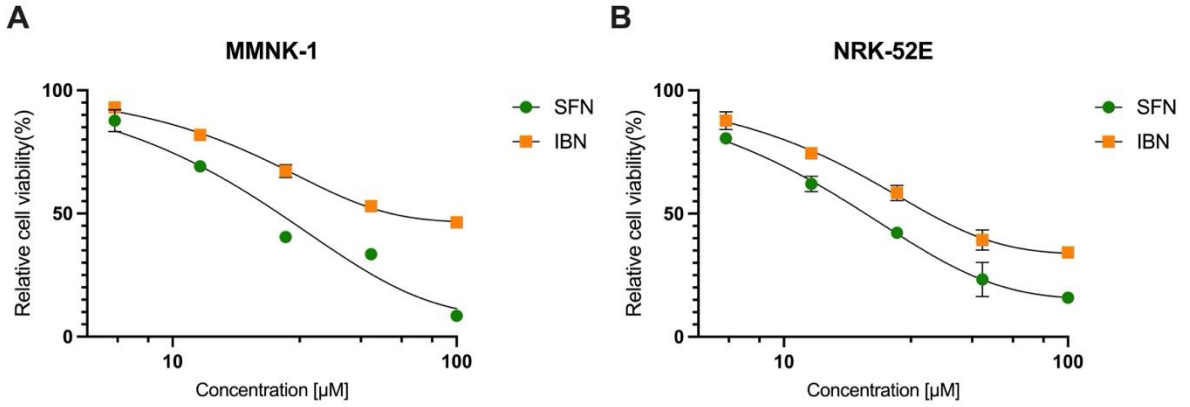

	SFN		IBN	
	IC_{50}	Emax	IC_{50}	Emax
MMNK-1	22.01 ± 0.83 μM	98.17 ± 1.36	20.82 ± 1.79 μM	57.81 ± 1.98
NRK-52E	18.14 ± 0.14 μM	90.30 ± 0.14	21.78 ± 0.78 μM	69.60 ± 1.13

Figure 2. Effect of ITCs on cell viability of non-cancerous cells. Cell viability of **(A)** MMNK-1 and **(B)** NRK-52E was assessed by SRB assay after 24 h of treatment with

different concentrations of SFN and IBN. Data were presented as mean ± SEM from independent experiments (n = 3).

Effect of IBN on cell cycle distribution

Based on the cell viability results, 10 μM and 25 μM IBN were selected as the low and high lethal concentrations, respectively, on the basis of the 24 h IC_{50} values. Cell cycle analysis showed that IBN caused S-phase arrest at the low concentration and G1-phase arrest at the high concentration (**Figure 3**).

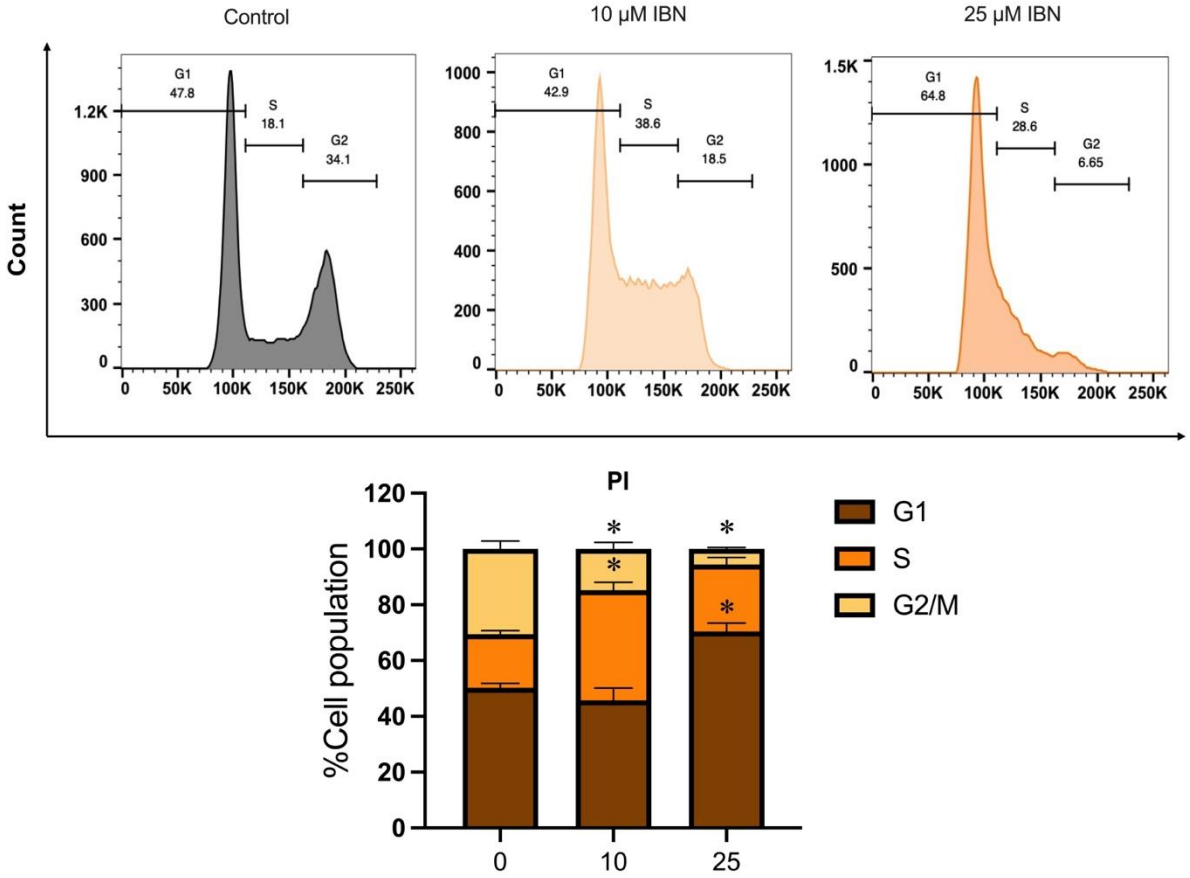

Figure 3. Effect of IBN in KKU-452 cells on cell cycle distribution. KKU-452 were treated with IBN for 12 h. Cell cycle was determined by flow cytometry to determined cells in each phase. Flow cytometry histograms (Upper panel) and Corresponding bar graphs (Lower panel) were provided. Data were presented as mean ± SEM from independent experiments (n = 3). *p<0.05 compared to the control group

Effect of IBN on apoptotic induction

The apoptotic effect of IBN was evaluated using both qualitative AO/EB staining and quantitative Annexin V/PI staining. In the AO/EB assay, untreated cells exhibited uniform green fluorescence, indicating viable cells. In contrast, treatment with IBN at the high concentration resulted in bright green nuclei, characteristic of early apoptotic cells with chromatin condensation, and orange/yellow nuclei, indicating late apoptotic cells with loss of membrane integrity (**Figure 4A**). To confirm these findings quantitatively, Annexin V/PI staining followed by flow cytometry was performed. The results showed that IBN significantly induced apoptosis at the high concentration (**Figure 4B and 4C**).

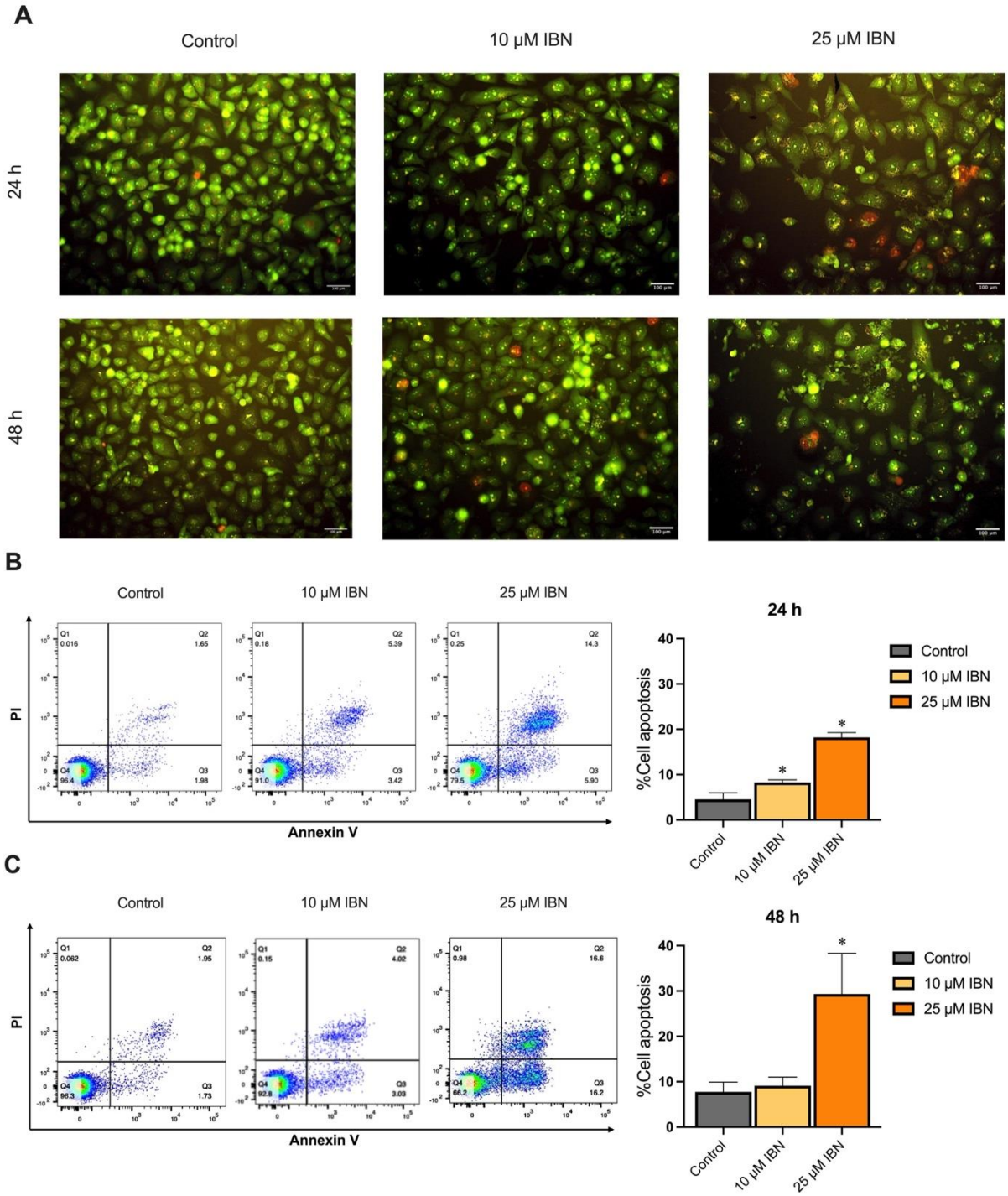

Figure 4. Effect of IBN in KKU-452 cells on programmed cell death. KKU-452 were treated with IBN for 24 h and 48 h. (A) Cellular morphology of KKU-452 was captured via bright field images at 10x magnification after exposure to 10 μM and 25 μM of IBN. Apoptosis was determined by flow cytometry to assess apoptotic cell (Q2+Q3) at 24 h (B) and 48h (C). Data were presented as mean ± SEM from independent experiments (n = 3). *p < 0.05 compared to the control group

Effect of IBN on cell migration

The effect of IBN on CCA cell migration was evaluated using a wound healing assay following treatment with sub-lethal concentrations of IBN (3.12 and 6.25 μM) for 18 h. A significant inhibition of wound closure was observed at 6.25 μM, with the migration rate reduced to 53% compared with the untreated control (100%) (**Figure 5**).

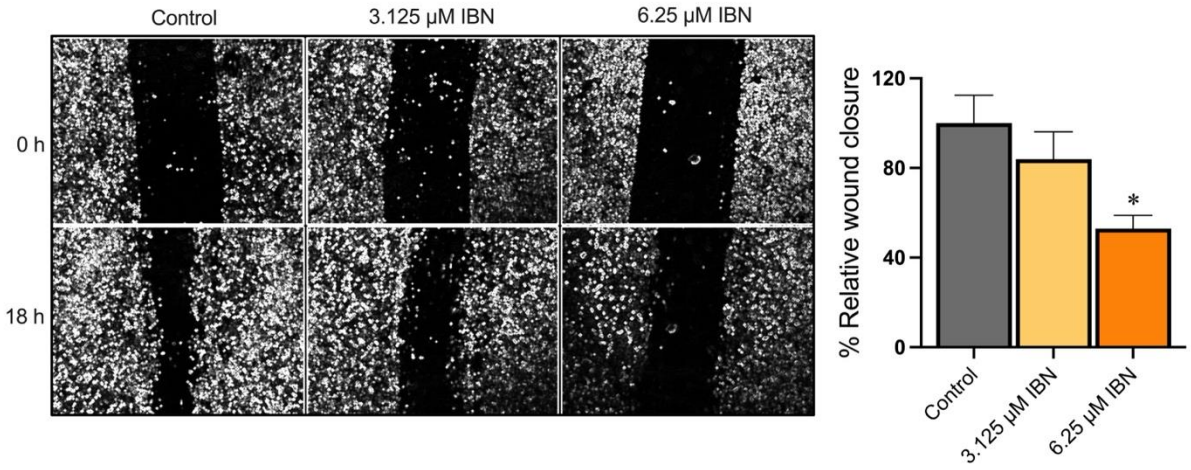

Figure 5. Effect of iberin in KKU-452 cells on cell migration. Anti-migration was determined by wound healing assay. Images of the wound area were captured at 4x magnification at 0h and 18h after treatment with 3.123μM or 6.25μM iberin, and the bar graph quantifies the percentage of wound closure. Data were presented as mean ± SEM from independent experiments (n = 3). *p < 0.05 compared to the control group

Discussion

ITCs have attracted considerable interest because of their broad range of biological activities, particularly their anticancer properties. Among these compounds, IBN has been reported to exert antitumor activity in several malignancies, including breast, brain, and liver cancers[12], suggesting that IBN may be of interest for further investigation in cancer research. Despite these findings, the effect of IBN on CCA has not been well characterized. Given the highly aggressive nature of CCA and the limited availability of effective treatment options, the identification of new bioactive compounds remains an important area of investigation. Therefore, the present study evaluated the effects of IBN in CCA cells to provide initial evidence of its potential relevance in this cancer type.

We first evaluated the effect of IBN on cell viability in KKU-452 cells, an aggressive CCA cell line that represents a relevant experimental model for this malignancy in the Asian population. Our findings demonstrated that IBN reduced cell viability in a time- and concentration-dependent manner. Importantly, its potency was comparable to that of SFN, a well-characterized ITC with established anticancer activity. This observation is in line with previous studies showing that IBN exerts cytotoxic effects across several cancer cell lines, with reported IC_{50} values ranging approximately from 10 to 100 μM[7,13]. Collectively, these findings suggest that IBN may have relevant bioactivity against CCA cells. However, the effect of IBN on non-cancerous cells should also be considered when interpreting these findings.

The effects of IBN on non-cancerous cells were relatively similar to those observed in CCA cells. This suggests that, under the present conditions, IBN did not demonstrate clear selectivity for cancer cells over non-cancerous cells, and this effect may

depend on the cellular context. Previous studies of ITCs have reported inconsistent selectivity profiles, with some showing greater cytotoxicity toward cancer cells (i.e. hepatocellular carcinoma)[7], whereas others reported limited selectivity (i.e. laryngeal carcinoma)[14]. Although these findings warrant cautious interpretation of the anticancer activity of IBN, they do not exclude its biological relevance. Rather, they highlight the need for further investigation to identify treatment conditions and concentration ranges that may better define its biological actions.

The biological effects of IBN were then evaluated at low and high lethal concentrations (10 and 25 μM, respectively), which showed significant cytotoxicity. We first examined its effect on cell cycle distribution and found that IBN induced S-phase arrest at the low concentration and G1-phase arrest at the high concentration. Previous studies have reported that ITCs can induce S-phase arrest, potentially through activation of checkpoint kinases[15], whereas G1-phase arrest has been associated with suppression of cyclin–CDK activity[16]. The effects of ITCs on cell cycle progression may also depend on treatment conditions, with milder exposure often associated with arrest at G1 or S phase, while more severe stress conditions may lead to G2/M arrest[16,17]. Although the present data are insufficient to explain why IBN induced different arrest phases at the tested concentrations, these findings indicate that IBN is capable of disrupting cell cycle progression in CCA cells. In addition to its effect on cell cycle progression, IBN also promoted apoptotic cell death in CCA cells. These findings suggest that the reduction in cell viability observed following IBN treatment was not solely due to growth inhibition, but also involved activation of programmed cell death. These results are consistent with previous studies reporting the pro-apoptotic activity of IBN[12], which has been linked to mechanisms such as intracellular ROS generation and microtubule depolymerization[7]. Collectively, these observations suggest that apoptosis is one of the mechanisms underlying the anticancer effect of IBN in CCA cells.

Given the limited selectivity observed at lethal concentrations, the activity of IBN at sub-lethal concentrations was further investigated, with particular focus on cell migration. Using a wound healing assay, we found that IBN reduced CCA cell migration at sub-lethal concentrations (3.12 and 6.25 μM). This finding is consistent with previous report showing that ITCs can suppress cancer cell migration, potentially through modulation of signaling pathways involved in motility and invasion, such as PI3K/Akt and NRF2[18]. As cell migration is closely associated with tumor invasion and metastatic progression, these results suggest that IBN may also influence metastasis-related behavior in CCA cells.

Conclusion

In conclusion, the present study provides initial evidence that IBN exerts anticancer activity against CCA cells. IBN showed cytotoxic effects in CCA cells, and at lethal concentrations (≥10 μM), it disrupted cell cycle progression and induced apoptosis. In addition, at sub-lethal concentrations (≤ 6.25 μM), IBN reduced cell migration, suggesting that it may also affect behaviors related to cancer progression. However, the limited selectivity observed in non-cancerous cells indicates that its biological effects should be interpreted with caution. Based on the present findings, sub-lethal concentrations of IBN may represent a more favorable condition for further investigation. Additional studies are needed to better define its mechanisms of action, optimize its effective concentration range, and clarify its potential relevance in CCA.

Acknowledgement

The author, Nanthawut Buachaban, gratefully acknowledges the Postgraduate Study Support Grant from the Faculty of Medicine, Khon Kaen University. This study was supported by the Faculty of Medicine, Khon Kaen University, Thailand (Grant No. IN67065).

References

1. Brindley PJ, Bachini M, Ilyas SI, et al. Cholangiocarcinoma. *Nat Rev Dis Primers*. 2021;7(1):65. doi:10.1038/s41572-021-00300-2
2. Mazzaferro V, Gorgen A, Roayaie S, Droz Dit Busset M, Sapisochin G. Liver resection and transplantation for intrahepatic cholangiocarcinoma. *Journal of Hepatology*. 2020;72(2):364-377. doi:10.1016/j.jhep.2019.11.020
3. Doherty B, Nambudiri VE, Palmer WC. Update on the Diagnosis and Treatment of Cholangiocarcinoma. *Curr Gastroenterol Rep*. 2017;19(1):2. doi:10.1007/s11894-017-0542-4
4. Liu P, Zhang B, Li Y, Yuan Q. Potential mechanisms of cancer prevention and treatment by sulforaphane, a natural small molecule compound of plant-derived. *Mol Med*. 2024;30(1):94. doi:10.1186/s10020-024-00842-7
5. Wang W, Wang S, Howie AF, Beckett GJ, Mithen R, Bao Y. Sulforaphane, Erucin, and Iberin Up-Regulate Thioredoxin Reductase 1 Expression in Human MCF-7 Cells. *J Agric Food Chem*. 2005;53(5):1417-1421. doi:10.1021/jf048153j
6. Jadhav U, Ezhilarasan R, Smith SF, Smith MA, Mohanam S. Dietary Isothiocyanate Iberin Inhibits Growth and Induces Apoptosis in Human Glioblastoma Cells. *Journal of Pharmacological Sciences*. 2007;103(2):247-251. doi:10.1254/jphs.SC0060148
7. Pocasap P, Weerapreeyakul N, Thumanu K. Alyssin and Iberin in Cruciferous Vegetables Exert Anticancer Activity in HepG2 by Increasing Intracellular Reactive Oxygen Species and Tubulin Depolymerization. *Biomol Ther (Seoul)*. 2019;27(6):540-552. doi:10.4062/biomolther.2019.027
8. Saensa-ard S, Leuangwattanawanit S, Senggunprai L, et al. Establishment of cholangiocarcinoma cell lines from patients in the endemic area of liver fluke infection in Thailand. *Tumour Biol*. 2017;39(11):1010428317725925. doi:10.1177/1010428317725925
9. Maruyama M, Kobayashi N, Westerman KA, et al. Establishment of a highly differentiated immortalized human cholangiocyte cell line with SV40T and hTERT. *Transplantation*. 2004;77(3):446-451. doi:10.1097/01.TP.0000110292.73873.25
10. Best CJM, Tanzer LR, Phelps PC, et al. H-ras-transformed NRK-52E renal epithelial cells have altered growth, morphology, and cytoskeletal structure that correlates with renal cell carcinoma in vivo. *In Vitro CellDevBiol-Animal*. 1999;35(4):205-214. doi:10.1007/s11626-999-0028-2
11. Suarez-Arnedo A, Figueroa FT, Clavijo C, Arbeláez P, Cruz JC, Muñoz-Camargo C. An image J plugin for the high throughput image analysis of in vitro scratch wound healing assays. *PLOS ONE*. 2020;15(7):e0232565. doi:10.1371/journal.pone.0232565
12. Gong TT, Guo Q, Li X, et al. Isothiocyanate Iberin inhibits cell proliferation and induces cell apoptosis in the progression of ovarian cancer by mediating ROS accumulation and GPX1 expression. *Biomedicine & Pharmacotherapy*. 2021;142:111533. doi:10.1016/j.biopha.2021.111533
13. Jadhav U, Ezhilarasan R, Vaughn SF, Berhow MA, Mohanam S. Iberin induces cell cycle arrest and apoptosis in human neuroblastoma cells. *International Journal of Molecular Medicine*. 2550;19(3):353-361. doi:10.3892/ijmm.19.3.353
14. Devi JR, Thangam EB. Mechanisms of Anticancer Activity of Sulforaphane from Brassica oleracea in HEp-2 Human Epithelial Carcinoma Cell Line. *Asian Pacific Journal of Cancer*

Prevention. 2012;13(5):2095-2100. doi:10.7314/APJCP.2012.13.5.2095
15. Żuryń A, Krajewski A, Klimaszewska-Wiśniewska A, Grzanka A, Grzanka D. Expression of cyclin B1, D1 and K in non-small cell lung cancer H1299 cells following treatment with sulforaphane. *Oncology Reports*. 2562;41(2):1313-1323. doi:10.3892/or.2018.6919
16. Gamet-Payrastre L, Li P, Lumeau S, et al. Sulforaphane, a Naturally Occurring Isothiocyanate, Induces Cell Cycle Arrest and Apoptosis in HT29 Human Colon Cancer Cells. *Cancer Res*. 2000;60(5):1426-1433.
17. Li J, Zhou Y, Yan Y, Zheng Z, Hu Y, Wu W. Sulforaphane-cysteine downregulates CDK4 /CDK6 and inhibits tubulin polymerization contributing to cell cycle arrest and apoptosis in human glioblastoma cells. *Aging*. 2020;12(17):16837-16851. doi:10.18632/aging.103537
18. Zhang Y, Gilmour A, Ahn YH, de la Vega L, Dinkova-Kostova AT. The isothiocyanate sulforaphane inhibits mTOR in an NRF2-independent manner. *Phytomedicine*. 2021;86:None. doi:10.1016/j.phymed.2019.153062

PU.1 modRNA induces osteoclast formation from human peripheral blood mononuclear cells

Atima Khopimai[1], Kran Sununtha[2], Tipparat Parakaw[3], Puangwan Lapthanasupkul[4], Sirada Srihirun[3,*]

[1]Master Degree Student of Oral Biology and Integrative Biomedical Science Program, Department of Pharmacology, Faculty of Dentistry, Mahidol University, Ratchathewi, Bangkok 10400, Thailand
[2]Chakri Naruebodindra Medical Institute, Faculty of Medicine Ramathibodi Hospital, Mahidol University, Samut Prakan 10540, Thailand
[3]Department of Pharmacology, Faculty of Dentistry, Mahidol University, Ratchathewi Bangkok 10400, Thailand
[4]Department of Oral and Maxillofacial Pathology, Faculty of Dentistry, Mahidol University, Ratchathewi, Bangkok 10400, Thailand

Abstract

Osteoclasts, specialized cells responsible for bone resorption, play a crucial role in skeletal remodeling by degrading both the mineral and organic components of bone, thereby maintaining bone homeostasis and calcium balance. Most existing *in vitro* osteoclast models rely on animal cells or immortalized cell lines, which often fail to reflect human-specific regulatory pathways and functional responses. This study aims to generate osteoclast cells from human peripheral mononuclear cells (PBMCs) using modified RNA (modRNA) encoding the spleen focus-forming virus proviral integration 1 (*PU.1*), an initial transcription factor for osteoclast differentiation. Human PBMCs were isolated by the Histopaque density gradient method from the peripheral blood of healthy volunteers (n=3). Human macrophages were transfected with *PU.1* modRNA. Osteoclast-specific markers: tartrate-resistant acid phosphatase (TRAP), F-actin ring, and cathepsin K expression were evaluated. At day 1 post-transfection, the expression of *PU.1* in human macrophages increased by 2.53 ± 0.31, 1.97 ± 0.17, and 2.56 ± 0.45 -fold for 5, 10, and 20 ng, respectively. In addition, *PU.1* modRNA (10 ng/well) induced formation of $TRAP^+$ multinucleated cells, F-action ring formation, and expression of cathepsin K in human macrophages at day 5 after transfection. In conclusion, *PU.1* modRNA can induce osteoclast formation from human macrophages *in vitro*. This provides a new *in vitro* human osteoclast model for more precise studies of bone disease pathogenesis and a reliable platform for drug discovery in a human-relevant system.

Keywords: *PU.1*, modRNA, osteoclast, bone

Introduction

Osteoclasts, large multinucleated bone-resorbing cells generated from hematopoietic origin, are essential in maintaining alveolar bone homeostasis. The alveolar bone, a part of the jawbone, not only supports the structural teeth but also adsorbs the masticatory force produced by chewing (1, 2). Disrupting the balance between osteoblast as bone formation and osteoclast as bone resorption results in pathological conditions such as periodontitis (3). Therefore, osteoclasts have been the target for therapeutic intervention. PBMCs have become a valuable source for generating osteoclasts *in vitro*, allowing researchers to investigate osteoclast biology in a controlled environment. Using PBMCs, researchers can explore cellular processes relevant to human osteoclast formation without relying on animal models. This study focuses on PBMC-derived osteoclasts, offering insights into the specific pathways and molecular signals involved in their differentiation (4, 5).

The spleen focus-forming virus proviral integration 1 (*PU.1*) transcription factor has gained recognition as a crucial regulator of osteoclast differentiation and function (6). As a member of the Ets family of transcription factors, *PU.1* is essential for developing myeloid cells, including osteoclasts, macrophages, and other immune cells (7). *PU.1* plays a crucial role in regulating osteoclastogenesis by promoting the expression of osteoclast-specific genes such as tartrate-resistant acid phosphatase (TRAP) and cathepsin K (8). The involvement of *PU.1* in osteoclast differentiation and bone resorption processes has sparked significant interest, as it directly influences osteoclast activity, making it a promising gene for induction of osteoclast formation.

A gene delivery system using modRNA represents a powerful technique for inducing osteoclast differentiation. The exogenous expression of *PU.1* was driven by retrovirus-induced osteoclast formation in bone marrow-derived macrophages (9). However, the gene delivery system via virus vectors increases the risk of insertion mutagenesis to the host genome. The synthetic modRNA, a DNA-free technique, represents an alternative tool to induce protein expression in target cells. Because protein production induced by modRNA is synthesized in the cytoplasm (no nuclear translocation required), modRNA exerts fast and localized protein expression (10). This study aims to generate an osteoclast model from human PBMCs by modRNA of *PU.1*. The osteoclast characteristics, including TRAP-positive multinucleated cells, F-action ring formation and cathepsin K expression were investigated.

Methods

Construction of in vitro transcription (IVT) templates and synthesis of modRNA

PU.1 (GeneID 6688) and eGFP IVT templates were generated using the pGEM T easy vector and 120-A tract primers, as described previously (11). *PU.1* template was generated from U937-derived osteoclasts using conventional phorbol 12-myristate 13-acetate (PMA) and 1α, 25 di-hydroxy Vitamin D_3. Subsequent PCR of *PU.1* was isolated. ModRNA was synthesized with the HiScribe™ T7 High-yield RNA synthesis kit (New England Biolabs, Ipswich, MA, USA), using a custom ribonucleoside cocktail comprising CleanCap® Reagent AG (TriLink Biotechnologies, San Diego, CA, USA), pseudouridine triphosphate, adenosine triphosphate, guanosine triphosphate, and cytidine triphosphate, in accordance with the manufacturer's instructions. Reactions were incubated for 3 hours at 37 °C and then treated with DNase. The RNA was purified using RNA Clean &

Concentrator (Zymo Research, Irvine, CA, USA) and adjusted to 100 ng/μL with RNase-free water before freezing at -80 °C.

Human PBMCs isolation

This research was approved by the Ethical Committee of the Faculty of Dentistry/Faculty of Pharmacy, Mahidol University (COA.No. MU-DT/PY-IRB 2025/022.0104). Human peripheral blood was corrected from healthy volunteers (n = 3) who gave written informed consent according to the Declaration of Helsinki. Venous whole blood was placed and gently mixed in EDTA tubes. Blood was layered above Histopaque-1077 (Sigma-Aldrich, St. Louis, MO, USA) in 1:1 ratio and centrifuged at 400xg for 30 minutes. After centrifugation, blood samples were separated into 4 layers: plasma, PBMCs, Histopaque-1077, and red blood cells. The layer of PBMCs located between plasma and Histopaque-1077 was carefully aspirated into clean conical tubes and washed twice with PBS.

Culture and differentiation of macrophages from PBMCs

PBMCs were expanded with completed Dulbecco's modified Eagle's medium (DMEM) supplemented with 10% fetal bovine serum and 1% penicillin/streptomycin in the presence of 25 ng/ml human M-CSF (R&D Systems, Minneapolis, MN, USA). After 3 days of expansion, macrophages were collected by cell scrapper after washed once with PBS.

PU.1 modRNA transfection

PU.1 modRNA was transfected by MessengerMax Lipofectamine (Thermo Fisher Scientific, Waltham, MA, USA) according to the manufacturer's protocol. Cells were transfected with 5, 10, and 20 ng/well of *PU.1* modRNA in 48 well plates. A mixture of MessengerMax Lipofectamine and *PU.1* modRNA was added on top of the cells for transfection. Cell culture media was replaced by complete DMEM at 1, 3, and 5 days after transfection.

TRAP staining

TRAP staining was done on day 5 post-*PU.1* modRNA transfection using a TRAP staining kit (Cosmo Bio, Carlsbad, CA, USA). Brief, cells were washed with PBS and fixed with 10% formalin neutral buffer. After fixation, formalin was removed and washed 3 times with deionized water. The chromogenic substrates were added and incubated at 37 °C for 1 hour. TRAP-positive multinucleated cells (> 3 nuclei) were photographed and counted.

Immunofluorescence staining of F-action and cathepsin K

The cells were fixed with 4% paraformaldehyde at room temperature, permeabilized by incubation with 0.1% Triton-X-10 and blocked with 5% BSA. Then The cells were stained with 1:100 mouse anti-cathepsin K antibody (Santacruz, #sc-376803) for overnight. Rhodamine anti-mouse secondary antibody was incubated in dark. F-actin was stained by iFluoro488-phallodidin (Abcam, #ab176753) for 30 minutes before counter-stained nuclei by prolong gold anti-face DAPI (Invitrogen™, #P36935). Images were randomly taken using the spiral scan path of the confocal microscope.

Quantitative polymerase chain reaction (qPCR)

Total RNA was extracted at day 1 and 5 by a commercial entire RNA purification kit (Favorgen Biotech Corp., Taiwan). Complementary DNA was synthesized by using 1 μg of total RNA by iScript cDNA synthesis kit (Bio-rad, Hercules, CA). Quantitative real-time PCR was performed on Bio-rad real-time PCR system (CFX96) by using KAPA SYBR fast (KAPA biosystem Wilmington MA) as a real-time PCR indicator. The threshold cycle (Ct) value of the gene was normalized with the value of the housekeeping gene, *B2M* and targeting gene, *PU.1* and *CTSK*.

Statistical analysis

Data analysis was done using GraphPad Prism version 6 (GraphPad Software Inc., San Diego, CA). Data are means S.D. and analyzed by ANOVA and t-test. The level of significance was defined as a p-value < 0.05.

Results

Transfection Efficiency of PU.1 modRNA

To investigate the transfection efficiency of modRNA, *PU.1* modRNA was transfected into human macrophages and measured the expression *PU.1* by qPCR. The transfection of 5, 10 and 20 ng/well of *PU.1* modRNA significantly increased the expression of PU.1 in human macrophages by 2.53 ± 0.31, 1.97 ± 0.17, and 2.56 ± 0.45 -fold, respectively.

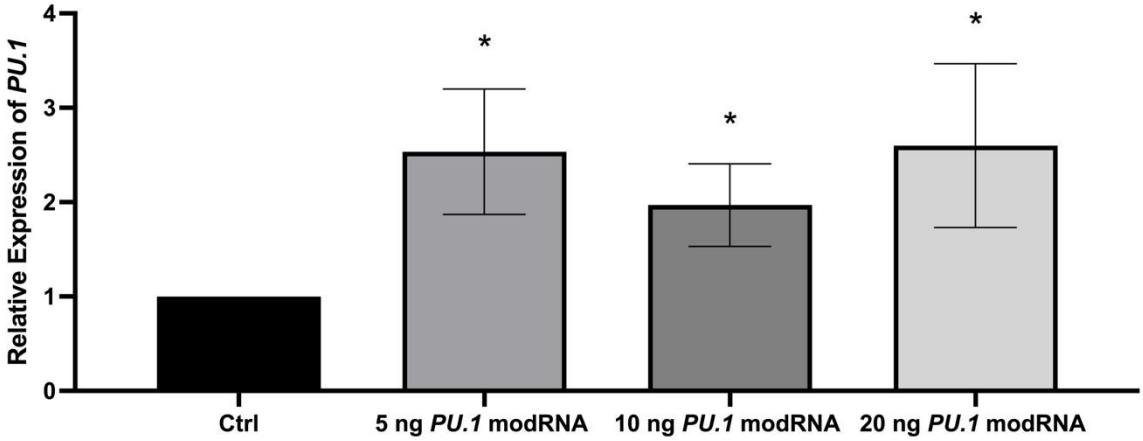

Figure 1. The expression of *PU.1* in human macrophages at 1 day post transfection. Human macrophages were transfected with 5, 10 and 20 ng/well of *PU.1* modRNA. The expression was measured by qPCR. Data are mean ± S.D. * p < 0.05 compared to the control group, analyzed by ANOVA (n = 3)

TRAP⁺ multinucleated cells induced by PU.1 modRNA

Osteoclasts express tartrate-resistant acid phosphatase (TRAP), a key osteoclast differentiation marker while losing their nonspecific esterase activity and forming multinucleated cells. The expression of TRAP was stained in human macrophages after transfected by 10 ng/well *PU.1* modRNA for 5 days. *PU.1* modRNA induced formation of large, multinucleated cells with purple cytoplasmic staining (Figure 2A). The numbers of TRAP⁺ multinucleated cells induced by *PU.1* modRNA significantly increased compared with control (Figure 2B).

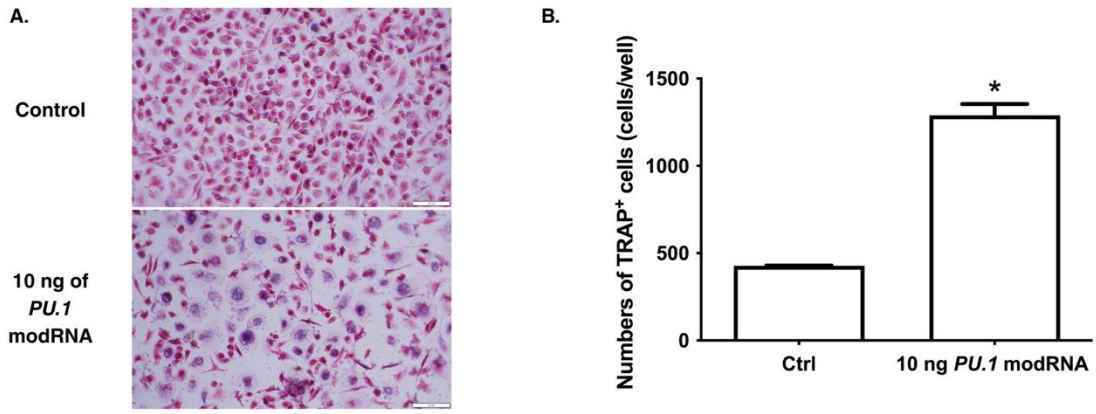

Figure 2. TRAP+ multinucleated cells induced by *PU.1* modRNA. (A) Representative images (A) and numbers (B) of TRAP+ multinucleated cells following treatment with lipofectamine (control) or transfection with 10 ng/well *PU.1* modRNA. Data are mean ± S.D. Scale bar = 100 μm * $p < 0.05$ compared to the control group, analyzed by t-test (n = 3).

PU.1 modRNA-induced expression of F-actin and cathepsin K

F-actin is essential for osteoclast bone adhesion and bone resorption, as it forms the sealing zone (actin ring) that isolates the resorption lacuna and enables effective acidification of the bone surface. Cathepsin K is a critical proteolytic enzyme responsible for degrading the organic bone matrix, particularly type I collagen, within the resorption compartment. Together, F-actin organization and Cathepsin K activity are fundamental for efficient osteoclastic bone resorption. *PU.1* modRNA induced formation of F-actin as well-defined continuous ring localized at the cell periphery. In addition to F-actin, *PU.1* modRNA also induced the expression of cathepsin K in the center of cells (Figure 3).

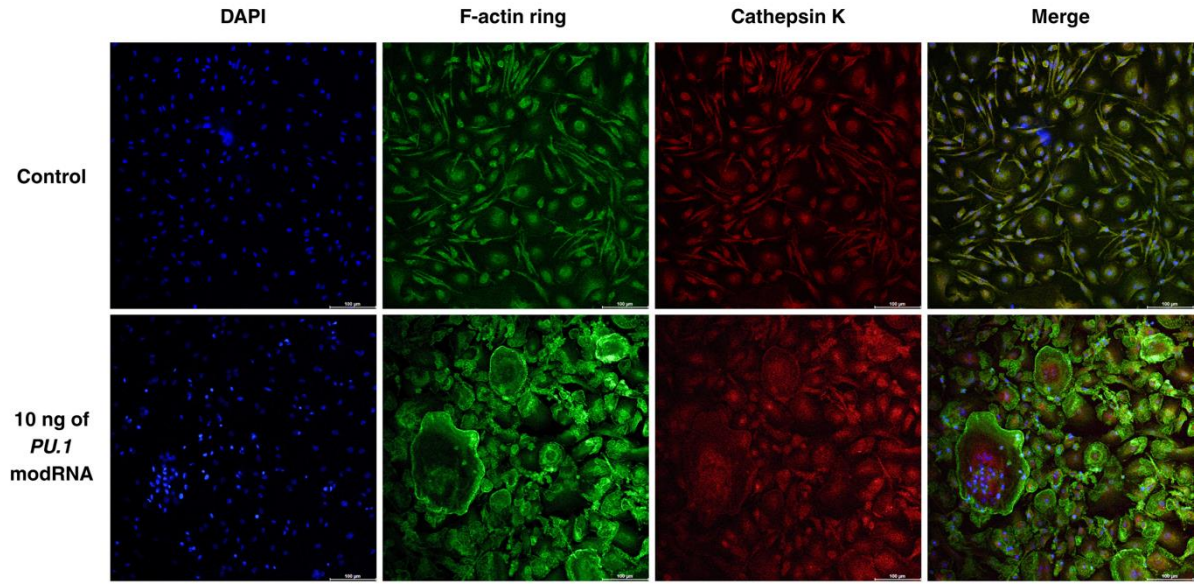

Figure 3. F-actin and cathepsin K expression induced by *PU.1* modRNA. Representative confocal images of F-actin and cathepsin K induced by *PU.1* modRNA in human macrophages at 5 days post-transfection. Scale bars = 100 μm

Discussion

Our research demonstrates that the delivery of *PU.1* modRNA successfully transforms primary human macrophages into osteoclasts in a short period of 5 days. The results from TRAP staining, and confocal microscopy confirm that this *PU.1* modRNA induces the key characteristics of osteoclastogenesis, such as the presence of multinucleation $TRAP^+$ cells, F-actin ring formation, and a significant increased cathepsin K expression. This creates a rapid and effective *in vitro* model of osteoclast generation.

The use of modRNA technology offers several advantages over traditional viral and DNA-based approaches. Viral vectors, such as lentiviruses and retroviruses, are known for their high transduction efficiency; however, they carry inherent risks of insertional mutagenesis and typically require extended incubation periods to achieve stable genomic integration and sustained transgene expression (12-14). In contrast, DNA-based transfection methods often exhibit low efficiency in primary human macrophages and may activate innate immune responses via cytosolic DNA-sensing pathways (15, 16). The modRNA, bypasses the need for nuclear entry, by inducing direct protein translation in the cytoplasm which accelerated onset of protein expression(17). This supports a significantly shortened timeline for cellular differentiation. Nevertheless, a key limitation of modRNA technology is the transient of mRNA-mediated protein expression (18, 19). While viral integration facilitates stable and long-term protein production, modRNA-driven expression is short-lived, thereby necessitating precise temporal control in experimental design and downstream analyses.

Although modRNA doses ranging from 5–20 ng/well significantly increased *PU.1* expression in human macrophages, 10 ng/well was identified as the optimal concentration, balancing effective transcriptional activation with cellular tolerance. In our study, a 5 ng/well enhanced *PU.1* transcript levels on Day 1; however, it was insufficient to support complete cellular maturation by Day 3. We hypothesized that at this low dose, protein expression levels did not reach the critical threshold required to activate downstream gene networks involved in cell fusion and F-actin organization. Notably, although the Day 1 transcriptional activity at the 5 ng dose (2.53-fold) was comparable to that observed at 20 ng (2.56-fold), the differentiation outcomes by Day 3 diverged substantially. This discrepancy suggests that mRNA expression levels may not directly correlate with protein translation, or that even subtle differences in initial PU.1 expression can critically influence commitment to the osteoclast lineage. In contrast, the 20 ng/well condition, despite demonstrating robust early expression, resulted in pronounced cytotoxicity and the absence of viable multinucleated cells by the end of the culture period. This effect is likely attributable to overactivation of innate immune sensing pathways (20, 21). Exogenous RNA can be recognized by pattern recognition receptors, including Toll-like receptors (TLRs) and RIG-I-like receptors, leading to the induction of pro-inflammatory signaling cascades and, in some cases, apoptosis(17, 22). Additionally, the high translational imposed by this modRNA dose may contribute to endoplasmic reticulum (ER) stress, further compromising cellular viability(12). Such stress responses are particularly relevant in primary human macrophages, which are highly sensitive to perturbations in protein homeostasis(21). Together, these findings highlight the importance of dose optimization in modRNA-based approaches to balance efficient gene expression with cellular viability.

Osteoclasts are generated from hematopoietic stem cells through the monocyte/macrophage lineage, and *PU.1* functions at multiple stages of this differentiation process (23). In early hematopoiesis, *PU.1* acts as a pioneer transcription factor that promotes myeloid differentiation while suppressing alternative cell fates such as erythroid or lymphoid lineages. This establishes the precursor pool necessary for osteoclastogenesis. In addition, *PU.1* directly regulates the expression of key receptors required for osteoclast differentiation, particularly the receptor M-CSF and RANKL. Without PU.1, precursor cells fail to express sufficient levels of these receptors, rendering them incapable of responding to osteoclastogenic signals (24). Our findings are consistent with previous studies demonstrating that overexpression of *PU.1* induced $TRAP^+$ multinucleated cell formation in mouse bone marrow–derived macrophages without RANKL (9). This result indicated that osteoclast generated by *PU.1* modRNA is one of an alternative *in vitro* model that can be utilized for osteoclast-related drug screening and therapeutic development.

Despite these promising findings, several limitations should be acknowledged and addressed in future studies. Although both morphological and molecular markers of osteoclast differentiation were validated, the functional bone-resorptive capacity has not yet been evaluated. Future investigations should incorporate functional assays, such as culturing cells on dentin slices or hydroxyapatite-coated surfaces, to quantify the formation of resorption pits. In addition, evaluating the long-term stability of the induced phenotype beyond Day 5 would provide important insights into the persistence and durability of modRNA-mediated reprogramming. Addressing these aspects will be essential for validating this model for high-throughput drug screening applications and to enable more comprehensive mechanistic studies of bone-related diseases.

Conclusion

In conclusion, transfection of modified RNA encoding *PU.1* represents a promising strategy to induce osteoclast differentiation from human macrophages, providing a rapid, controllable, and human-relevant approach to osteoclast generation. However, the bone resorption activity of osteoclast generated by this method need further study.

Acknowledgement

This study was supported by Mahidol University (Basic Research Fund: fiscal year 2022).

References

1. Cheenpracha S, Karalai C, Ponglimanont C, Subhadhirasakul S, Tewtrakul S. Anti-HIV-1 protease activity of compounds from Boesenbergia pandurata. Bioorg Med Chem. 2006;14(6):1710–4.
2. Daponte V, Henke K, Drissi H. Current perspectives on the multiple roles of osteoclasts: Mechanisms of osteoclast–osteoblast communication and potential clinical implications. eLife. 2024;13:e95083.
3. Omi M, Mishina Y. Roles of osteoclasts in alveolar bone remodeling. Genesis. 2022;60(8-9):e23490.

4. Tanaka Y, Nakayamada S, Okada Y. Osteoblasts and osteoclasts in bone remodeling and inflammation. Curr Drug Targets Inflamm Allergy. 2005;4(3):325–8.
5. Henriksen K, Karsdal MA, Taylor A, Tosh D, Coxon FP. Generation of human osteoclasts from peripheral blood. Methods Mol Biol. 2012;816:159–75.
6. Abdallah D, Jourdain ML, Braux J, Guillaume C, Gangloff SC, Jacquot J. An Optimized Method to Generate Human Active Osteoclasts From Peripheral Blood Monocytes. Front Immunol. 2018;9:632.
7. Paiva KBS, Granjeiro JM. Matrix Metalloproteinases in Bone Resorption, Remodeling, and Repair. Prog Mol Biol Transl Sci. 2017;148:203–303.
8. D'Alò F, Di Ruscio A, Guidi F, Fabiani E, Greco M, Rumi C. PU.1 and CEBPA expression in acute myeloid leukemia. Leuk Res. 2008;32(9):1448–53.
9. Jules J, Li YP, Chen W. C/EBPα and PU.1 exhibit different responses to RANK signaling for osteoclastogenesis. Bone. 2018;107:104–14.
10. Kim JH, Jin HM, Kim K, Song I, Youn BU, Matsuo K. The mechanism of osteoclast differentiation induced by IL-1. J Immunol. 2009;183(3):1862–70.
11. Suknuntha K, Tao L, Brok-Volchanskaya V, D'Souza SS, Kumar A, Slukvin I. Optimization of Synthetic mRNA for Highly Efficient Translation and its Application in the Generation of Endothelial and Hematopoietic Cells from Human and Primate Pluripotent Stem Cells. Stem Cell Rev Rep. 2018;14(4):525–34.
12. Kaur K, Zangi L. Modified mRNA as a Therapeutic Tool for the Heart. Cardiovascular Drugs and Therapy. 2020;34(6):871–80.
13. Kozak M, Hu J. DNA Vaccines: Their Formulations, Engineering and Delivery. Vaccines [Internet]. 2024;12(1):71.
14. Kwon S, Kwon M, Im S, Lee K, Lee H. mRNA vaccines: the most recent clinical applications of synthetic mRNA. Arch Pharm Res. 2022;45(4):245–62.
15. Ablasser A, Chen ZJ. cGAS in action: Expanding roles in immunity and inflammation. Science. 2019;363(6431):eaat8657.
16. Shi Y, Falahati R, Zhang J, Flebbe-Rehwaldt L, Gaensler KML. Role of antigen-specific regulatory CD4+CD25+ T cells in tolerance induction after neonatal IP administration of AAV-hF.IX. Gene Therapy. 2013;20(10):987–96.
17. Karikó K, Muramatsu H, Welsh FA, Ludwig J, Kato H, Akira S. Incorporation of pseudouridine into mRNA yields superior nonimmunogenic vector with increased translational capacity and biological stability. Mol Ther. 2008;16(11):1833–40.
18. Zangi L, Lui KO, von Gise A, Ma Q, Ebina W, Ptaszek LM. Modified mRNA directs the fate of heart progenitor cells and induces vascular regeneration after myocardial infarction. Nature Biotechnology. 2013;31(10):898–907.
19. Vavilis T, Stamoula E, Ainatzoglou A, Sachinidis A, Lamprinou M, Dardalas I. mRNA in the Context of Protein Replacement Therapy. Pharmaceutics [Internet]. 2023; 15(1):[166 p.].
20. Muslimov A, Tereshchenko V, Shevyrev D, Rogova A, Lepik K, Reshetnikov V. The Dual Role of the Innate Immune System in the Effectiveness of mRNA Therapeutics. International Journal of Molecular Sciences [Internet]. 2023;24(19):14820.
21. Schott J, Reitter S, Philipp J, Haneke K, Schäfer H, Stoecklin G. Translational regulation of specific mRNAs controls feedback inhibition and survival during macrophage activation. PLoS Genet. 2014;10(6):e1004368.
22. Chen F, Hasegawa H, Schmitt-Ulms G, Kawarai T, Bohm C, Katayama T. TMP21 is a presenilin complex component that modulates γ-secretase but not ε-secretase activity. Nature. 2006;440(7088):1208–12.

Combined Effects of Metformin and Palbociclib on Cell Viability in Tamoxifen-Resistant Breast Cancer Cells

Nanticha Wilawan[1], Kitiya Rujimongkon[1], Patthamapon Adchariyasakulchai[1], Wannarasmi Ketchart[1,*]

[1]Department of Pharmacology, Faculty of Medicine, Chulalongkorn University, Bangkok, 10330, Thailand

Abstract

Breast cancer is one of the leading health concerns in women, with the five-year survival rate of metastatic breast cancer patients being as low as 30%. Furthermore, breast cancer cells may acquire resistance to endocrine therapy through alterations in estrogen receptor (ER) expression or changes in growth factor signaling pathways. People with type 2 diabetes have a higher risk of developing various cancers, including breast cancer. Notably, metformin, a common anti-diabetic drug, has demonstrated anticancer properties beyond its glucose-lowering effect, making it a promising repurposed agent for breast cancer treatment. This study aims to investigate the effect of metformin and palbociclib on cell viability in wild-type ER+ breast cancer cells (MCF-7) and tamoxifen-resistant breast cancer cells (MCF-7/LCC2) and to determine whether combining metformin with palbociclib produces a synergistic effect on cancer cell viability. The results demonstrated that, at 72 hours, the IC_{50} values of metformin were 25.692 mM in MCF-7 cells and 2.576 mM in MCF-7/LCC2 cells, whereas those of palbociclib were 1.632 μM and 4.731 μM in MCF-7 and MCF-7/LCC2 cells, respectively. Furthermore, the combination of metformin and palbociclib tended to synergistically reduce cancer cell viability, as evidenced by combination index (CI) values < 1 at 0.457, 0.789, and 2.576 mM of metformin combined with 1.107 and 4.731 μM of palbociclib in MCF-7/LCC2.The findings indicate that the combination of metformin and palbociclib represents a potentially effective treatment strategy for patients with tamoxifen-resistant breast cancer.

Keywords: Metformin, palbociclib, endocrine therapy, tamoxifen-resistant breast cancer cells, synergistic effect

Introduction

Breast cancer continues to be a serious health issue for women, with less than 30% of patients with metastatic breast cancer surviving for five years.[1] Although adjuvant endocrine therapy reduces breast cancer mortality by nearly 40%, resistance remains common in advanced disease, often leading to tumor recurrence.2 Breast cancer cells can develop resistance to endocrine therapy through changes in ER expression or growth factor signaling pathways, which is associated with poorer prognosis.[3,4]

Palbociclib, a potent CDK4/6 inhibitor, prevents cell progression into the S phase by disrupting the interaction between CDK4/6 and cyclin D proteins.[5,6] Palbociclib is considered a key therapeutic agent for the treatment of hormone receptor-positive, HER2-negative, and metastatic breast cancer.[7] Importantly, the majority of endocrine-resistant breast cancers have an intact downstream Rb pathway, suggesting that CDK4/6 inhibitor

therapy may be effective in these patients.2 However, its efficacy as a single agent is limited, and higher doses have been associated with toxicity and adverse effects.[8,9]

Type 2 diabetes (T2D) patients have a higher risk of developing various cancers, including breast cancer, compared to those without diabetes.[10] Metformin, a major biguanide derived from Galega officinalis, is a first-line treatment for T2D.[11] A 2005 Scottish study found that metformin lowers cancer risk in T2D patients, suggesting antitumoral properties.[12] Beyond its role in regulating blood sugar levels, metformin has gained increasing attention in oncology research and is being investigated as a potential therapeutic option for breast cancer treatment.[13]

Accordingly, the results outlined above suggest that metformin exhibits a reduction in cell viability and may act synergistically with palbociclib in tamoxifen-resistant breast cancer cells.

Methods

Cell culture and reagent

The wild-type ER+ breast cancer cell lines (MCF-7) were obtained from the American Type Culture Collection (Manassas, VA, USA). Tamoxifen-resistant cell lines (MCF-7/LCC2) were generously provided by Dr. Robert Clarke of the Lombardi Cancer Center, Georgetown University, Washington, DC, USA. The cell lines were maintained in MEM supplemented with 5% fetal bovine serum (FBS; Gibco, USA), 1% penicillin–streptomycin, and 1% amphotericin B (Invitrogen, MA, USA). All cultures were maintained in an incubator at 37°C in a humidified atmosphere of 95% air and 5% CO_2.

Palbociclib was purchased from Abcam (Cambridge, UK), while Metformin was purchased from Sigma-Aldrich (St. Louis, MO, USA).

Cell viability assay

The MCF7, and MCF-7/LCC2 cells were seeded at a density of 5x103 cells/well in 96-well plate and incubated overnight before the treatment. After that cells were treated with palbociclib at the concentration of 0-50 μM, and metformin at the concentration of 0-50 mM for 72 hours. The concentration ranges for palbociclib and metformin were established based on previous studies and preliminary experiments, covering values below and above the IC50 value. After incubation, MTT (5 mg/mL) was added to the wells and allowed to react for 4 hours at 37 °C and the formazan crystals were solubilized in dimethyl sulfoxide (DMSO) and determined the O.D. at 570 nm with microplate reader.

Vehicle controls were included for each treatment. DMSO at the highest concentration served as the control for palbociclib-treated groups, and complete MEM medium (CM) was used as the control for metformin-treated cells to account for potential solvent effects.

Combination Index (CI) analysis

Metformin and palbociclib were combined at non-constant ratios, with concentrations chosen at or below their individual IC_{50} values to cover both effective concentrations and those with reduced toxicity. This approach enhanced the assessment of possible synergistic effects. In detail, cells received combinations at ¼ IC_{50}, ½ IC_{50}, and IC_{50} concentrations for each drug.

The synergistic, additive, or antagonistic effects of the drug combinations were quantitatively evaluated using the Combination Index (CI) derived from the Chou-Talalay

assay. All CI values were calculated and analyzed using the specialized CompuSyn software. The combination Index value represents the effect of drug combination; CI < 1 (Synergistic effect); CI = 1 (Additive effect); and CI > 1 (Antagonistic effect)

Statistical analysis

Data were presented as the mean ± S.D. from three independent experiments. Differences between groups were determined by one-way ANOVA and subsequently analyzed using Tukey's multiple comparison post-hoc test. All analyses and graphs generation were performed with GraphPad Prism10. The significant values were accepted at $p < 0.05$

Results

Metformin and palbociclib demonstrated a reduction in cell viability in both wild-type ER+ breast cancer (MCF-7) and tamoxifen-resistant breast cancer cells (MCF-7/LCC2).

Metformin and palbociclib reduced cell viability in both MCF-7 and MCF-7/LCC2 cells lines, as determined by the MTT assay. After 72 hours of treatment, the IC_{50} values of metformin were 25.692 mM in MCF-7 cells and 2.576 mM in MCF-7/LCC2 cells (Figure 1a, b), while the IC_{50} values of palbociclib were 1.632 μM in MCF-7 cells and 4.731 μM in MCF-7/LCC2 cells (Figure 1c, d).

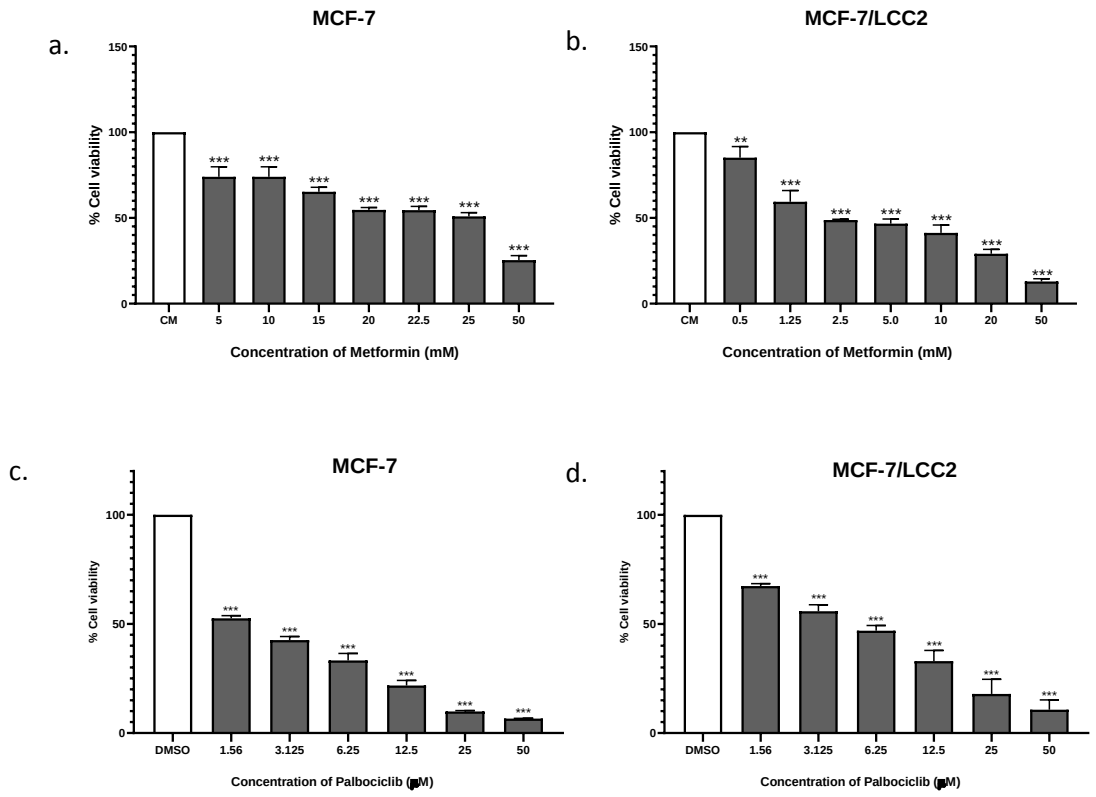

Figure 1. Metformin and palbociclib reduced cell viability in both wild-type ER+ breast cancer cells (MCF-7) and tamoxifen-resistant breast cancer cells (MCF-7/LCC2). The data present the percentage of cell viability for MCF-7 and MCF-7/LCC2 cells following 72 hours of treatment. (a, b) Cells were treated with metformin (0–50 mM), and (c, d) with palbociclib (0–50 μM), in MCF-7 and MCF-7/LCC2 cells, respectively. Results are expressed as mean ± SD of three independent experiments. *p-value < 0.05; **p < 0.01; ***p < 0.001 vs. control.

Combined effects of metformin and palbociclib in tamoxifen-resistant breast cancer cells (MCF-7/LCC2).

The combination of metformin and palbociclib tended to have inhibitory effects on cancer cell viability (Figure 2a). Synergistic effects were observed at non-constant concentration ratios, specifically at ¼ IC50, ½ IC50, and IC50 of each drug, corresponding to metformin concentrations of 0.457, 0.789, and 2.576 mM combined with palbociclib at 1.107 and 4.731 μM in MCF-7/LCC2 cells (Figure 2b).

The normalized isobologram analysis demonstrated that co-treatment with metformin and palbociclib produced a synergistic effect at specific concentrations, as data points fell below the line of additivity in the isobologram (Figure 2c). This synergistic interaction was further confirmed by combination index (CI) values of less than 1.

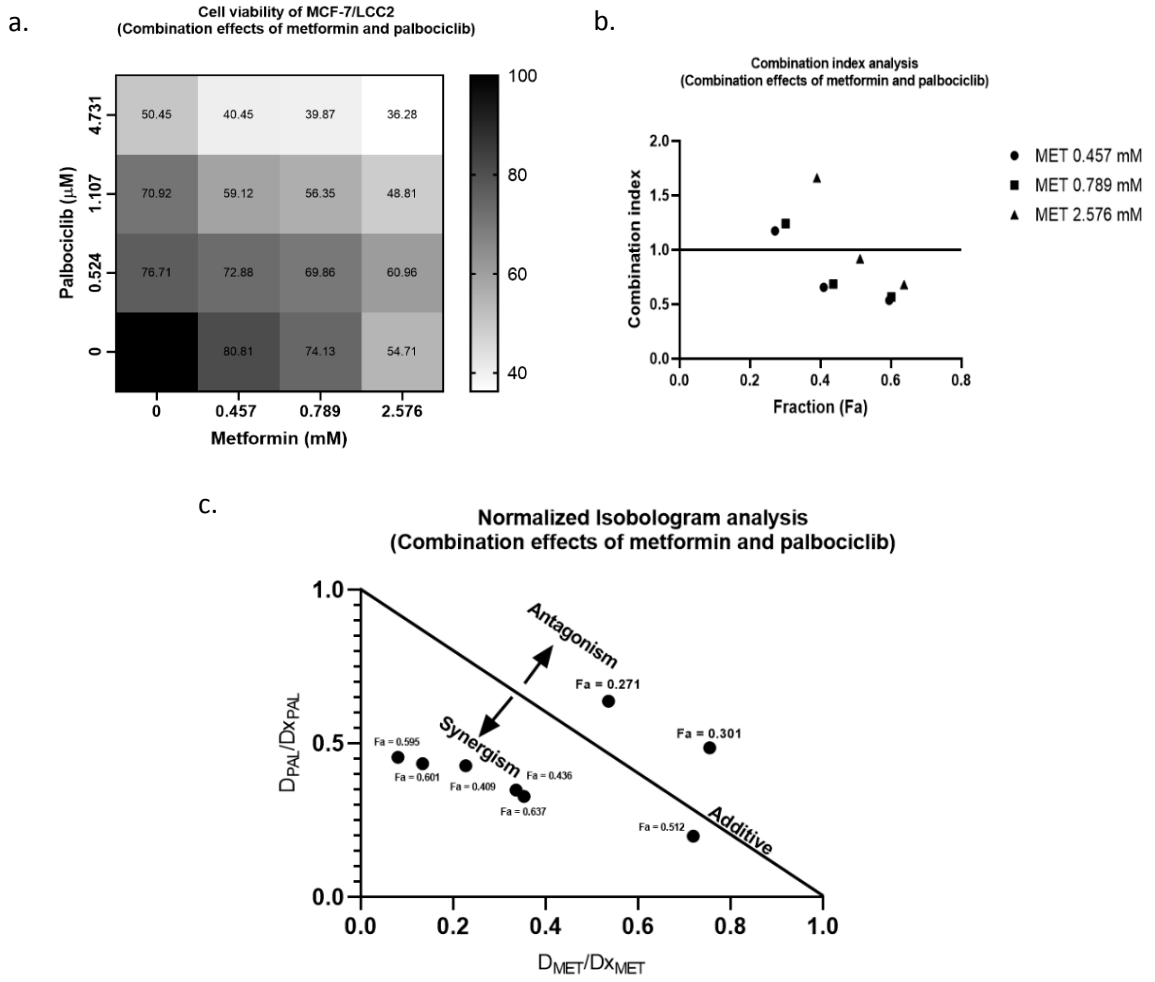

Figure 2. The combination effect of metformin and palbociclib in tamoxifen-resistant breast cancer cells (MCF-7/LCC2). (a.) % Cell viability of MCF-7/LCC2 cell lines treated with metformin at 0.457-2.576 mM and palbociclib at 0.524-4.731 μM for 72 hours. (b.) Combination index (CI) analysis was generated using the CompuSyn program based on the Chou-Talalay method. The CI value indicates the nature of drug interaction;CI < 1 (Synergistic effect); CI = 1 (Additive effect); and CI > 1 (Antagonistic effect) (c.) Normalized isobologram analysis illustrating the drug interaction between metformin (MET) and palbociclib (PAL). All data are presented as mean ± SD from three independent experiments. Statistical significance is denoted as *$p < 0.05$, **$p < 0.01$, and ***$p < 0.001$ vs. control.

Discussion

Metformin has been reported to exhibit anticancer activity by targeting multiple cancer hallmarks, including angiogenesis, cell proliferation, glucose metabolism, epithelial-to-mesenchymal transition, cell cycle progression, DNA damage response, and inflammation.[14] Its anticancer effects are primarily driven by AMPK activation, which suppresses downstream signaling pathways such as PI3K/AKT/mTOR, RAS/MAPK, and Wnt, and when combined with targeted therapies, these effects can be further enhanced.[15] In addition, Palbociclib is a selective CDK4/6 inhibitor that targets the Cyclin D1–CDK4/6 complex, leading to the induction of G1 phase cell cycle arrest by preventing phosphorylation of the retinoblastoma (Rb) protein, thereby inhibiting cell cycle progression.6 In this research, we have shown that metformin and palbociclib effectively suppresses cell viability in both wild-type ER+ breast cancer (MCF-7) and tamoxifen-resistant breast cancer (MCF-7/LCC2) cell lines. Additionally, the combination of metformin with palbociclib enhanced the reduction in cell viability in both cell lines compared to either treatment alone. Although the metformin concentrations used in this study exceed typical clinical plasma levels, they are consistent with those reported in previous in vitro studies, as concentrations of 1–40 mM are commonly required to produce measurable biological effects. This observation may be explained by the fundamental gap between in vitro and in vivo conditions, as cancer cells grown in culture media containing high levels of glucose and growth factors in the media can reduce cellular sensitivity to the drug, requiring higher concentrations to achieve a measurable effect.[16]

Previous reports have shown that metformin effectively inhibited both MCF-7 and SKBR3 breast cancer cell lines, particularly in the SKBR3 cells, which are known to overexpress HER2.15 Interestingly, our previous studies also found that MCF-7/LCC2 cells similarly overexpress HER2.[17] Supporting this, another report demonstrated that metformin-induced AMPK activation results in a dose-dependent decrease in HER2 phosphorylation (pHER2) levels.[18] Therefore, metformin and palbociclib exhibited a synergistic effect in MCF-7/LCC2 cells, which may be associated with HER2-related signaling pathways.

However, further experiments are required to fully investigate the molecular mechanisms that explain the synergistic effects observed between metformin and palbociclib, particularly in terms of how their combined action enhances anticancer activity in human breast cancers.

Conclusion

The results indicate that metformin and palbociclib have an inhibitory effect on the viability of both cell lines, wild-type estrogen receptor-positive (ER+) breast cancer cells

(MCF-7) and tamoxifen-resistant breast cancer cells (MCF-7/LCC2), in a concentration-dependent manner at 72 hours. Moreover, the combination of metformin and palbociclib demonstrated a synergistic effect in tamoxifen-resistant breast cancer cells (MCF-7/LCC2).

Acknowledgement

The study was supported by H.M. the King Bhumibol Adulyadej's 72nd Birthday Anniversary Scholarship. We would like to thank Prof. Robert Clarke M.D., Georgetown University Medical center, Washington DC, USA, for providing the tamoxifen-resistant breast cancer cell lines (MCF-7/LCC2).

References

1. Riggio AI, Varley KE, Welm AL. The lingering mysteries of metastatic recurrence in breast cancer. Br J Cancer. 2021;124(1):13-26.
2. Ertel A, Dean JL, Rui H, Liu C, Witkiewicz AK, Knudsen KE, Knudsen ES. RB-pathway disruption in breast cancer: differential association with disease subtypes, disease-specific prognosis and therapeutic response. Cell Cycle. 2010;9(20):4153-63.
3. Sweeney EE, McDaniel RE, Maximov PY, Fan P, Jordan VC. Models and Mechanisms of Acquired Antihormone Resistance in Breast Cancer: Significant Clinical Progress Despite Limitations. Horm Mol Biol Clin Investig. 2012;9(2):143-63.
4. Patel HK, Bihani T. Selective estrogen receptor modulators (SERMs) and selective estrogen receptor degraders (SERDs) in cancer treatment. Pharmacol Ther. 2018;186:1-24.
5. Morikawa A, Henry NL. Palbociclib for the Treatment of Estrogen Receptor-Positive, HER2-Negative Metastatic Breast Cancer. Clin Cancer Res. 2015;21(16):3591-6.
6. Portman N, Alexandrou S, Carson E, Wang S, Lim E, Caldon CE. Overcoming CDK4/6 inhibitor resistance in ER-positive breast cancer. Endocr Relat Cancer. 2019;26(1):R15-r30.
7. Mohamed Ebid AI, Fahim Genina YM, Shawky Haffez HR, Ahmed Hakam SH, Hassan Kassem LM, Mohamed AbdelMotaleb SM. Palbociclib in endocrine-resistant metastatic breast cancer: real-world outcomes. Expert Rev Anticancer Ther. 2026;26(2):263-72.
8. Finn RS, Dering J, Conklin D, Kalous O, Cohen DJ, Desai AJ, et al. PD 0332991, a selective cyclin D kinase 4/6 inhibitor, preferentially inhibits proliferation of luminal estrogen receptor-positive human breast cancer cell lines in vitro. Breast Cancer Res. 2009;11(5):R77.
9. Spring LM, Zangardi ML, Moy B, Bardia A. Clinical Management of Potential Toxicities and Drug Interactions Related to Cyclin-Dependent Kinase 4/6 Inhibitors in Breast Cancer: Practical Considerations and Recommendations. Oncologist. 2017;22(9):1039-48.
10. Giovannucci E, Harlan DM, Archer MC, Bergenstal RM, Gapstur SM, Habel LA, et al. Diabetes and cancer: a consensus report. Diabetes Care. 2010;33(7):1674-85.
11. Nathan DM, Buse JB, Davidson MB, Ferrannini E, Holman RR, Sherwin R, Zinman B. Medical management of hyperglycemia in type 2 diabetes: a consensus algorithm for the initiation and adjustment of therapy: a consensus statement of the American Diabetes Association and the European Association for the Study of Diabetes. Diabetes Care. 2009;32(1):193-203.
12. Evans JM, Donnelly LA, Emslie-Smith AM, Alessi DR, Morris AD. Metformin and reduced risk of cancer in diabetic patients. Bmj. 2005;330(7503):1304-5.
13. Bashraheel SS, Kheraldine H, Khalaf S, Moustafa AA. Metformin and HER2-positive breast cancer: Mechanisms and therapeutic implications. Biomed Pharmacother. 2023;162:114676.
14. Rocha GZ, Dias MM, Ropelle ER, Osório-Costa F, Rossato FA, Vercesi AE, et al. Metformin amplifies chemotherapy-induced AMPK activation and antitumoral growth. Clin Cancer Res. 2011;17(12):3993-4005.

15. Mahmoudi G, Ehteshaminia Y, Kokhaei P, Jalali SF, Jadidi-Niaragh F, Pagheh AS, et al. Enhancement of targeted therapy in combination with metformin on human breast cancer cell lines. Cell Commun Signal. 2024;22(1):10.
16. Dowling RJ, Niraula S, Stambolic V, Goodwin PJ. Metformin in cancer: translational challenges. J Mol Endocrinol. 2012;48(3):R31-43.
17. Sakunrangsit N, Ketchart W. Plumbagin inhibited AKT signaling pathway in HER-2 overexpressed-endocrine resistant breast cancer cells. Eur J Pharmacol. 2020;868:172878.
18. Kim JS, Kim MY, Hong S. Synergistic Effects of Metformin and Trastuzumab on HER2 Positive Gastroesophageal Adenocarcinoma Cells In Vitro and In Vivo. Cancers (Basel). 2023;15(19).

We gratefully acknowledge the sponsorship from…

GOLD SPONSORS

- Bara Scientific Co., Ltd.

- Fortis Trading Co.,Ltd.

SILVER SPONSORS

- Abhaiphubet Chaopraya Hospital Foundation

- Analytik Jena Instruments (Thailand) Co., Ltd.

- ANH Scientific Marketing Co.,Ltd.

- Applied Chemical and Instrument Co., Ltd.

- Chengdu Techman Software Co.,Ltd.

SILVER SPONSORS

- DKSH Holding Ltd.
- iCrotech Co., Ltd.
- K.A. Science Technology Co., Ltd.
- Kyberlife
- Lifomics Co., Ltd.
- Rightsign trading Co., Ltd.
- Theera Trading Co., Ltd.
- U2Bio (Thailand) Co., Ltd.
- Ward Medic Ltd.